SAPIENZA
UNIVERSITÀ DI ROMA

Particle-based modeling of dynamics in presence of obstacles

Alessandro Ciallella

PhD Thesis in Mathematical Models for Engineering, Electromagnetics and Nanosciences

Advisor: Prof. Emilio N. M. Cirillo

Department of Basic and Applied Sciences for Engineering

(XXX Cycle)

Acknowledgments

Foremost, I would like to thank my advisor, Emilio Cirillo: thanks to his patience and support, he guided me in this research over the past few years showing a genuine enthusiasm, dedication and confidence in my work.

I am also particularly grateful to Mario Pulvirenti for his wise advice and for having supported me since my Master's Degree studies.

Thanks to the coauthors of my works Petru L. Curseu, Adrian Muntean and Julien Sohier, and to Daniele Andreucci and Giada Basile for helpful discussions.

Thanks to the reviewers of this thesis, Francesca R. Nardi and Rutger A. van Santen, for their valuable comments and remarks.

I also wish to thank Claudia, my family, my Ph.D. colleagues, especially the Room 24 guys, my friends, for being part of my life.

Contents

Introduction

The aim of this dissertation is to study the effects of the presence of obstacles in the dynamics of some particle–based models. The interest is due to the existence of non–trivial phenomena observed in systems modeling different contexts, from biological scenarios to pedestrian dynamics. Indeed, obstacles can interfere with the motion of particles producing opposite effects, both "slowing down" and "speeding up" the dynamics , depending on the one hand on the model and on the other hand depending on some features of the obstacles, such as position, size, shape. In many different contexts it is required to pay great attention to this matter.

Particle–based models are of interest in the study of different realistic situations, from traffic flow, pedestrian dynamics, and granular flows, to ions or neutrons dynamics, colloids diffusion, biological and chemical models. There exist cases in which some features of the model are well understood. Let us think for instance to particles undergoing a Brownian motion. In this case it is well known how particles diffuse. Indeed, the mean square distance traveled by particles is proportional to time, and this is called classical Fickian diffusion. The classical diffusion has been the paradigm in numerous applications ranging from polymeric solutions, emulsions, colloidal suspension to several biological systems.

Nevertheless, is it possible to see a different unexpected behavior, for instance in experimental data? Can the environment influence significantly the dynamics? It is observed in many experimental measures that the mean square displacement of biomolecules scales as a power law with exponent smaller than one. This phenomenon, called *anomalous diffusion*, is largely present in nature, for instance in crowded biological media, polymeric networks, and porous materials. The common observation in this phenomena seems to be that the environment is densely packed. For instance it happens in cells, where different macromolecules such as proteins, lipids and sugars present in cellular cytosol can occupy from 5 to 40% of the total cellular volume [24]. This so–called called *macromolecular crowding* is believed to be the reason of the observed slowing down of the transport. Those macromolecules play the role of ob-

stacles for the diffusion of smaller molecules [38, 45]. Among the models proposed to theoretically study the phenomenon of the anomalous diffusion, we want to mention some Monte Carlo methods proposed in [23, 49]. The authors use a lattice model to investigate how obstacles size, shape, and density influence the motion of both a single agent and a population of agents, estimating the exponent of the power law of the mean squared displacement.

So, in the case of anomalous diffusion, obstacles in a way produce a slowing down effect on agents dynamics, as it is in general intuitive to expect talking about obstacles. Is it always true?

It is not difficult to find models in which the presence of obstacles can surprisingly facilitate the motion of particles. Let us think for instance to the *Braess paradox*: it has been noticed that adding a barrier or a constraint in a road network can actually increase the traffic flow or the human crowd flow [9, 39].

In granular flows it has been studied how obstacles close to the exit can prevent clogging. In experimental observations on the flow of granular media, when the particles pass through a constriction, it has been observed the drop of the flow or even the complete arrest of the flow due to particle interactions (for a review of the phenomenon of clogging of granular materials in bottleneck see for instance [53]). Several examples of this phenomenon at different scale are well known. Everyone can observe this effect in a saltcellar, but this phenomenon can happen in a silo, forcing a production line to stop, or in a dense suspension of colloidal particles when they try to pass through microchannels [31, 32], or even at smaller scale, for electrons of the liquid helium surface which pass through nanoconstrictions [47]. This outward flow drop is explained as the consequence of the tendency of particles to form arches close to the outlet. In the case of three–dimensional spherical grains discharging from a silo by gravity, the probability of arches to be formed has been studied as a function of the ratio between the size of the outlet size and the diameter of the beads [51] (see [50] for a earlier two–dimensional analogous result). This probability decreases when the ratio grows up to a critical value, beyond which no jamming can occur.

How is it possible to increase the flux trough a bottleneck? In the case of granular flows a solution that has been implemented is to place an obstacle above the silo exit. Even if it is contrary to common intuition, the choice of obstacles properly selected and placed avoids the jamming because it prevents arches to be formed or to become stable. Experimental evidence of this phenomenon is presented in [52], while in [2] it has been verified in particle–based simulations.

In pedestrian flows (see, e.g., [7, 33, 34, 37] for reviews of models and related prob-

lems), there is large and growing literature on the role that obstacles plays in the dynamics . For instance in [19], great attention is payed to the possible ways to handle obstacles, introducing a new modeling technique in obstacle parametrization and management that guarantees also the opacity of the obstacle, i.e., the choice of the authors is to model pedestrians dynamics in such a way that agents cannot see through obstacles.

Similarly to the granular dynamics, the effect of clogs reduction by adding obstacles, such as a suitable positioning of columns, is deeply investigated in the study of pedestrian flows [33]. Although they reduce the accessible space, they slow down the motion reducing the "faster–is–slower" effect. It has also been noticed that a suitable positioning of an obstacle close to the exit facilitates the evacuation of people in panic situations. Indeed the obstacle tends to decrease the internal pressure among pedestrian and breaks the symmetry in front of the exit, resulting in a faster outflow (see e.g. [1, Section 6.3] and [35, 36]). The clogging at the door is reduced because pedestrians can accumulate close to the obstacle and avoid the congestion in front of the exit, producing the so called "waiting room" effect [25]. By preventing the clogging at the door, a well–positioned obstacle reduce also the probability of injuries under panicked escape.

Other works inspired our study. In the study of transport of active matter in microscopic systems, for instance in drug-delivery design scenarios [40], ion moving in molecular cytosol [3–5], percolation of aggressive acids through reactive porous media [20], it is important to evaluate the efficiency of a medical treatment, the properties of ionic currents through cellular membranes, the durability of a highly permeable material. This is strictly connected to the time spent by the individual particle (colloid, ion, acid molecule) in the constraining geometry of the external environment.

This motivates the interest in studying the *residence time* of particles, i.e., the typical time that an agent of the system needs to cross a finite space, possibly overcoming some kind of barriers. This is one of the aims of the papers [15, 16] where it has been considered a particle system undergoing an asymmetric simple exclusion dynamics on a two–dimensional finite strip, at contact at two opposite side with two mass reservoirs at different density levels (see [29] for a diffusion hopping model with convection). It has been studied the effect of the presence of a barrier even when a drift acts on particles. The study of the dynamics has been carried out by numerical simulation and, in some cases, also analytically. The authors find non–trivial results when comparing the residence time in presence of the barrier with the residence

time when the obstacle is absent. The residence time reveals to be not monotonic as function of the size of the obstacle and this opens to the possibility to optimize the residence time by adding a suitable barrier.

All previously reported examples remind us that when the number of agents and interactions grows, for instance because of the presence of the obstacles, the possibility of unexpected phenomena increases. In all previous examples, the interaction of particles among each other plays a crucial role in the surprising effect due to the presence of obstacles. We want to show that obstacles can induce non–trivial effects even in simpler models, when particles of the system are not interacting among themselves [11–13].

The main problem in this dissertation is the study of the dynamics of some particle models in a finite region of the plane $\mathbb{R}^2$. Firstly, we consider the geometry of a rectangular strip with two opposite sides that are open boundaries, that we will think as the vertical side of the strip. These vertical sides are at contact with two infinite mass reservoirs at equilibrium at different densities ρ_L and ρ_R. Since we are interested in studying how obstacles influence the dynamics, we will consider the presence of large fixed reflective obstacles at rest into this strip. We consider also the horizontal boundaries of the strip to be reflective boundaries. Particles enter into and exit from the strip when they reach the open vertical sides.

In the first part of the thesis we consider, inside the strip, particles moving according to the Markov process solving the linear Boltzmann transport equation (LBTE). The linear Boltzmann equation is an important kinetic equation that is frequently used for mathematical modeling of different systems, from neutron and electron dynamics to radiation transfer and cometary flow. The LBTE is a case of the Boltzmann transport equation obtained by assuming that particles interact only with the medium in which they are passing through, but they do not interact among themselves. It represents the evolution of the density of particles subjected to random collisions while traveling freely. It describes the process of a particle that moves freely and that has random transitions in the velocity. The transitions can be interpreted as an interaction with a medium present in the environment, but the particles are not interacting among themselves. The linear Boltzmann equation arises also as the correct kinetic description of the Lorentz gas model in suitable limits.

We are interested in focusing on both collective and individual behavior. We will present both theoretical and numerical results.

One interesting problem is to compute the stationary state to which the solution $f(x, v, t)$ representing the distribution of particles tends at large time. The computa-

tion of the stationary state of the LBTE is commonly used for instance in radiation therapy, in particular in dosimetry. In [46] a survey of numerical methods for the stationary LBTE (Grid–Methods solver and Monte Carlo methods) is presented.

The stationary state of the linear Boltzmann equation will be totally characterized in the diffusive limit, corresponding to the limit in which the particles average free path between two consecutive jumps in the velocity tends to zero. We will prove the existence and uniqueness of the stationary state and the convergence in the L^∞ setting of the stationary solution of the LBTE to the stationary solution of the heat equation with mixed boundary conditions: Dirichlet boundary condition with values the density of the reservoirs on the open boundaries and homogeneous Neumann boundary condition on the horizontal sides and on the boundary of the obstacles. The stationary profile of the particle density will be even numerically constructed with a Monte Carlo algorithm by simulating one by one the motion of single particles and averaging over the obtained trajectories.

We will give great attention to the investigation of the residence time of particles. We let particles start their motion from the left open boundary and we compute the time that they spend into the strip until they eventually leave the channel through the right side. We discard the particles exiting through the left boundary in this computation. We compute, by averaging, the typical time needed to cross the strip and we analyze its dependence on the size and position of a reflecting obstacle positioned inside the strip. Surprisingly, the presence of reflective obstacles in the strip influences the residence time in some non–monotonic ways, depending on the size and the position of the obstacles. It is worth noticing that, for suitable dispositions of obstacles, in the strip we measure a residence time smaller than in the empty strip case, that is in absence of obstacles, and that there are cases in which the same obstacle, placed in different positions, can produce both the effects, i.e. decreasing or increasing the residence time. An unexpected symmetry in the position of the obstacle, with respect to the center of the strip, emerges from this Monte Carlo data. The evaluation of the residence time will be performed numerically.

In the second part of the thesis we will study a simpler model to fully understand the residence time behavior we found for the linear Boltzmann dynamics. We consider a 2D finite lattice with an equivalent geometry as before. The lattice is a rectangular strip, where we may place a rectangular fixed obstacle. Again, the left and right side of the strip are open boundaries, while the upper and lower sides and the boundaries of the obstacles are reflective boundaries. We consider particles moving performing a simple symmetric random walk. We first study numerically the residence time behav-

ior. We show that the behavior of the residence time exhibits the same dependence on the features of the obstacles observed when particles moved following the linear Boltzmann equation.

We would like to evaluate exactly the expected residence time in this model, to give a complete interpretation of previous numerical tests. To do this, we construct his reduced 1D version.

We consider the one–dimensional lattice whose length is equal to the horizontal length of the previous 2D lattice. We consider a simple symmetric random walk except that in two sites, defects, where the probability to jump backwards and forwards are suitably chosen. Since we want to mimic as good as possible the 2D case we interpret the singular sites as the horizontal coordinates of the vertical sides of the 2D obstacle. The probability of possible moves that we assign to a particle on a defected sites is still $1/2$ in the direction opposite with respect to the obstacle and λ in the direction toward the obstacle. To compare the residence time in the one–dimensional case to the results of two–dimensional experiments, here we call p the ratio between the height of the obstacle and the height of the 2D strip. The particle on a defect site hits the "obstacle" and it does not move with probability $p/2 = 1/2 - \lambda$, while it jumps in the direction of the obstacle with probability $\lambda = (1 - p)/2$. With this choice, calculating the residence time for this 1D model via Monte Carlo simulations, we find good correspondence between the results of the 1D and the 2D model. Moreover, in the case of this 1D toy model reduction we are able to compute exactly the residence time in function of the position and the "size" of the barrier. So we will construct a 5 state reduced picture of the 1D model, that permit us to produce exact calculation of the residence time for the 1D model.

We have found that the residence time has a complex dependence on the geometrical parameters of the obstacle. The final result is the balance of two effects. On the one hand the particle in presence of obstacle spends more time in the regions on the left and on the right of the obstacle, on the other hand it spends less time in the central region (the channels above and below the obstacle) with respect to the case of absence of obstacle. This is due to the fact that the obstacle makes more difficult to access to the central region, so it forces the particle to stay for a longer time in the other two regions. The final effect will be the balance of the two effects.

In the third part of the thesis we will focus on a different question. We will consider a crowd of people moving in an unknown area in condition of lack of visibility. Our aim is to investigate how cooperation can slow down people in finding the exit with respect to an individual behavior.

We consider particles moving on a squared 2D lattice, representing a corridor, where there is an exit, a site at the center of one side, that is not visible to pedestrian due to the absence of visibility. Particles move undergoing a variation of the simple symmetric random walk, where the closest sites do not have all the same probability to be reached because this depends on a possible interaction among particles. So, on one hand we consider particles to explore the environment randomly due to the absence of visibility, on the other we want to mimic the tendency of pedestrians to follow other people in the hope they will help them to found a way out. This *herding effect*, especially visible in crowds in panic situation, is represented by a tendency for particles to jump in the neighboring site where the largest group of particles is present. In this model there is no simple exclusion, particles can jump on an occupied site, but we study the effect of a buddying threshold of no–exclusion per site. If on the site there are too many people (above the threshold), we assume it to become unattractive for other particles. In this model, proposed in [17, 18], if we consider the threshold to be 0 (so pedestrians are not attracted by other people), we recover particles moving via independent simple symmetric random walks (individual behavior).

We have to consider how pedestrians act when they reach a wall. We will mimic via a parameter the tendency of people to follow the walls when trying to reach the exit and we consider also the presence of an obstacle into the lattice [14].

Our results will be numerical studies of how the buddying threshold influence the overall exit flux (evacuation rate) and the evacuation time in different cases (different geometries due to obstacle and different effects of the wall) as function of the total number of particles present in the lattice. To study the overall exit flux we consider the stationary case in which the same number of particles is present in the corridor at every time. This means that when a particle finds the exit and goes out of the lattice, we insert a new one at the opposite side of the lattice. Instead, in the study of the evacuation time we are interested in the time needed to let all the particles leave the corridor.

We find that the tendency of people to follow the walls in every considered case favor the evacuation. Another general effect is that the more is present the tendency to form large groups, i.e., the bigger the buddying threshold is, the more the evacuation will be inefficient. The presence of obstacles influences the dynamics. While in the computation of the residence time in both previous models the result was symmetric in the position of the same obstacle with respect to the center of the strip, now there is a strong asymmetry in the effect of the same obstacle placed in different position. We find that obstacles can favor effectively the evacuation flux and decrease the evacuation time if they are placed suitably far from the exit, closer to the opposite

side, while on the contrary obstacles close to the exit hinder the evacuation.

Finally, we will dedicate the last part of this thesis to the Lorentz model. In the original version, Lorentz [42] discussed the motion of a ballistic particle which is elastically scattered off by randomly placed, hard spherical obstacles to lay a microscopic basis for Drude's electric conductivity of metals.

The Lorentz model is a classical model that describes transport in a spatially heterogeneous medium. This is a classical model for finite velocity random motions: particles perform uniform linear motion up to the instant of contact with static disks when they are elastically reflected. The Lorentz model is a system of non–interacting particles moving in a region where static small spheres (scatterers) are distributed according to a Poisson probability measure.

Thus at high obstacle density, a tracer faces a heterogeneous environment characterized by a significant excluded volume and a highly ramified remaining space and may display many facets of anomalous transport like subdiffusion, crossover phenomena, immobilized particles and long-time tails (see for instance [38], Sect.3.3). In different limits such as Boltzmann–Grad limit or suitable low density limit the connection with the linear Boltzmann equation has been investigated in several works such as [6, 8, 30, 48]. Since we do not have a complete proof at the moment, we will just dedicate some comments to the study of the convergence of the particle density of the Lorentz model to the solution of the linear Boltzmann equation, that we expect to hold even in our geometry in a suitable low density limit.

Chapter 1

Linear Boltzmann

We introduce the linear Boltzmann equation in our domain: a rectangular strip with large reflective obstacles. We claim our results concerning the characterization of the stationary solution. We construct a Monte Carlo algorithm to simulate the dynamics and we use it to construct numerically the stationary states and to evaluate the residence time in presence of obstacles. Finally we prove the results on the stationary solution of the equation.

1.1 Model and results

We consider a system of light particles moving in the two–dimensional space. We choose as the domain a subset Ω of the finite strip $(0, L_1) \times (0, L_2) \subset \mathbb{R}^2$. This strip has two open boundaries, that we think as the left side $\partial\Omega_L = \{0\} \times (0, L_2)$ and the right side $\partial\Omega_R = \{L_1\} \times (0, L_2)$. The strip is in contact on the left side and on the right side with two mass reservoirs at equilibrium with particle mass densities ρ_L and ρ_R, respectively. Particles traveling into Ω are instead specularly reflected upon colliding with the upper side $(0, L_1) \times \{L_2\}$ and lower side $(0, L_1) \times \{0\}$ of the strip.

We consider the case in which large fixed obstacles are placed in the strip so that the domain Ω is a connected set. These obstacles are convex sets with smooth reflective boundaries. We consider a generic configuration of a finite number of obstacles with positive mutual distance and positive distance from the sides of the strip. In the sequel we will call $\partial\Omega_E$ the union of the obstacle boundaries and the upper and lower sides of the strip (see Figure 1.1). Therefore, when a particle reaches $\partial\Omega_E$ it experiences a specular reflection.

The linear Boltzmann equation is a kinetic linear equation, combining free transport and scattering off of a medium. This equation consists of two terms: a free

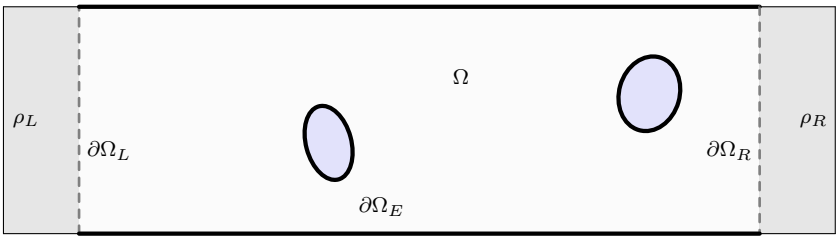

Figure 1.1: Domain Ω: strip with large fixed obstacles, where $\partial\Omega_L$ and $\partial\Omega_R$ are the vertical open boundaries and $\partial\Omega_E$ are reflective boundaries.

transport term and a collision operator $\mathcal{L}$.

Let us consider the phase space $\Omega \times S^1$, where $S^1 := \{v \in \mathbb{R}^2 : |v| = 1\}$. We will consider the operator $\mathcal{L}$ with elastic collision kernel. The equation for $(x, v) \in \Omega \times S^1$ and positive times t reads

$$(\partial_t + v \cdot \nabla_x) g(x, v, t) = \eta_\varepsilon \mathcal{L} g(x, v, t), \qquad x \in \Omega,\ v \in S^1,\ t \geq 0 \tag{1.1}$$

where, by the elastic collision rule $v' = v - 2(n \cdot v)n$, the operator $\mathcal{L}$ is defined for any $f \in L^1(S^1)$ as

$$\mathcal{L} f(v) = \lambda \int_{-1}^{1} [f(v') - f(v)] \, \mathrm{d}\delta. \tag{1.2}$$

Here $n = n(\delta)$ is the outward pointing normal to a circular scatterer of radius 1 at the point of collision among the particle with velocity v and the scatterer. So $\delta = \sin\alpha$ if α is the angle of incidence between v and n that has δ as impact parameter (see Figure 1.2); $\lambda > 0$ is a fixed parameter.

We denote by g_ε the solution of the equation corresponding to the value of η_ε, that is a positive parameter that we let go to $+\infty$ as ε goes to 0^+. The choice of the kernel and the related parameters will be discussed at the end of this Section.

The equation describes the evolution of the density of particles, moving of linear motion and having random collisions, against a circular scatterer, that preserve the energy. The time between two consecutive jumps in the velocities is distributed with exponential law with mean value $(\lambda\eta_\varepsilon)^{-1}$. Since both random collisions and hits against the elastic boundaries preserve the energy, the modulus of the velocity of a particle moving in Ω is constant, so we consider it to be equal to one.

On the elastic boundary $\partial\Omega_E$ we impose reflective boundary condition and on the

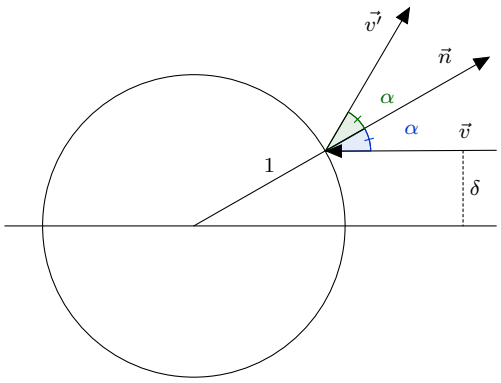

Figure 1.2: Elastic collision with a scatterers: impact parameter δ and angle of incidence α.

open boundary $\partial\Omega_L \cup \partial\Omega_R$ we set Dirichlet condition:

$$\begin{cases} g(x,v',t) = g(x,v,t) & x \in \partial\Omega_E,\ v\cdot n < 0,\ t \geq 0 \\ g(x,v,t) = f_B(x,v) & x \in \partial\Omega_L \cup \partial\Omega_R,\ v\cdot n > 0,\ t \geq 0, \end{cases} \tag{1.3}$$

where f_B is defined in (1.4) below and v' is given by the elastic collision rule $v' = v - 2(n\cdot v)n$. Here we denote by $n = n(x)$ the inward pointing normal on the boundary $\partial\Omega$ of the domain. We consider as initial datum the function $f_0(x,v) \in L^\infty(\Omega \times S^1)$ and we define f_B (not depending on t) as

$$f_B(x,v) := \begin{cases} \rho_L/2\pi & x \in \partial\Omega_L,\ v\cdot n > 0 \\ \rho_R/2\pi & x \in \partial\Omega_R,\ v\cdot n > 0, \end{cases} \tag{1.4}$$

where $1/2\pi$ is the density of the uniform distribution on S^1.

We are interested in the study of the stationary problem associated to (1.1)-(1.3):

$$\begin{cases} v\cdot\nabla_x g^S(x,v) = \eta_\varepsilon \mathcal{L} g^S & x \in \Omega,\ v \in S^1 \\ g^S(x,v') = g^S(x,v) & x \in \partial\Omega_E,\ v\cdot n < 0 \\ g^S(x,v) = f_B(x,v) & x \in \partial\Omega_L \cup \partial\Omega_R,\ v\cdot n > 0. \end{cases} \tag{1.5}$$

We want to investigate the behavior of the solution g^S_ε of (1.5) and prove its convergence to the stationary solution of the diffusion problem in Ω with mixed boundary

conditions given by

$$\begin{cases} \Delta\rho(x) = 0 & x \in \Omega \\ \rho(x) = \rho_L & x \in \partial\Omega_L \\ \rho(x) = \rho_R & x \in \partial\Omega_R \\ \partial_n\rho(x) = 0 & x \in \partial\Omega_E. \end{cases} \tag{1.6}$$

Theorem 1.1. *If $\varepsilon > 0$ is sufficiently small there exists a unique stationary solution $g_\varepsilon^S \in L^\infty(\Omega \times S^1)$ of (1.5).*

Theorem 1.2. *The stationary solution g_ε^S of (1.5) verifies*

$$g_\varepsilon^S \to \rho \tag{1.7}$$

as $\varepsilon \to 0$, where $\rho(x)$ is the solution to the problem (1.6). The convergence is in $L^\infty(\Omega \times S^1)$.

The choice of the elastic collision kernel for the operator $\mathcal{L}$ defined in (1.2) is due to the physical model we have in mind. We are considering a particle moving with initial velocity $v \in S^1$ and hitting an hard circular scatterer whose position is random. The random impact parameter δ chosen uniformly in $[-1, 1]$ allows to individuate this collision. In a similar way we could let the particle move following the Lorentz process, that is moving freely in a region where static small disks of radius ε are distributed according to a Poisson probability measure and elastically colliding with those disks. In this case for suitable choices of the mean value of the Poisson distribution in terms of ε and η_ε it could be possible to prove that the diffusive limit for the linear Boltzmann equation and the Lorentz process in a (small disks) low density limit are asymptotically equivalent in the limit $\varepsilon \to 0$ (see Chapter 4, [6] for the case of an infinite $2D$ slab with open boundary).

1.2 Stationary state: numerical study

We investigate, here, the stationary solution of the linear Boltzmann equation from a numerical point of view. Our algorithm directly simulates the motion of single particles following the linear Boltzmann equation. In the simulations we exploit the interpretation of the linear Boltzmann equation as the equation describing a stochastic jump process in the velocities and we directly simulate the motion of single particles.

We will show that the numerical stationary solution that we construct is close to the solution of the associated Laplace problem (1.6) if the scale parameter ε is

small enough, that is to say if the average time t_m between two consecutive hits is sufficiently small. This time will be called in the sequel *mean flight time*.

We will construct the solution of the Laplace problem (1.6) in our geometry by using the *COMSOL Multiphysics* software.

We proceed in the following way: we consider particles entering in Ω from the reservoirs. A particle starts its trajectory from the left boundary $\partial\Omega_L$ or from the right boundary $\partial\Omega_R$, where the mass density is ρ_L and ρ_R respectively. Therefore the number of particles we let enter from each side is chosen to be proportional to ρ_L and ρ_R. In other words, we select the starting side of the particle with probability $\rho_{\mathrm{L}}/(\rho_{\mathrm{L}}+\rho_{\mathrm{R}})$ (left side) and $\rho_{\mathrm{R}}/(\rho_{\mathrm{L}}+\rho_{\mathrm{R}})$ (right side) respectively. Then we draw uniformly the position x in $\partial\Omega_{\mathrm{L}}$ or $\partial\Omega_{\mathrm{R}}$ and the velocity v in S^1 with $v\cdot n(x)>0$, $n(x)$ inward-pointing normal.

Once the particle started, it moves with uniform linear motion until it hits a scatterers or the elastic boundary $\partial\Omega_E$. We pick t_h, the time until the hit with a scatterers, following the exponential law of mean t_m, with t_m a fixed parameter. The particle travels with velocity v for a time t_h. If during this time it hits the elastic boundary $\partial\Omega_E$, its velocity changes performing an elastic collision. At time t_h we simulate an hit with a scatterers by picking an impact parameter δ uniformly in $[-1,1]$ and changing the velocity from v to $v'=v-2(v\cdot n)n$, where $\delta=\sin\alpha$ and $n=n(\delta)$ is the outward pointing normal to the scatterers such that the angle of incidence between n and v is α (see Figure 1.2).

We proceed as before by letting the particle move until it leaves Ω by reaching again the open boundary $\partial\Omega_L\cup\partial\Omega_R$. Then the particle exits from the system and we are ready to simulate another particle. We simulate a number N of particles.

The random number generator we use in our simulation is the Mersenne Twister [43, 44].

We want to construct the stationary solution of equation (1.1)-(1.3). Note that we can simulate particles one by one since in the considered model particles are not interacting. Moreover, being the stationary state not dependent on the initial datum f_0, we consider in this algorithm only particles starting from the reservoirs. We assume that in the stationary state the density of particles in a region is proportional to the total time spent by all particles in that region. Moreover, due to isotropy, there is no preferential direction for the velocity, so the stationary g_ε^S is not dependent on v.

We divide the space Ω in equal small square cells. For every particle we calculate the time that it spends in every cell. Then we calculate the total time that particles spend in each cell. For t_m going to zero and N very big, in every infinitesimal region of Ω the stationary density has to be proportional to the total time spent by particles

in that region. Considering sufficiently small cells, for t_m small enough and a number of particles simulated N big enough, the total time spent in the cell we calculate is proportional to our numerical stationary solution.

We construct with our algorithm a grid of sojourn times in the cells. The last step we have to do is to normalize it. It is sufficient to multiply by a constant, obtained by imposing the correct value of g_ε^S in a point (e.g., the boundary datum). We call our numerical solution $h_{t_m}(x)$. So we fix a cell in contact with the reservoir where we calculated a sojourn time t_c and consider the value f_B of the stationary solution. We choose as multiplication constant $c = f_B(x)/t_c$. So the simulated solution $h_{t_m}(x)$ is constructed by multiplying the sojourn time in each cell for this constant c.

In the sequel we will show that for t_m sufficiently small and N big enough, the simulated solution $h_{t_m}(x)$ well approximates the solution $\rho(x)$ of the associated Laplace problem.

All the simulations we are going to discuss in this Section are performed with $N = 5 \cdot 10^7$ particles.

Let us preliminary consider the case of $\Omega = (0,4) \times (0,1)$ in absence of obstacles. We fix mass densities at the reservoirs $\rho_L = 1$ and $\rho_R = 0.5$. In this first case there is no dependence on the vertical coordinate in the solution of the Laplace problem (1.6). Indeed we know that the problem has analytic solution $\rho(x_1, x_2) = 1 - x_1/8$, where we are denoting by $(x_1, x_2) \in \mathbb{R} \times \mathbb{R}$ the spatial coordinates x in Ω. We divide the domain in 200×50 equal square cells and we consider simulations with different values of t_m, to understand which values of the mean time t_m provide a good approximation of the solution we are looking for.

In Figures 2.3 and 2.4 we show that the choice of t_m of the order of 10^{-2} is suitable for our purpose. Indeed in Figures 2.3 we compare the simulated solution h_{t_m} with the analytic solution for the values $t_m = 2 \cdot 10^{-1}$, $t_m = 10^{-1}$, $t_m = 2 \cdot 10^{-2}$. We see in a $3D$ plot and in a $2D$ plot, obtained from the previous one by averaging on the x_2 variable, that h_{t_m} becomes closer to $\rho(x_1)$ when t_m decreases. So in Figures 2.4 we fix the parameter $t_m = 10^{-2}$ and we verify that h_{t_m} is close to the function $\rho(x_1)$ showing the relative error $|h_{t_m} - \rho|/\rho$.

We consider now the more interesting case with presence of obstacles in the strip. Our domain Ω is the strip $(0,4) \times (0,1)$ minus the obstacles. We fix again mass densities at the reservoirs $\rho_L = 1$ and $\rho_R = 0.5$. We fix again $t_m = 10^{-2}$, since we have shown that in the empty case this choice for the exponential clock allows to construct a numerical solution h_{t_m} that is close to the analytical solution $\rho(x_1, x_2)$ of the associated Laplace problem (1.6). We propose different situations for the domain Ω and we show in Figures 2.5 - 2.7 that in each case the simulation algorithm works correctly. We

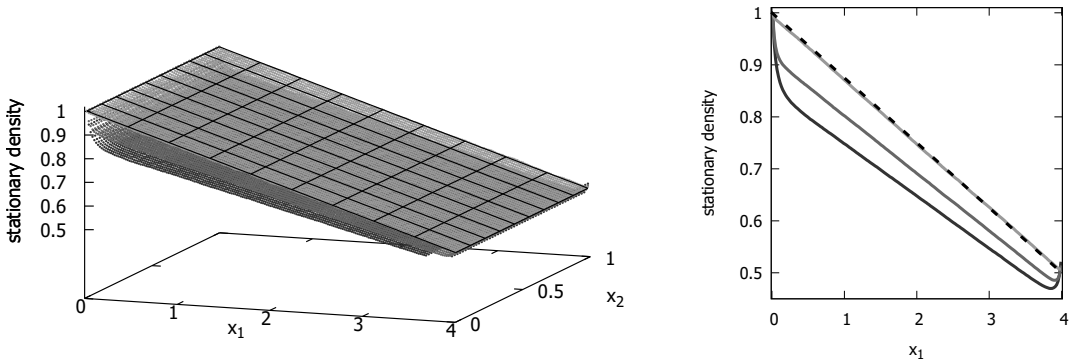

Figure 2.3: Plot of the simulated solutions h_{t_m} in a $3D$ plot and in a $2D$ plot constructed by averaging on the x_2 variable: in dark gray $t_m = 2 \cdot 10^{-1}$, in gray $t_m = 10^{-1}$, in light gray $t_m = 2 \cdot 10^{-2}$. In black (grid and dashed line) the analytic solution ρ of the associated Laplace problem.

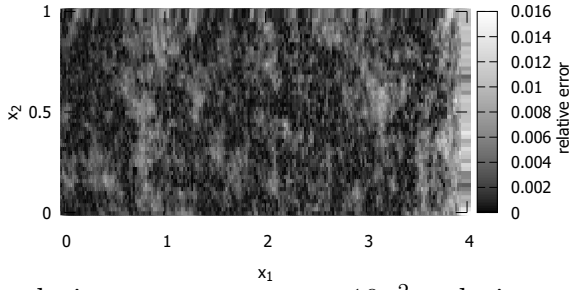

Figure 2.4: Simulation parameter $t_m = 10^{-2}$: relative error $|h_{t_m} - \rho|/\rho$.

compare our numerical solution with the solution $\rho(x_1, x_2)$ of the associated Laplace problem (1.6). We show the plots of the h_{t_m} and ρ and the map of the relative error $|h_{t_m} - \rho|/\rho$ as in Figure 2.4 .

The first case we consider is the presence of a big squared obstacle with side $8 \cdot 10^{-1}$, in different positions into the strip. In Figure 2.5 the results on two different positions are presented.

Another interesting case is the presence of a very thin and tall obstacle placed vertically inside the strip. We show it in Figure 2.6, by picking a thin obstacle of height of $8 \cdot 10^{-1}$.

The last case we want to present is the presence in the strip of two obstacles. In Figure 2.7 we consider two different situations: in the first we set in the strip two squared obstacles with sides $6 \cdot 10^{-1}$ long, in the second we place into the strip two rectangular obstacles of sides $4 \cdot 10^{-1}$ and $7 \cdot 10^{-1}$.

Note that due to the presence of obstacles the solutions are not independent of

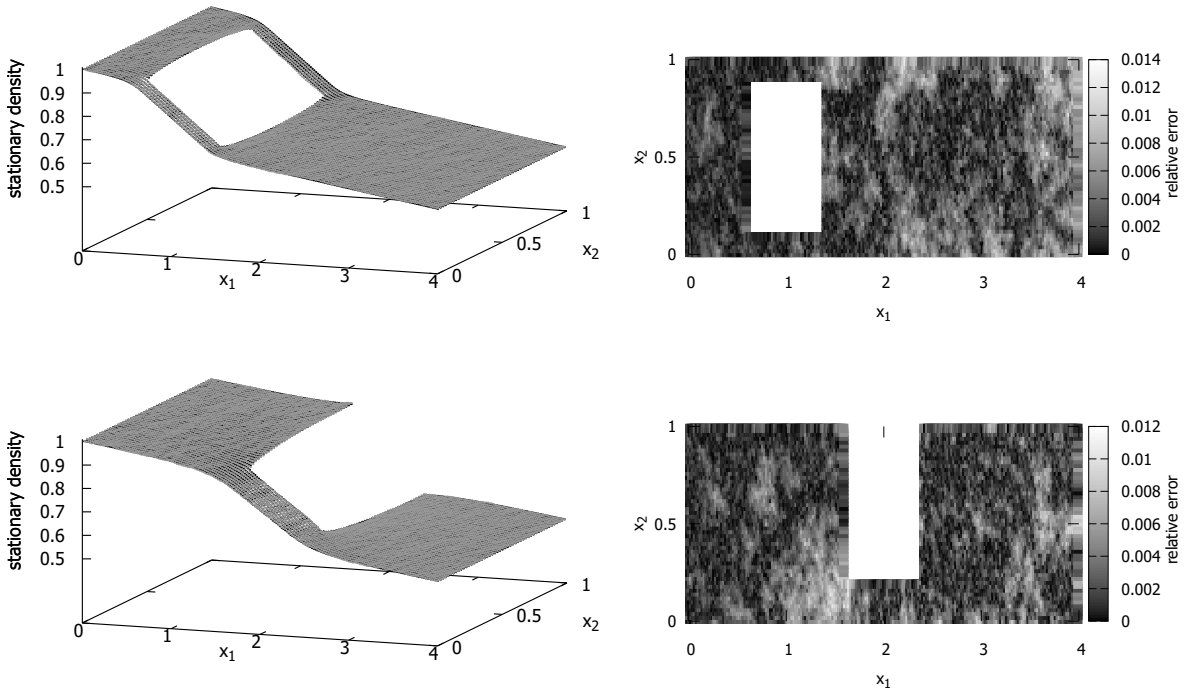

Figure 2.5: Simulation parameter $t_m = 10^{-2}$: on the left in gray the numerical solution h_{t_m} and in black the solution ρ of the associated Laplace problem; on the right the relative error $|h_{t_m} - \rho|/\rho$. Into the strip there is a square obstacle with side $8 \cdot 10^{-1}$.

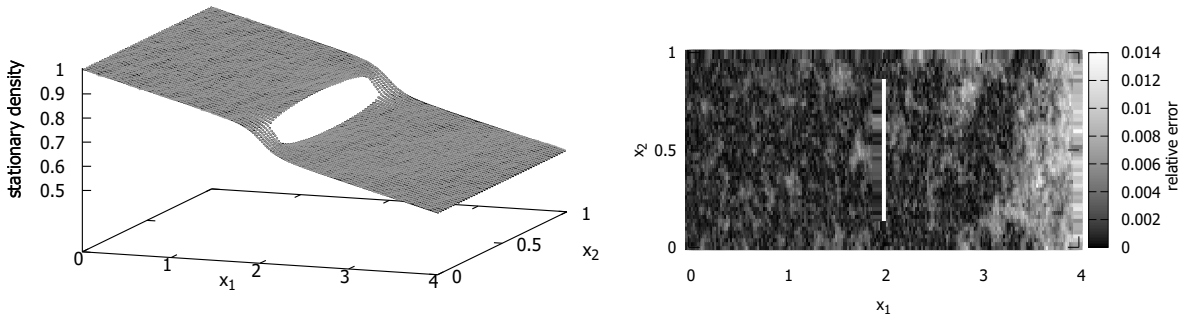

Figure 2.6: Simulation parameter $t_m = 10^{-2}$: on the left in gray the numerical solution h_{t_m} and in black the solution ρ of the associated Laplace problem; on the right the relative error $|h_{t_m} - \rho|/\rho$. In the strip is placed a very thin obstacle with height of 0.8.

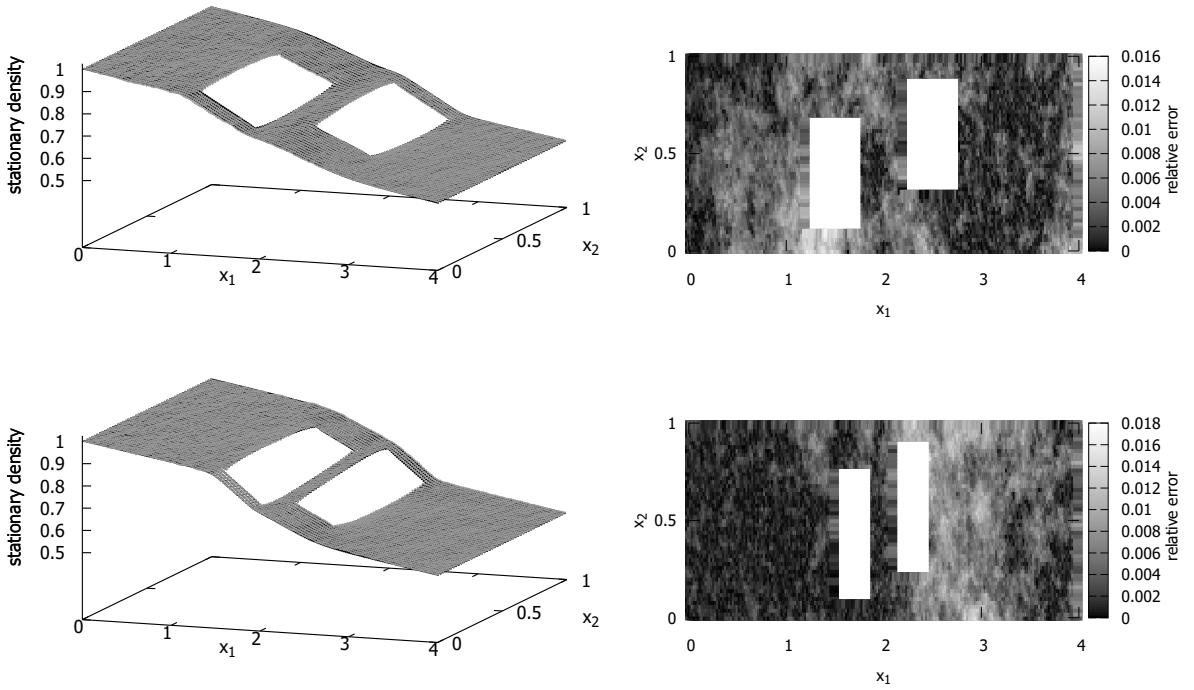

Figure 2.7: Simulation parameter $t_m = 10^{-2}$: on the left in gray the numerical solution h_{t_m} and in black the solution ρ of the associated Laplace problem; on the right the relative error $|h_{t_m} - \rho|/\rho$. In the first line we show the case of two squared obstacles with side $6 \cdot 10^{-1}$, in the second one a couple of rectangular obstacles, taller and thinner than the squares.

the vertical coordinate x_2 anymore as it was in the empty strip case. However, we can notice that before and beyond the obstacles in the x_1 direction the stationary states are closer to a flat state than in the empty case, with a steeper slope in the tight channels at sides of the obstacles. The total stationary mass flux through any vertical line $\{x_1\} \times (0,1) \cap \Omega$ does not depend on x_1. Indeed, this should follow from the Fick's law, that we expect to be valid also in presence of obstacles (in absence of obstacle, being the limiting problem one–dimensional, the Fick's law holds as shown in [6]), together with the divergence theorem and the fact that the boundary conditions are homogeneous on $\partial\Omega_E$. The Fick's law would tell us that, in presence of obstacles, the total flux on the lines $\{x_1 = a\} \cap \Omega$ is smaller than in the empty case, as it is possible to see focusing on the vertical lines before the obstacles. In this sense, and opposite to what happen in the case of the study of the residence time, we find on the flux the intuitive result we expected.

1.3 Residence time

We consider the domain $(0, L_1) \times (0, L_2)$ with the same boundary conditions as in Section 1.1, namely, reflecting horizontal boundaries and open vertical boundaries. As before Ω denotes a subset of this domain obtained by placing large fixed reflecting obstacles. Particles in Ω move according to the Markov process solving the linear Boltzmann equation and described in detail in Section 1.2.

In Section 1.2 we investigated the stationary state of the system and we demonstrated that, provided the mean flight time t_m is sufficiently small, the stationary state is very well approximated by the solution of the Laplace problem (1.6) even in presence of obstacles. We have also noted that, due to the presence of obstacles, the total flux crossing the strip is smaller with respect to the one measured in absence of obstacles. This implies that if we consider a fixed number of particles entering the strip throught the left boundary, the number of them exiting through the right boundary decreses when an obstacle is inserted. In our simulations we remark that the ratio between the number of particles exiting through the left boundary in presence of an obstacle and in the empty strip case does not depend very much on the geometry of the obstacle and, in the worst case we considered, it is approximatively equal to $1/5$. Detailed data for the different cases we studied are reported in the figure captions of this section.

In this section, on the other hand, we focus on those particles that do the entire trip, that is to say they enter through the left boundary and eventually exit the strip through the right one. Limiting our numerical computation to these particles, we measure the average time needed to cross the strip, also called the residence time and discuss its dependence on the size and on the position of a large fixed obstacle placed in the strip. The surprising result is that the residence time is not monotonic with respect to the obstacle parameters, such as position and size. More precisely, we show that obstacles can increase or decrease the residence time with respect to the empty strip case depending on their side lengths and on their position. Moreover, in some cases, by varying only one of these parameters a transition from the increasing effect to the decreasing effect is observed.

In some cases we observe that the residence time measured in presence of an obstacle is smaller than the one measured for the empty strip. In other words, we find that the obstacle is able to select those particles that cross the strip in a smaller time. More precisely, particles that succeed to cross the strip do it faster than they would in absence of obstacles.

We now discuss the different cases we considered. All numerical details are in

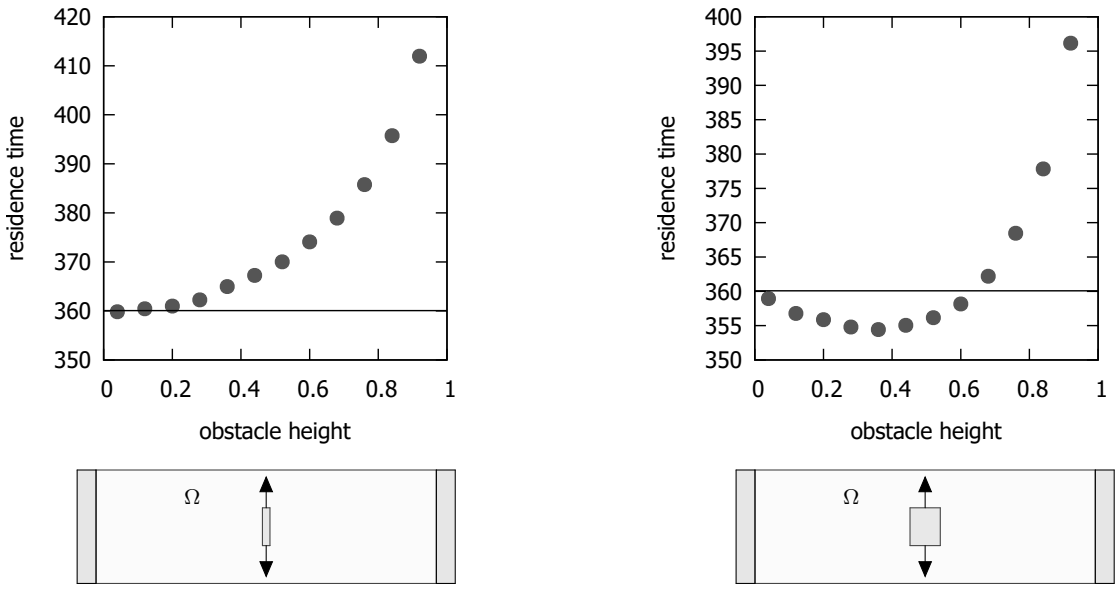

Figure 3.8: Residence time vs. height of a centered rectangular obstacle with fixed width $4 \cdot 10^{-2}$ (on the left) and $4 \cdot 10^{-1}$ (on the right). Simulation parameters: $L_1 = 4$, $L_2 = 1$, $t_m = 2 \cdot 10^{-2}$, total number of inserted particles 10^8, the total number of particles exiting through the right boundary varies from $5.3 \cdot 10^5$ to $3.6 \cdot 10^5$ (on the left) and from $5.3 \cdot 10^5$ to $2.1 \cdot 10^5$ (on the right) depending on the obstacle height. The solid lines represent the value of the residence time measured for the empty strip (no obstacle).

the figure captions. The statistical error is not represented in the pictures since it is negligible and it could not be appreciated in the graphs. In each figure we draw a graph reporting the numerical data and a schematic picture illustrating the performed experiment. We first describe our result and at the end of this section we propose a possible interpretation.

In Figure 3.8 we report the residence time as a function of the obstacle height. The obstacle is placed at the center of the strip and its width is very small on the left and larger on the right. We notice that in the case of a thin barrier, the residence time increases with the height of the obstacle. On the other hand, for a wider obstacle, we do not find this a priori intuitive result, but we observe a not monotonic dependence of the residence time on the obstacle height. In particular, it is interesting to remark that if the obstacle height is chosen smaller that 0.65 the residence time is smaller than the one measured for the empty strip. This effect is even stronger if the width of the obstacle is increased (Figure 3.9).

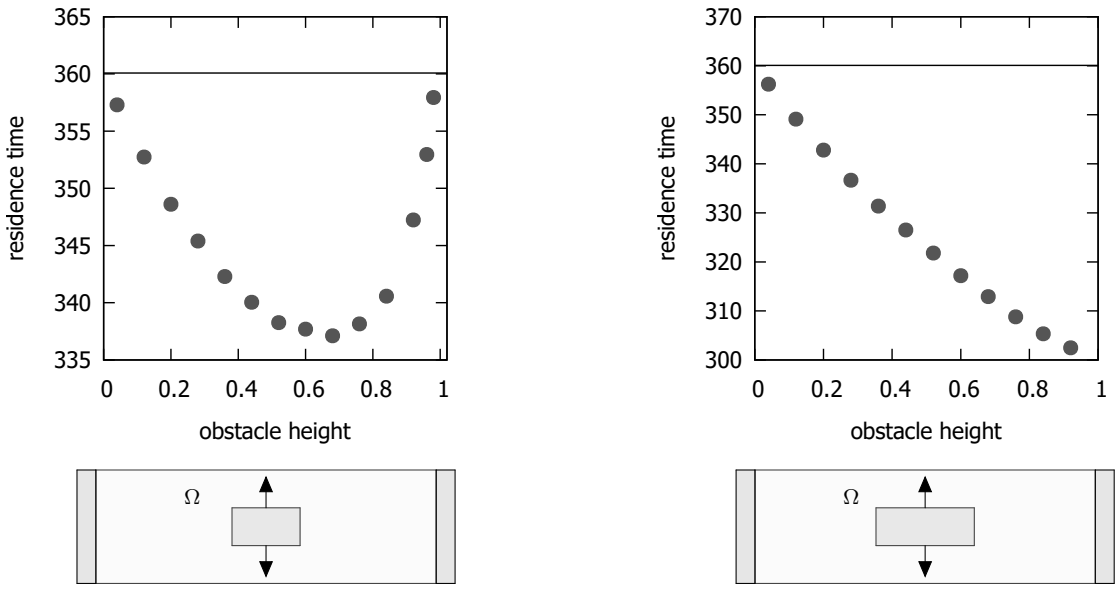

Figure 3.9: Residence time vs. height of a centered rectangular obstacle with fixed width $8 \cdot 10^{-1}$ (on the left) and $12 \cdot 10^{-1}$ (on the right). Simulation parameters: $L_1 = 4$, $L_2 = 1$, $t_m = 2 \cdot 10^{-2}$, total number of inserted particles 10^8, the total number of particles exiting through the right boundary varies from $5.2 \cdot 10^5$ to $1.4 \cdot 10^5$ (on the left) and from $5.2 \cdot 10^5$ to $1.1 \cdot 10^5$ (on the right) depending on the obstacle height. The solid lines represent the value of the residence time measured for the empty strip (no obstacle).

In the left panel of Figure 3.10 we report the residence time as a function of the obstacle width. The obstacle is placed at the center of the strip and its height is fixed to 0.8. When the barrier is thin the residence time is larger than the one measured in the empty strip case. But, when the width is increased, the residence time decreases and at about 0.7 it becomes smaller than the empty case value. The minimum is reached at about 2.3, then the residence time starts to increase and when the width of the obstacles equals that of the strip the residence time becomes equal to the empty strip value. This last fact is rather obvious, indeed, in this case the strip reduces to two independent channels having the same width of the original strip.

In the right panel of Figure 3.10 a centered square obstacle is considered. We note that the residence time happens to be a monotonic decreasing function of the obstacle side length.

In Figure 3.11 we show that, and this is really surprising, the residence time is not monotonic even as a function of the position of the center of the obstacle. In

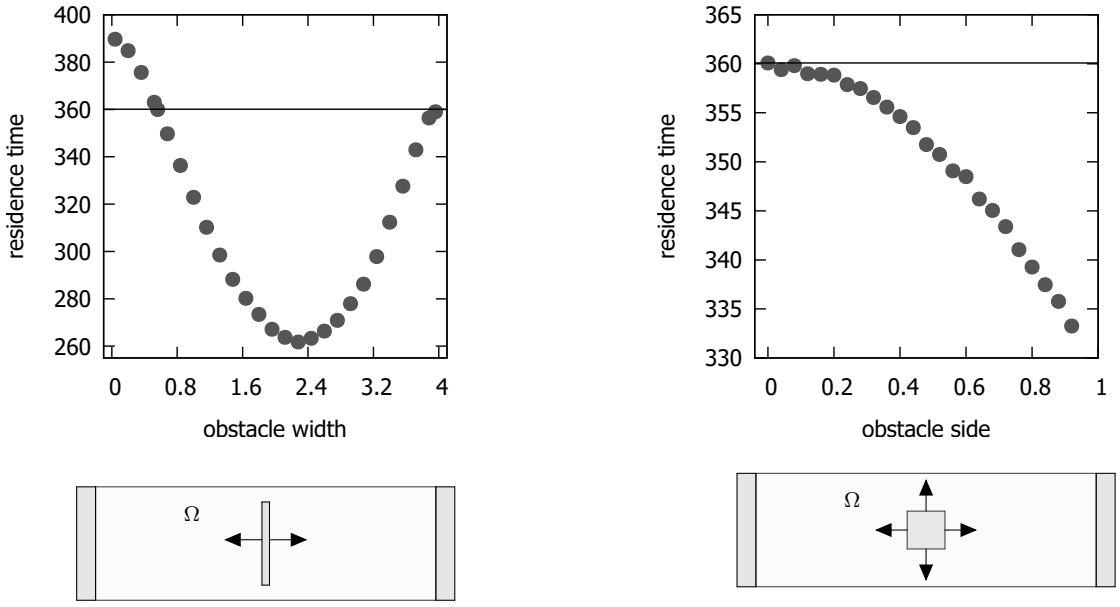

Figure 3.10: Residence time vs. width of a centered rectangular obstacle with fixed height 0.8 (on the left) and vs. the side length of a centered squared obstacle (on the right). Simulation parameters: $L_1 = 4$, $L_2 = 1$, $t_m = 2 \cdot 10^{-2}$, total number of inserted particles 10^8, the total number of particles exiting through the right boundary varies from $4.2 \cdot 10^5$ to $1.1 \cdot 10^5$ (on the left) and from $5.3 \cdot 10^5$ to $1.3 \cdot 10^5$ (on the right) depending on the obstacle width. The solid lines represent the value of the residence time measured for the empty strip (no obstacle).

the left panel a squared obstacle of side length 0.8 is considered, whereas in the right panel a thin rectangular obstacle 0.04×0.8 is placed in the strip. In both cases the residence time is not monotonic and attains its minimum value when the obstacle is placed in the center of the strip. It is worth noting, that in the case on the left when the position of the center lays between 1.5 and 2.5 the residence time in presence of the obstacles is smaller than the corresponding value for the empty strip.

Summarizing, the numerical experiments reported in Figures 3.8–3.11 show that the residence time strongly depends on the obstacle geometry and position. In particular it is seen that large centered obstacles favor the selection of particles crossing the strip faster than in the empty strip case.

A possible interpretation of these results can be given. The strip $(0, L_1) \times (0, L_2)$ is partitioned in the three rectangles L (the part on the left of the obstacles), R (the part on the right of the obstacles), and $C = (0, L_1) \times (0, L_2) \setminus (L \cup R)$. The phenomenon we reported above can be explained as a consequence of two competing effects: the

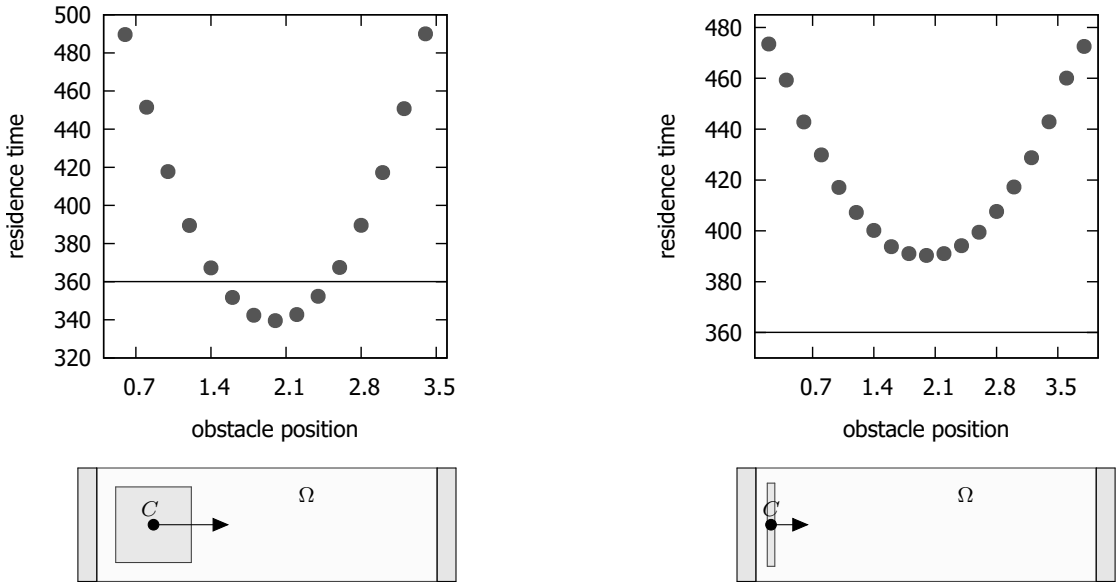

Figure 3.11: Residence time vs. position of the center of the obstacle. The obstacle is a square of side length 0.8 on the left and a rectangle of side lengths 0.04 and 0.8 on the right. Simulation parameters: $L_1 = 4$, $L_2 = 1$, $t_m = 2 \cdot 10^{-2}$, total number of inserted particles 10^8, the total number of particles exiting through the right boundary is stable at the order of $2.6 \cdot 10^5$ (on the left) and of $4 \cdot 10^5$ (on the right) not depending on the obstacle position. The solid lines represent the value of the residence time measured for the empty strip (no obstacle).

total time spent by a particle in the channels between the obstacle and the horizontal boundaries is smaller with respect to the time typically spent in C in the empty strip case because the obstacle makes the channels more difficult to access. So a particle crosses the channels in average less times with respect to the empty strip case (once the particle is in the channel it spends the same time in C in both the empty strip case and the obstacle case since in C the obstacle acts as the horizontal boundary). On the other hand the times spent in L and in R are larger if compared to the times spent there by a particle in the empty strip case, due to the fact that it is more difficult to leave these regions and enter in the channels flanking the obstacle. The increase or the decrease of the residence time compared to the empty strip case depends on which of the two effects dominates the particle dynamics.

In Figure 3.12 we consider the geometry in the right panel of Figure 3.8. We compute the average time spent by particles in small squared cells (0.02×0.02). This local residence time in presence of the obstacle is larger than the one measured in the

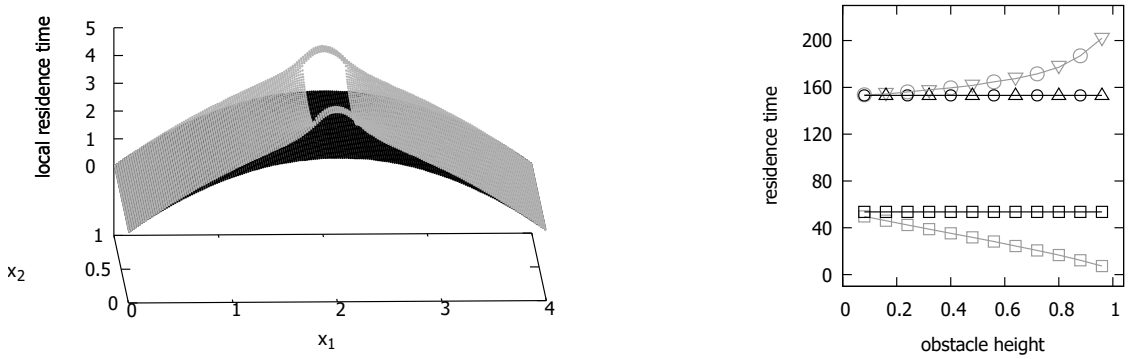

Figure 3.12: As in the right panel in Figure 3.8. In the left panel the height of the obstacle is equal to 0.8. Left panel: the mean time spent by particles crossing the strip in each point of the strip (0.02×0.02 cells have been considered) for the empty strip case (black) and in presence of the obstacle (gray). Right panel: residence time in regions L (circles), C (squares), and R (triangles) in presence of the obstacle (gray) and for the empty strip case (black).

empty strip, indeed the gray surface in the picture is always above the black one. But, if the total residence time spent in the regions L, C, and R is computed, one discovers that the time spent in the region C decreases in presence of the obstacle, whereas the time spent in L and R increases. Note that the local residence time in the cells belonging to the channels in C is larger with respect to the empty strip case, but the total time in C is smaller due to the fact that the available volume in C is decreased by the presence of the obstacle. Hence, the result in the right panel in Figure 3.8 can be explained as follows: if the height of the obstacle is smaller than 0.6 the effect in C dominates the one in L and R so that the total residence time decreases. On the other hand, when the height is larger than 0.6 the increase of the residence time in L and R dominates its decrease in C, so that the total residence time increases.

The Figure 3.13, referring to the geometry in the left panel in Figure 3.10, and the Figure 3.14, referring to the geometry in the left panel in Figure 3.11, can be discussed similarly. We just note that in Figures 3.12 and 3.13 the circles and triangles, which correspond to the residence time in L and R, coincide due to the symmetry of the system. Indeed, in both cases the center of the obstacle is at the center of the strip.

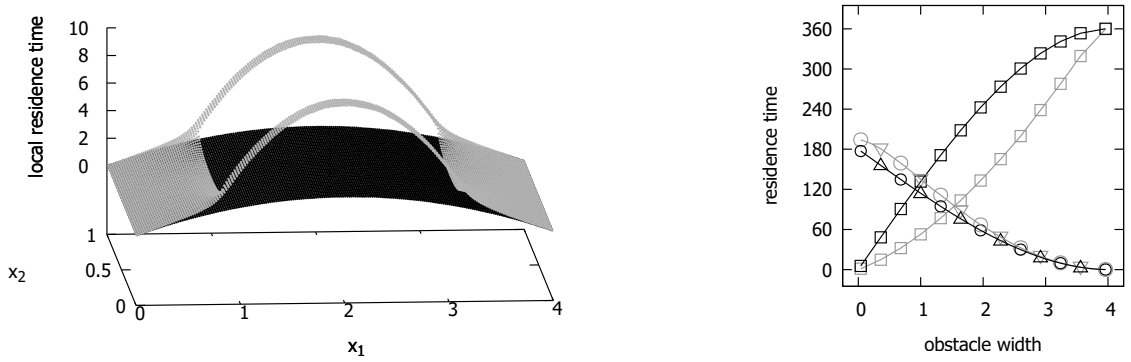

Figure 3.13: As in Figure 3.12 for the geometry in the left panel in Figure 3.10. In the left panel the width of the obstacle is 2.28.

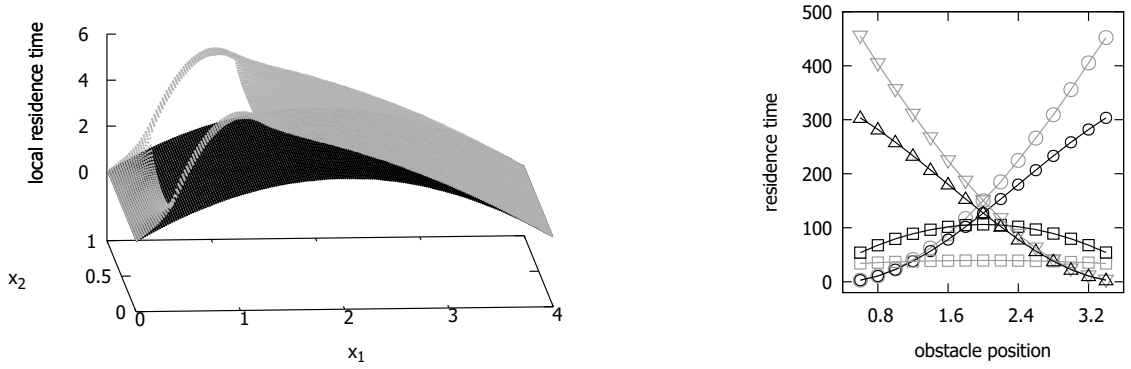

Figure 3.14: As in Figure 3.12 for the geometry in the left panel in Figure 3.11. In the left panel the position of the center of the obstacle is 0.8.

1.4 Proof of results

We prove Theorems 1.1 and 1.2. We firstly construct the solution of the linear Boltzmann problem in form of a Dyson series. Then we are able to prove the existence and uniqueness of the associated stationary problem. To do this we exploit the diffusive limit of the linear Boltzmann equation in a L^∞ setting and in a bigger domain containing Ω, by means of the Hilbert expansion method (see [6, 10, 26]). The stationary solution is constructed in the form of a Neumann series to avoid the exchange of the limits $t \to \infty$, $\varepsilon \to 0$, following the idea of [6]. Eventually we prove the convergence of the stationary state to the solution of the mixed Laplace problem. This also requires the Hilbert expansion method. The auxiliary results stated are proved after the main theorems.

Let us consider the problem (1.1)-(1.3) with the datum $g_\varepsilon(x, v, 0) = f_0(x, v) \in L^\infty(\Omega \times S^1)$. We can express the operator defined in (1.2) as $\mathcal{L}f(v) = 2\lambda(\mathcal{K} - \mathcal{I})f(v)$,

where

$$(\mathcal{K}f)(v) = \frac{1}{2}\int_{-1}^{1} \mathrm{d}\delta\, f(v') \tag{4.8}$$

and $\mathcal{I}$ is the identity. Therefore the equation (1.1) can be written as

$$\partial_t f + (v\cdot\nabla_x + 2\eta_\varepsilon\lambda\mathcal{I})f = 2\eta_\varepsilon\lambda\mathcal{K}f. \tag{4.9}$$

We want to exploit the Duhamel's principle and express the solution as a series expansion. We consider the semigroup generated by $\mathcal{A} = (v\cdot\nabla_x + 2\eta_\varepsilon\lambda\mathcal{I})$. We recall that in the whole plane $\mathbb{R}^2$ this semigroup acts as $e^{-t\mathcal{A}}f(x,v) = e^{-2\lambda\eta_\varepsilon t}f(x - vt, v)$, while the semigroup generated only by the transport term $v\cdot\nabla_x$ would be $e^{-t\,v\cdot\nabla}f(x,v) = f(x-vt,v)$.

We want to consider the semigroup generated by $\mathcal{A}$ on our domain Ω initial datum f_0 and boundary conditions (1.3). Recall that $\partial\Omega_E$ is a specular reflective boundary while on $\partial\Omega_L \cup \partial\Omega_R$ the system is in contact with reservoirs with particle densities $f_B(x,v)$. Since the equation describes the evolution of a particle moving in the space with velocity of modulus one, having random collisions with impact parameter δ, for any sequence of collision times and impact parameters t_i, δ_i we can construct the backward trajectory of a particle as long as it stays in Ω. Indeed the backward trajectory for a particle in (x,v) at time t starts by letting the particle move with velocity $-v$. For a time $t-t_1$ it does not hit any scatterers, but if the particle reaches the elastic boundary $\partial\Omega_E$ during this time, the velocity $-v$ becomes $-v'$ following the elastic collision rule $-v' = -(v - 2(n\cdot v)n)$, where n is the inward pointing normal to Ω. After a time $t-t_1$ the particle performs a collision with impact parameter δ_1 that produces the velocity $-v_1$. Then again the particles travels for a time $t_1 - t_2$ elastically colliding if touching the boundary $\partial\Omega_E$ and so on until it reaches a reservoir or it has traveled for a total time t.

In the same way, given the sequence x, v, t_1, …, t_m, δ_1, …, δ_m, we define the flow $\Phi_m^{-t}(x,v,t_1,\dots,t_m,\delta_1,\dots,\delta_m)$ as the backward trajectory starting from x with velocity v and having m transition in velocity obtained after a time $t-t_1$, …, $t_i - t_{i+1}$, …, t_m $(i = 1,\dots,m-1)$ by a scattering with an hard disk with impact parameter respectively δ_i $(i = 1,\dots,m)$. We impose that the trajectories described by this flow $\Phi^{-t}(x,v)$ make a change of velocity from v to $v' = v - 2(n\cdot v)n$ any time the elastic boundary $\partial\Omega_E$ is reached.

We define the function $\tau = \tau(x,v,t,t_1,\dots,t_m,\delta_1,\dots,\delta_m)$ that represents the time when the particle that is in (x,v) at time t leaves a reservoirs and it enters into the strip. So if the backward trajectory having collision times and parameters

$t_1, \dots, t_m, \delta_1, \dots, \delta_m$ reaches the boundary $\partial\Omega_L \cup \partial\Omega_R$ in the time interval $[0,t]$, then it happens after a backward time $t-\tau$. If the trajectory $\Phi^{-s}(x,v)$ never hits the boundary $\partial\Omega_L \cup \partial\Omega_R$ for any time $s \in [0,t]$ we set $\tau = 0$.

We are now able to write the solution $g_\varepsilon(x,v,t)$ using the Duhamel's principle. The semigroup generated by $\mathcal{A}$ on our domain has a transport term that we can express thanks to the flow $\Phi^{-t}(x,v)$, and the transported datum is f_B or f_0 depending on the case the backward trajectory touches a reservoir in the time interval $[0,t]$ on not. We use the function τ to distinguish these two cases. We consider the collision operator $2\lambda\eta_\varepsilon\mathcal{K}$ as the source term for the linear problem (4.9). So we construct the following expression for g_ε

(4.10)
$$\begin{aligned} g_\varepsilon(x,v,t) =& e^{-2\lambda\eta_\varepsilon t} f_0(\Phi_0^{-t}(x,v))\chi(\tau=0) + e^{-2\lambda\eta_\varepsilon(t-\tau)} f_B(\Phi_0^{-(t-\tau)}(x,v))\chi(\tau>0) + \\ &+ \lambda\eta_\varepsilon \int_0^t e^{-2\lambda\eta_\varepsilon(t-t_1)} 2\mathcal{K} g_\varepsilon(\Phi_0^{-(t-t_1)}(x,v),t_1)\chi(\tau<t_1)\,\mathrm{d}t_1. \end{aligned}$$

The notation χ represents the characteristic function.

The meaning of (4.10) is clear: we separate the contribution given to g_ε from trajectories transporting the initial datum f_0, having no collisions with scatterers and never hitting a reservoirs in the time interval $[0,t]$; the contribution from trajectories transporting the initial datum f_B exiting from a reservoirs at time τ and than moving in Ω until the time t without colliding any scatterers; finally the last term is the contribution due to trajectories having the last collision with a scatterers at time t_1 and never touching the reservoirs in the time interval $[t_1,t]$.

We iterate the procedure by using (4.10) again for the g_ε in the last integral and from (4.8) we find:

(4.11)
$$\begin{aligned} g_\varepsilon(x,v,t) =& e^{-2\lambda\eta_\varepsilon t} f_0(\Phi_0^{-t}(x,v))\chi(\tau=0) + e^{-2\lambda\eta_\varepsilon(t-\tau)} f_B(\Phi_0^{-(t-\tau)}(x,v))\chi(\tau>0) \\ &+ \lambda\eta_\varepsilon \int_0^t \mathrm{d}t_1 e^{-2\lambda\eta_\varepsilon(t-t_1)} \int_{-1}^1 \mathrm{d}\delta_1 \Big[e^{-2\lambda\eta_\varepsilon t_1} f_0(\Phi_1^{-t}(x,v,t_1,\delta_1))\chi(\tau=0) \\ &+ e^{-2\lambda\eta_\varepsilon(t_1-\tau)} f_B(\Phi_1^{-(t-\tau)}(x,v,t_1,\delta_1))\chi(\tau>0)\chi(\tau<t_1) \\ &+ \lambda\eta_\varepsilon \int_0^{t_1} \mathrm{d}t_2\, e^{-2\lambda\eta_\varepsilon(t_1-t_2)} \int_{-1}^1 \mathrm{d}\delta_2 g_\varepsilon(\Phi_1^{-(t-t_2)}(x,v,t_1,\delta_1),t_2)\chi(\tau<t_2) \Big]. \end{aligned}$$

By successive iterations we write the series expansion for the density of particles

$g_\varepsilon(x,v,t)$ as

(4.12)

$$g_\varepsilon(x,v,t) = e^{-2\lambda\eta_\varepsilon t} f_0(\Phi_0^{-t}(x,v))\chi(\tau=0) + \sum_{m\geq 1} e^{-2\lambda\eta_\varepsilon t}(\lambda\eta_\varepsilon)^m \int_0^t \mathrm{d}t_1 \dots \int_0^{t_{m-1}} \mathrm{d}t_m$$
$$\int_{-1}^1 \mathrm{d}\delta_1 \dots \int_{-1}^1 \mathrm{d}\delta_m \chi(\tau=0) f_0(\Phi_m^{-t}(x,v,t_1,\dots,t_m,\delta_1,\dots,\delta_m))$$
$$+ e^{-2\lambda\eta_\varepsilon(t-\tau)} f_B(\Phi_0^{-(t-\tau)}(x,v))\chi(\tau>0) + \sum_{m\geq 1}(\lambda\eta_\varepsilon)^m \int_0^t \mathrm{d}t_1 \dots \int_0^{t_{m-1}} \mathrm{d}t_m \int_{-1}^1 \mathrm{d}\delta_1 \dots$$
$$\int_{-1}^1 \mathrm{d}\delta_m \chi(\tau<t_m)\chi(\tau>0) e^{-2\lambda\eta_\varepsilon(t-\tau)} f_B(\Phi_m^{-(t-\tau)}(x,v,t_1,\dots,t_m,\delta_1,\dots,\delta_m)) =$$
$$= g_\varepsilon^{in}(x,v,t) + g_\varepsilon^{out}(x,v,t).$$

Note that the series are clearly convergent in $L^{+\infty}$.

In (4.12) the terms with $\chi(\tau=0)$ define g_ε^{in} that represents the contributions to g_ε due to trajectories that stay in Ω for every time in $[0,t]$ while the terms with $\chi(\tau>0)$ define g_ε^{out} that collects the contributions due to trajectories leaving a mass reservoir at time $\tau>0$.

Note that g_ε^{out} solves the problem (1.1)-(1.3) with initial datum $f_0=0$.
We will use the shorthand notation $\Phi^{-s}(x,v)$ instead of $\Phi_m^{-s}(x,v,t_1,\dots,t_m,\delta_1,\dots,\delta_m)$ where it is clear by the context to which sequence of collisions we refer. Moreover, the terms with zero collision will be included in the series as the $m=0$ terms.

We denote by S_ε acting on any $h\in L^\infty(\Omega\times S^1)$ the Markov semigroup associated to the g_ε^{in} term in (4.12) for an initial datum h, namely

(4.13)

$$(S_\varepsilon(t)h)(x,v) = \sum_{m\geq 0} e^{-2\lambda\eta_\varepsilon t}(\lambda\eta_\varepsilon)^m \int_0^t \mathrm{d}t_1 \dots \int_0^{t_{m-1}} \mathrm{d}t_m \int_{-1}^1 \mathrm{d}\delta_1 \dots \int_{-1}^1 \mathrm{d}\delta_m \chi(\tau=0) h(\Phi^{-t}(x,v)),$$

so that in (4.12) $g_\varepsilon^{in}(t) = S_\varepsilon(t) f_0$.

Proposition 4.1. *There exists $\varepsilon_0>0$ such that for any $\varepsilon<\varepsilon_0$ and for any $h\in L^\infty(\Omega\times S^1)$ it holds*

$$\|S_\varepsilon(\eta_\varepsilon)h\|_\infty \leq \alpha\|h\|_\infty, \qquad \alpha<1. \tag{4.14}$$

Note that in the estimate (4.14) we are considering $t=\eta_\varepsilon$ and the estimate is saying that there is a strictly positive probability for a backward trajectory to exit from Ω in a time of the order of η_ε.

Proof of Theorem 1.1. From (4.12) the stationary solution g_ε^S of the problem (1.5) verifies

$$g_\varepsilon^S = g_\varepsilon^{out}(t_0) + S_\varepsilon(t_0) g_\varepsilon^S,$$

for every $t_0 > 0$. We can formally write it by iterating the previous one in the form of the Neumann series

$$g_\varepsilon^S = \sum_{N\geq 0} (S_\varepsilon(t_0))^N g_\varepsilon^{out}(t_0). \tag{4.15}$$

In order to verify the existence and uniqueness of g_ε^S we show that the (4.15) converges. Indeed from Proposition 4.1 and (4.15), chosen $t_0 = \eta_\varepsilon$

$$\|g_\varepsilon^S\|_\infty \leq \sum_{N\geq 0} \|(S_\varepsilon(\eta_\varepsilon))^N g_\varepsilon^{out}\|_\infty \leq \sum_{N>0} \alpha^N \|g_\varepsilon^{out}(\eta_\varepsilon)\|_\infty \leq \frac{1}{1-\alpha}\|g_\varepsilon^{out}\|_\infty \leq \frac{\max\{\rho_L, \rho_R\}}{1-\alpha}.$$

As a consequence the Neumann series (4.15) converges in L^∞ and identifies a single element in L^∞. Choosing an arbitrary t_0 bigger than η_ε of the same order of η_ε and thanks to the semigroup property of S_ε it follows that g_ε^S does not depend on the time t_0. So there exists a unique stationary solution $g_\varepsilon^S \in L^\infty(\Omega \times S^1)$ satisfying (1.5). □

In order to prove Theorem 1.2 we need some properties of the linear Boltzmann operator $\mathcal{L}$ defined in (1.2). We summarize them in the next lemma.

Lemma 4.1. *Let $\mathcal{L}$ be the operator defined in (1.2), then $\mathcal{L}$ is a selfadjoint operator on $L^2(S^1)$ and has the form $\mathcal{L} = 2\lambda(\mathcal{K} - \mathcal{I})$ where $\mathcal{K}$ is a selfadjoint and compact operator (in $L^2(S^1)$). Moreover, $\mathcal{K}$ is positive and its spectrum is contained in $[0, 1]$. The value 0 is the only accumulation point for the spectrum and 1 is a simple eigenvalue. So it holds that $\{\mathrm{Ker}\mathcal{L}\}^\perp = \{h \in L^2(S^1) : \int_{S^1} \mathrm{d}v\ h(v) = 0\}$ and there exists $C > 0$ such that for any $h \in L^\infty(S^1)$ that verifies $\int_{S^1} \mathrm{d}v\ h(v) = 0$ we have*

$$\|\mathcal{L}^{-1} h\|_\infty \leq C\|h\|_\infty. \tag{4.16}$$

Proof of Lemma 4.1. The existence and the estimate of norm of $\mathcal{L}^{-1}$ are discussed in Lemma 4.1 from Section 4.1 of [6]. The compactness of the operator $\mathcal{K}$ and the spectral property of $\mathcal{L}$ are discussed in [26]. □

Proof of Theorem 1.2. The proof makes use of the Hilbert expansion (see e.g. [6, 10, 26]). Assume that g_ε^S has the following form

$$g_\varepsilon^S(x, v) = g^{(0)}(x) + \sum_{k=1}^{+\infty} \left(\frac{1}{\eta_\varepsilon}\right)^k g^{(k)}(x, v),$$

where $g^{(k)}$ are not depending on η_ε. We require $g^{(0)}$ to satisfy the same Dirichlet boundary conditions as the whole solution g_ε^S on $\partial\Omega_L \cup \partial\Omega_R$:

$$\begin{cases} g^{(0)}(x) = \rho_L & x \in \partial\Omega_L \\ g^{(0)}(x) = \rho_R & x \in \partial\Omega_R. \end{cases} \tag{4.17}$$

By imposing that g_ε^S solves (1.5) and by comparing terms of the same order we get the following chain of equations:

$$v \cdot \nabla_x g^{(k)} = \mathcal{L} g^{(k+1)}, \qquad k \geq 0,$$

where we used that $\mathcal{L}g^{(0)}(x) = 0$ since $g^{(0)}$ is independent of v. The first two equations read

(i) $v \cdot \nabla_x g^{(0)}(x) = \mathcal{L} g^{(1)}(x, v)$,

(ii) $v \cdot \nabla_x g^{(1)}(x, v) = \mathcal{L} g^{(2)}(x, v)$.

Let us consider the first one. By the Fredholm alternative, this equation has a solution if and only if the left hand side belongs to $(\mathrm{Ker}\mathcal{L})^\perp$. We recall that the null space of $\mathcal{L}$ is constituted by the constant functions (with respect to v), so we can solve equation (i) if and only if the left hand side belongs to $(\mathrm{Ker}\mathcal{L})^\perp = \{h \in L^2(S^1)$ such that $\int_{S^1} \mathrm{d}v\, h(v) = 0\}$ (see Lemma 4.1). Since $v \cdot \nabla_x g^{(0)}(x)$ is an odd function of v, it belongs to $(\mathrm{Ker}\mathcal{L})^\perp$. So we can invert the operator $\mathcal{L}$ and set

$$g^{(1)}(x, v) = \mathcal{L}^{-1}(v \cdot \nabla_x g^{(0)}(x)) + \zeta^{(1)}(x), \tag{4.18}$$

where $\zeta^{(1)}(x) \in \mathrm{Ker}\,\mathcal{L}$ and $\mathcal{L}^{-1}(v \cdot \nabla_x g^0)$ is an odd function of v since $\mathcal{L}^{-1}$ preserves the parity, namely it maps odd (even) function of v in odd (even) functions (see [26]).

We integrate equation (ii) with respect to the uniform measure on S^1. We can notice that $\int_{S^1} \mathrm{d}v\, v \cdot \nabla_x \zeta^{(1)}(x) = 0$ ($\zeta^{(1)}$ depends only on x, so the function in the integral is odd in the velocity) and $\int_{S^1} \mathrm{d}v\, \mathcal{L}g^{(2)} = 0$ (since operator $\mathcal{L}$ preserves mass), so by (4.18) we obtain

$$\frac{1}{2\pi}\left(\int_{S^1} \mathrm{d}v\; v \cdot \nabla_x (\mathcal{L}^{-1}(v \cdot \nabla_x g^{(0)}(x))) \right) = 0. \tag{4.19}$$

By expanding the scalar product and using the linearity of $\mathcal{L}^{-1}$ we get

$$-\sum_{i,j=1}^{2} D_{i,j} \partial_{x_i} \partial_{x_j} g^{(0)}(x) = 0. \tag{4.20}$$

We define the 2×2 matrix $D_{i,j} = \frac{1}{2\pi} \int_{S^1} \mathrm{d}v\, v_i(-\mathcal{L}^{-1})v_j$ and we observe that $D_{ij} = 0$ if $i \neq j$ as follows by the change $v_i \to -v_i$ while $D_{11} = D_{22} = D > 0$ thanks to the isotropy and the spectral property of the operator (see [26]). Hence D is given by the formula (4.33)

$$D = \frac{1}{4\pi} \int_{S^1} \mathrm{d}v\; v \cdot (-\mathcal{L})^{-1} v,$$

and the integrated equation (ii) becomes

$$\frac{1}{2\pi} \left(\int_{S^1} \mathrm{d}v\; v \cdot \nabla_x (\mathcal{L}^{-1}(v \cdot \nabla_x g^{(0)}(x))) \right) = 0 \Leftrightarrow -D\Delta_x g^{(0)}(x) = 0. \tag{4.21}$$

We require $g^S_\varepsilon(x,v)$ to satisfy the reflective boundary condition $g^S_\varepsilon(x,v') = g^S_\varepsilon(x,v)$ on $\partial\Omega_E$. By imposing it on the first term $g^{(1)}(x,v) = g^{(1)}(x,v')$ for every $x \in \partial\Omega_E$, $v \cdot n < 0$, from (4.18) we obtain

$$\mathcal{L}^{(-1)}(v \cdot \nabla_x g^{(0)}) + \zeta^{(1)}(x) = \mathcal{L}^{(-1)}(v' \cdot \nabla_x g^{(0)}) + \zeta^{(1)}(x). \tag{4.22}$$

By means of the elastic collision rule $v' = v - 2(v \cdot n)n$, the linearity of $\mathcal{L}^{-1}$ allow us to write

$$\mathcal{L}^{(-1)}((v - 2(v \cdot n)n) \cdot \nabla_x g^{(0)}) = \mathcal{L}^{(-1)}(v \cdot \nabla_x g^{(0)}) - 2(n \cdot \nabla_x g^{(0)})\mathcal{L}^{(-1)}(v \cdot n).$$

Left and right members in (4.22) are the same if and only if $(n \cdot \nabla_x g^{(0)})\mathcal{L}^{(-1)}(v \cdot n) = 0$. Since $\int_{S^1} \mathrm{d}v\, v \cdot n = 0$ we get $\mathcal{L}^{(-1)}(v \cdot n) \neq 0$, so the only possibility is $(n \cdot \nabla_x g^{(0)}) = 0$. Therefore $g^{(0)}(x)$ has to satisfy the Neumann boundary conditions $\partial_n g^{(0)}(x) = 0$, for all $x \in \partial\Omega_E$.

From the previous one, (4.21) and (4.17) we have shown that the term $g^{(0)}(x)$ solves the problem

$$\begin{cases} \Delta_x g^{(0)}(x) = 0 & x \in \Omega \\ g^{(0)}(x) = \rho_L & x \in \partial\Omega_L \\ g^{(0)}(x) = \rho_R & x \in \partial\Omega_R \\ \partial_n g^{(0)}(x) = 0 & x \in \partial\Omega_E. \end{cases} \tag{4.23}$$

We can deal with this mixed problem following the method of [41], Chapt. II. Furthermore, regularity results guarantee $g^0 \in C^\infty(\overline{\Omega})$ (see [27], Chapt. 6).

Since (4.19) shows that $\int_{S^1} \mathrm{d}v\; v \cdot \nabla_x g^{(1)} = 0$, we can invert $\mathcal{L}$ in equation (ii) to obtain

$$g^{(2)}(x,v) = \mathcal{L}^{-1}(v \cdot \nabla_x \mathcal{L}^{-1}(v \cdot \nabla_x g^{(0)}(x))) + \mathcal{L}^{-1}(v \cdot \nabla_x \zeta^{(1)}(x)) + \zeta^{(2)}(x), \tag{4.24}$$

where $\zeta^{(2)}$ belongs to the kernel of $\mathcal{L}$.

Now, integrating the third equation $v \cdot \nabla_x g^{(2)}(x) = \mathcal{L} g^{(3)}(x, v)$ with respect to the uniform measure on S^1, we find thanks to (4.24)

$$\begin{aligned} &\int_{S^1} \mathrm{d}v \; v \cdot \nabla_x (\mathcal{L}^{-1}(v \cdot \nabla_x \mathcal{L}^{-1}(v \cdot \nabla_x g^{(0)}(x)))) + \\ &+ \int_{S^1} \mathrm{d}v \; v \cdot \nabla_x (\mathcal{L}^{-1}(v \cdot \nabla_x \zeta^{(1)}(x))) + \int_{S^1} \mathrm{d}v \; v \cdot \nabla_x (\zeta^{(2)}(x)) = 0. \end{aligned} \tag{4.25}$$

The last integral is null because of the independence of $\zeta^{(2)}(x)$ from v. The first integral is null because the function in the integral is an odd function of the velocity thanks to the fact that the operator $\mathcal{L}^{-1}$ preserves the parity. The (4.25) becomes

$$\int_{S^1} \mathrm{d}v \; v \cdot \nabla_x (\mathcal{L}^{-1}(v \cdot \nabla_x \zeta^{(1)}(x))) = -D \Delta_x \zeta^{(1)}(x) = 0 \tag{4.26}$$

Since there are no restriction on the choice of the boundary condition, we impose the Dirichlet data $\zeta^{(1)}(x) = 0$ on the boundary $\partial\Omega_L \cup \partial\Omega_R$. So that by the previous and (4.26) we find $\zeta^{(1)}(x) \equiv 0$ and hence $g^{(1)}(x, v) = \mathcal{L}^{-1}(v \cdot \nabla_x g^{(0)}(x))$.

Because of the (4.21) the first term of the right hand side of equation (4.24) is null too. So (4.24) reduces to $g^{(2)}(x, v) = \zeta^{(2)}(x)$.

Moreover from the third equation we get, by inverting $\mathcal{L}$,

$$g^{(3)}(x, v) = \mathcal{L}^{-1}(v \cdot \nabla_x g^{(2)}(x, v)) + \zeta^{(3)}(x) = \mathcal{L}^{-1}(v \cdot \nabla_x \zeta^{(2)}(x)) + \zeta^{(3)}(x),$$

with $\zeta^{(3)}(x)$ belonging to Ker$\mathcal{L}$.

By integrating on S^1 the fourth equation $v \cdot \nabla_x g^{(3)} = \mathcal{L} g^{(4)}$ and by exploiting that $\int_{S^1} \mathrm{d}v \; \mathcal{L} g^4(x, v) = 0$ and that $\int_{S^1} \mathrm{d}v \; v \cdot \nabla_x \zeta^{(3)}(x) = 0$ we find

$$\int_{S^1} \mathrm{d}v \; v \cdot \nabla_x (\mathcal{L}^{-1}(v \cdot \nabla_x \zeta^{(2)}(x))) = -D \Delta_x \zeta^{(2)}(x) = 0. \tag{4.27}$$

We choose zero boundary condition at the reservoirs, namely $\zeta^{(2)}(x) = 0$ on $\partial\Omega_L \cup \partial\Omega_R$, so we find $\zeta^{(2)}(x) \equiv 0$. Then $g^{(2)}(x, v) \equiv 0$.

We can now write the expansion for g_ε^S as

$$g_\varepsilon^S = g^{(0)} + \frac{1}{\eta_\varepsilon} g^{(1)} + \frac{1}{\eta_\varepsilon} R_{\eta_\varepsilon}. \tag{4.28}$$

The remainder R_{η_ε} satisfies

$$v \cdot \nabla_x R_{\eta_\varepsilon} = \eta_\varepsilon \mathcal{L} R_{\eta_\varepsilon}. \tag{4.29}$$

We required $g^{(0)}$ to satisfy the same boundary conditions as the whole solution at contact with the reservoirs, namely on $\partial\Omega_L \cup \partial\Omega_R$, so the boundary conditions for R_{η_ε} read

$$\begin{cases} R_{\eta_\varepsilon}(x,v) = -\mathcal{L}^{-1}(v\cdot\nabla_x g^{(0)}(x)) & x\in\partial\Omega_L\cup\partial\Omega_R\,,\ v\cdot n(x)>0,\\ R_{\eta_\varepsilon}(x,v') = R_{\eta_\varepsilon}(x,v) & x\in\partial\tilde{\Omega}_E\,,\ v\cdot n(x)<0. \end{cases} \tag{4.30}$$

Note that the problem (4.29)-(4.30) has the form of (1.5). From Theorem 1.1 we know that it admits a unique solution in L^∞.

From the (4.28), thanks to the the fact that both $g^{(1)}$ and R_{η_ε} are bounded in L^∞ norm, we conclude that $g_\varepsilon^S \to g^{(0)}$. □

In order to prove Proposition 4.1 we follow the strategy of the proof of Proposition 3.1 in [6]. Here we have the additional difficulty of the specular reflective boundaries of horizontal sides of the strip and the presence of the obstacles in Ω. In the proof are exploited the diffusive limit of the linear Boltzmann equation in a L^∞ setting and in a bigger domain containing Ω as stated in Proposition 4.2 below and the properties of $\mathcal{L}$ summarized in Lemma 4.1.

We construct the extended domain Λ as the infinite strip constructed by removing the left and right sides of Ω and keeping the upper and lower elastic boundaries at $x_2 = 0$ and $x_2 = L_2$ and the obstacles into Ω (see Figure 4.15). We call $\partial\Lambda_E$ the union of upper and lower sides of Λ with the obstacles boundaries.

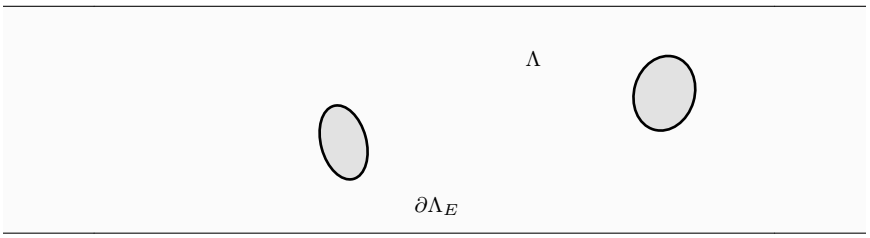

Figure 4.15: Domain Λ: infinite strip with big fixed obstacles: the whole boundaries of Λ is a specular reflective boundary.

We introduce $h_\varepsilon : \Lambda\times S^1\times[0,T]\to\mathbb{R}^+$ the solution of the following rescaled linear Boltzmann equation

$$\begin{cases} (\partial_t + \eta_\varepsilon v\cdot\nabla_x)h_\varepsilon = \eta_\varepsilon^2\mathcal{L}h_\varepsilon & x\in\Lambda\\ h_\varepsilon(x,v',t) = h_\varepsilon(x,v,t) & x\in\partial\Lambda_E,\ v\cdot n<0,\ t\geq 0\\ h_\varepsilon(x,v,0) = \rho_0(x) & x\in\Lambda, \end{cases} \tag{4.31}$$

where $\rho_0(x)$ is a smooth function of the only variable x (local equilibrium).

Proposition 4.2. *Let h_ε be the solution of (4.31), with an initial datum $\rho_0 \in C^\infty(\overline{\Lambda})$ such that there exists $M > 0$ with $\rho_0(x) = 0$ if $|x| > M$ and $\partial_n \rho_0(x) = 0$ for $x \in \partial\Lambda_E$. Then, as $\varepsilon \to 0$, h_ε converges to the solution of the heat equation*

$$\begin{cases} \partial_t \rho - D\Delta\rho = 0 & x \in \Lambda \\ \rho(x,0) = \rho_0(x) & x \in \Lambda \\ \partial_n \rho(x,t) = 0 & x \in \partial\Lambda_E,\ t \geq 0, \end{cases} \tag{4.32}$$

where the diffusion coefficient D is given by the formula

$$D = \frac{1}{4\pi} \int_{S^1} \mathrm{d}v\ v \cdot (-\mathcal{L})^{-1} v. \tag{4.33}$$

The convergence is in $L^\infty([0,T]; L^\infty(\Lambda \times S^1))$.

Proof of Proposition 4.1. The semigroup S_ε defined in (4.13) can be equivalently written as extended to functions belonging to $L^\infty(\Lambda \times S^1)$, namely

$$\begin{aligned} (S_\varepsilon(t)f)(x,v) =& \chi_\Omega(x) \sum_{m \geq 0} e^{-2\lambda\eta_\varepsilon t} (\lambda\eta_\varepsilon)^m \int_0^t \mathrm{d}t_1 \dots \int_0^{m-1} \mathrm{d}t_m \\ & \int_{-1}^1 \mathrm{d}\delta_1 \dots \int_{-1}^1 \mathrm{d}\delta_m \chi(\tau = 0) f(\Phi^{-t}(x,v)) \chi_\Omega(\Phi^{-t}(x)), \end{aligned} \tag{4.34}$$

for any $f \in L^\infty(\Lambda \times S^1)$, where χ_Ω is the characteristic function of Ω and $\Phi^{-t}(x)$ is the first component (the position) of $\Phi^{-t}(x,v)$, the backward flux individuated by x, v, $t_1, \dots, t_m$, $\delta_1, \dots, \delta_m$. The addition of $\chi_\Omega(\Phi^{-t}(x))$ guarantees together with $\chi(\tau = 0)$ that the dynamics stay internal to Ω. Moreover, the following estimate holds

$$S_\varepsilon(t)f \leq \|f\|_\infty \sum_{m \geq 0} e^{-2\lambda\eta_\varepsilon t} (\lambda\eta_\varepsilon)^m \int_0^t \mathrm{d}t_1 \dots \int_0^{m-1} \mathrm{d}t_m \int_{-1}^1 \mathrm{d}\delta_1 \dots \int_{-1}^1 \mathrm{d}\delta_m \chi_\Omega(\Phi^{-t}(x)).$$

We construct $\chi_\Omega^\delta \in C^\infty(\overline{\Lambda})$, a mollified version of χ_Ω, $\chi_\Omega^\delta \geq \chi_\Omega$, $\chi_\Omega^\delta \leq 1$ and $\Omega \subset supp(\chi_\Omega^\delta) \subset (-\delta, L_1 + \delta) \times [0, L_2]$. So we can write

$$S_\varepsilon(t)f \leq \|f\|_\infty \sum_{m \geq 0} e^{-2\lambda\eta_\varepsilon t} (\lambda\eta_\varepsilon)^m \int_0^t \mathrm{d}t_1 \dots \int_0^{m-1} \mathrm{d}t_m \int_{-1}^1 \mathrm{d}\delta_1 \dots \int_{-1}^1 \mathrm{d}\delta_m \chi_\Omega^\delta(\Phi^{-t}(x)). \tag{4.35}$$

Note that the series in (4.35) defines a function F which solves

$$\begin{cases} (\partial_t + v \cdot \nabla_x) F(x,v,t) = \eta_\varepsilon \mathcal{L} F(x,v,t) & x \in \Lambda \\ F(x,v',t) = F(x,v,t) & x \in \partial\Lambda_E,\ v \cdot n < 0,\ t \geq 0 \\ F(x,v,0) = \chi_\Omega^\delta(x) & x \in \Lambda. \end{cases} \tag{4.36}$$

Defining $G_\varepsilon(x,v,t)$ as $F(x,v,\eta_\varepsilon t)$, G_ε solves (4.31) with initial datum $\rho_0 = \chi^\delta_\Omega$. Thanks to Proposition 4.2 we know that at time $t=1$

$$\|G_\varepsilon(1) - \rho^\delta(1)\|_\infty \leq \omega(\varepsilon)$$

where ρ^δ solves (4.32) with initial datum χ^δ_Ω and $\omega(\varepsilon)$ denotes a positive function vanishing with ε. Moreover, we can notice that the function ρ^δ is the solution of a diffusion equation with initial datum $0 \leq \chi^\delta_\Omega \leq 1$ with support in a bounded subset of the infinite strip Λ. By the strong maximum principle we know that for the positive time $t=1$, it holds that $\rho^\delta(x,1) < 1$. Therefore for ε small enough

$$\begin{aligned} \|S_\varepsilon(\eta_\varepsilon)f\|_\infty \leq & \|f\|_\infty \|S_\varepsilon(\eta_\varepsilon)\chi^\delta_\Omega\|_\infty \leq \|f\|_\infty(\|G_\varepsilon(1) - \rho^\delta(1)\|_\infty + \|\rho^\delta(1)\|_\infty) \\ \leq & \|f\|_\infty(\omega(\varepsilon) + \|\rho^\delta(1)\|_\infty) < \alpha\|f\|_\infty, \quad \alpha < 1, \end{aligned} \tag{4.37}$$

where we have used (4.35) for $t = \eta_\varepsilon$. □

Proof of Proposition 4.2. Let $h_\varepsilon : \Lambda \times S^1 \times [0,T]$ the solution of (4.31). We use the Hilbert expansion technique to prove that h_ε converges to the solution of the heat equation (4.32). We search h_ε of the form

$$h_\varepsilon(x,v,t) = h^{(0)}(x,t) + \sum_{k=1}^{+\infty} \left(\frac{1}{\eta_\varepsilon}\right)^k h^{(k)}(x,v,t),$$

with coefficient $h^{(k)}$ not depending on η_ε. By imposing that h_ε solves (4.31) and comparing terms of the same order we find the identity $\mathcal{L}h^{(0)}(x,t) = 0$ and the chain of equations

$$\begin{aligned} v \cdot \nabla_x h^{(0)} =& \mathcal{L}h^{(1)} \\ \partial_t h^{(k)} + v \cdot h^{(k+1)} =& \mathcal{L}h^{(k+2)} \qquad \text{for } k \geq 0. \end{aligned}$$

We impose that $h^{(0)}$ satisfy the same initial condition of the whole solution h_ε, namely

$$h^{(0)}(x,0) = \rho_0(x).$$

Let us start from the first equation (i) $v \cdot \nabla_x h^{(0)} = \mathcal{L}h^{(1)}$. Thanks to the Fredholm alternative and by proceeding as in the proof of Theorem 1.2, we can solve equation (i) if and only if the left hand side belongs to $(\mathrm{Ker}\mathcal{L})^\perp = \{h \in L^2(S^1) \text{ s. t. } \int_{S^1} \mathrm{d}v\ h(v) = 0\}$. Since $v \cdot \nabla_x h^{(0)}(x)$ is an odd function of v, it belongs to $(\mathrm{Ker}\mathcal{L})^\perp$. So we can invert the operator $\mathcal{L}$ finding

$$h^{(1)}(x,v,t) = \mathcal{L}^{-1}(v \cdot \nabla_x h^{(0)}(x,t)) + \zeta^{(1)}(x,t). \tag{4.38}$$

where $\zeta^{(1)}(x,t)$ is a function to be determined in the kernel of $\mathcal{L}$. Recall that $\mathcal{L}^{-1}$ preserves the parity.

We integrate the second equation (ii) $\partial_t h^{(0)} + v \cdot \nabla_x h^{(1)} = \mathcal{L} h^{(2)}$ with respect to the uniform measure on the sphere S^1. Thanks to the equation (4.38) and the observations that $\int_{S^1} \mathrm{d}v\, \mathcal{L} h^{(2)} = 0$ and $\int_{S^1} \mathrm{d}v\, v \cdot \nabla_x \zeta^{(1)}(x,t) = 0$, it holds

$$\frac{1}{2\pi} \int_{S^1} \mathrm{d}v\, \partial_t h^{(0)}(x,t) + v \cdot \nabla_x (\mathcal{L}^{-1} v \cdot \nabla_x h^{(0)}(x,t)) = 0. \tag{4.39}$$

As in the proof of Theorem 1.2 defining $D_{i,j} = \frac{1}{2\pi} \int_{S^1} \mathrm{d}v\, v_i (-\mathcal{L}^{-1}) v_j$, we find that the diffusion coefficient D is given by the formula (4.33)

$$D = \frac{1}{4\pi} \int_{S^1} \mathrm{d}v\; v \cdot (-\mathcal{L})^{-1} v$$

so that the heat equation for $h^{(0)}$ is

$$\partial_t h^{(0)} - D \Delta_x h^{(0)} = 0. \tag{4.40}$$

$h_\varepsilon(x,v)$ has to satisfy the reflective boundary condition $h_\varepsilon(x,v',t) = h_\varepsilon(x,v,t)$ on $\partial\Lambda_E$. By imposing it on the first term $h^{(1)}(x,v,t) = h^{(1)}(x,v',t)$ for every $x \in \partial\Omega_E$, $v \cdot n < 0$, we obtain proceeding in the same way of the proof of Theorem 1.2 that $h^{(0)}(x,t)$ has to satisfy the Neumann boundary conditions $\partial_n h^{(0)}(x,t) = 0$, for all $x \in \partial\Lambda_E$.

We have so shown that the term $h^{(0)}(x,t)$ solves the problem

$$\begin{cases} \partial_t h^{(0)} - \Delta_x h^{(0)} = 0 & x \in \Lambda \\ h^{(0)}(x,0) = \rho_0(x) & x \in \Lambda \\ \partial_n h^{(0)}(x,t) = 0 & x \in \partial\Lambda_E. \end{cases} \tag{4.41}$$

In particular $h^{(0)}(t) \in L^\infty(\Lambda \times S^1)$ for any $t \geq 0$.

The equation (4.40) allow us to verify that when integrating the equation (ii) the left hand side vanishes. It implies that we can invert operator $\mathcal{L}$ finding

$$h^{(2)}(x,v,t) = \mathcal{L}^{-1}(\partial_t h^{(0)}(x,t) + v \cdot \nabla_x (\mathcal{L}^{-1}(v \cdot \nabla_x h^{(0)}(x,t))) + v \cdot \nabla_x \zeta^{(1)}(x,t)) + \zeta^{(2)}(x,t), \tag{4.42}$$

where $\zeta^{(2)}(x,t)$ is a function in $\operatorname{Ker} \mathcal{L}$.

Next equation is (iii) $\partial_t h^{(1)} + v \cdot \nabla_x h^{(2)} = \mathcal{L} h^{(3)}$. When integrating it with respect to the uniform measure on S^1, we exploit the fact that the operator $\mathcal{L}^{-1}$ preserves the parity. So, substituting $h^{(1)}$ and $h^{(2)}$ with their expressions given by (4.38) and (4.42), the only terms surviving give the equation for $\zeta^{(1)}$

$$\partial_t \zeta^{(1)}(x,t) - D \Delta_x \zeta^{(1)}(x,t) = 0. \tag{4.43}$$

Since there are no restrictions on the choice of the initial condition for $\zeta^{(1)}$, we fix $\zeta^{(1)}(x,0)=0$. So $\zeta^{(1)}(x,t)\equiv 0$ for any (x,t) and the expression for $h^{(1)}$ reduces to

$$h^{(1)}(x,v,t)=\mathcal{L}^{-1}(v\cdot\nabla_x h^{(0)}(x,t)).$$

By the Lemma 4.1 and the smoothness of $h^{(0)}$ we have

$$\sup_{t\in[0,T]}\|h^{(1)}(t)\|_\infty\le C\sup_{t\in[0,T]}\|\nabla_x h^{(0)}(t)\|_\infty<+\infty.$$

In the same way, by Lemma 4.1 and smoothness of $h^{(0)}$ it follows that the first term in the expression of $h^{(2)}$, i.e. $h_1^{(2)}=\mathcal{L}^{-1}(\partial_t h^{(0)}(x,t)+v\cdot\nabla_x(\mathcal{L}^{-1}(v\cdot\nabla_x h^{(0)}(x,t))))$, is in $L^\infty([0,T];L^\infty(\Lambda\times S^1))$, as well as its spatial derivatives.

Observe now that the left hand side of equation (iii) has null integral on S^1 due to (4.43). By inverting $\mathcal{L}$ we obtain the formula for $h^{(3)}$

(4.44)
$$\begin{aligned}h^{(3)}(x,v,t)=&\mathcal{L}^{-1}(\partial_t h^{(1)}+v\cdot\nabla_x h^{(2)}(x,v,t))+\zeta^{(3)}(x,t)\\=&\mathcal{L}^{-1}(\partial_t\mathcal{L}^{-1}(v\cdot\nabla_x h^{(0)}(x,t))+v\cdot\nabla_x(h_1^{(2)}(x,v,t)+\zeta^{(2)}(x,t)))+\zeta^{(3)}(x,t),\end{aligned}$$

where $\zeta^{(3)}\in\operatorname{Ker}\mathcal{L}$. We integrate now the equation (iv) $\partial_t h^{(2)}+v\cdot\nabla_x h^{(3)}=\mathcal{L}h^{(4)}$ with respect to the uniform measure on S^1. We find the equation for $\zeta^{(2)}(x,t)$

$$\partial_t\zeta^{(2)}-D\Delta_x\zeta^{(2)}=S(x,t),\tag{4.45}$$

where the source $S(x,t)$ is given by

$$\begin{aligned}S(x,t)=&-\frac{1}{2\pi}\int_{S^1}\mathrm{d}v\,v\cdot\nabla_x\mathcal{L}^{-1}(\partial_t\mathcal{L}^{-1}(v\cdot\nabla_x h^{(0)}(x,t)))\\&-\frac{1}{2\pi}\int_{S^1}\mathrm{d}v\,v\cdot\nabla_x\mathcal{L}^{-1}(v\cdot\nabla_x h_1^{(2)}(x,v,t))).\end{aligned}$$

We consider as initial datum $\zeta^{(2)}(x,0)=0$, so we have $\zeta^{(2)}\in L^\infty([0,T];L^\infty(\Lambda))$ and its spatial derivative as well, since $S\in L^\infty([0,T];L^\infty(\Lambda))$.

We write the the expansion truncated at order η_ε^{-2} for the solution:

$$h_\varepsilon(x,v,t)=h^{(0)}(x,t)+\frac{1}{\eta_\varepsilon}h^{(1)}(x,v,t)+\frac{1}{\eta_\varepsilon^2}h^{(2)}(x,v,t)+\frac{1}{\eta_\varepsilon}R_{\eta_\varepsilon}(x,v,t).\tag{4.46}$$

We have shown that $h^{(i)}(t)\in L^\infty(\Lambda\times S^1)$ for $i=0,1,2$. Now we have to prove that even,the remainder R_{η_ε} is in L^∞.

The remainder R_{η_ε} satisfies the equation

$$(\partial_t+\eta_\varepsilon v\cdot\nabla_x)R_{\eta_\varepsilon}=\eta_\varepsilon^2\mathcal{L}R_{\eta_\varepsilon}-T_{\eta_\varepsilon}\tag{4.47}$$

with initial condition

$$R_{\eta_\varepsilon}(x,v,0) = -h^{(1)}(x,v,0) - \frac{1}{\eta_\varepsilon} h^{(2)}(x,v,0)$$

and boundary conditions

$$R_{\eta_\varepsilon}(x,v',t) = R_{\eta_\varepsilon}(x,v,t) \qquad x \in \partial\Lambda_E,\ v\cdot n < 0.$$

The term T_{η_ε} on the left hand side of (4.47) is $T_{\eta_\varepsilon} = \partial_t h^{(1)} + \frac{1}{\eta_\varepsilon}\partial_t h^{(2)} + v\cdot\nabla_x h^{(2)}$. So $T_{\eta_\varepsilon} \in L^\infty([0,T]; L^\infty(\Lambda\times S^1))$ and thanks to the smoothness hypothesis on ρ_0 also the initial datum $R_{\eta_\varepsilon}(x,v,0)$ belongs to L^∞.

By denoting by $S_{\eta_\varepsilon}(t)$ the semigroup associated to the generator $\eta_\varepsilon(v\cdot\nabla_x - \eta_\varepsilon\mathcal{L})$ with reflective boundary conditions on $\partial\Lambda_E$, the equation (4.47) becomes

$$R_{\eta_\varepsilon}(t) = S_{\eta_\varepsilon}(t)R_{\eta_\varepsilon}(0) + \int_0^t \mathrm{d}s\, S_{\eta_\varepsilon}(t-s)T_{\eta_\varepsilon}(s).$$

By means of the series expansion found in (4.35), the solution can be written in the following way:

$$\begin{aligned} R_{\eta_\varepsilon}(x,v,t) =& \sum_{m\geq 0} e^{-2\lambda\eta_\varepsilon^2 t}(\lambda\eta_\varepsilon)^m \int_0^{\eta_\varepsilon t}\mathrm{d}t_1\ldots\int_0^{m-1}\mathrm{d}t_m\int_{-1}^1\mathrm{d}\delta_1\ldots\int_{-1}^1\mathrm{d}\delta_m R_{\eta_\varepsilon}(0)(\Phi^{-\eta_\varepsilon t}(x,v)) \\ &+\int_0^t \mathrm{d}s\sum_{m\geq 0} e^{-2\lambda\eta_\varepsilon^2(t-s)}(\lambda\eta_\varepsilon)^m \int_0^{\eta_\varepsilon(t-s)}\mathrm{d}t_1\ldots\int_0^{m-1}\mathrm{d}t_m\int_{-1}^1\mathrm{d}\delta_1\ldots\int_{-1}^1\mathrm{d}\delta_m T_{\eta_\varepsilon}(0)(\Phi^{-\eta_\varepsilon(t-s)}(x,v),s). \end{aligned}$$

Therefore we can estimate

$$\sup_{t\in[0,T]}\|R_{\eta_\varepsilon}(t)\|_\infty \leq \|R_{\eta_\varepsilon}(0)\|_\infty + T\sup_{t\in[0,T]}\|T_{\eta_\varepsilon}(t)\|_\infty \leq C < +\infty.$$

So the remainder is uniformly bounded too. Hence from the estimates and (4.46) it follows that h_ε converges to $h^{(0)}$ in L^∞ for $\eta_\varepsilon\to\infty$.

□

Chapter 2

Random Walk

We consider a 2D finite rectangular lattice where a rectangular fixed obstacle is present. We consider particles performing a simple symmetric random walk and we study numerically the residence time behavior. We give a complete interpretation of the resulting residence times, even by constructing the reduced 1D picture of the lattice: a simple symmetric random walk on an interval with two singular sites, that mimics the 2D case. We calculate the residence time for this 1D model via Monte Carlo simulations, finding good correspondence between the results of the 1D and the 2D model. Finally we produce exact calculation of the residence time for the 1D model.

2.1 The 2D model

A particle performs a symmetric simple random walk on the 2D strip Λ made of the points (x_1, x_2) with $x_1 = 1, \ldots, L_1$ and $x_2 = 1, \ldots, L_2$. The 1 and the 2 directions are respectively called *horizontal* and *vertical*. The particle starts at a site in the first column on the left, namely, at a site $(1, x_2)$ with $x_2 = 1, \ldots, L_2$ chosen at random with uniform probability. At each time step the particle performs a move to one of the four neighboring sites with the same probability $1/4$. If the target site is in the horizontal boundary, made of the sites $(x_1, 0)$ and $(x_1, L_2 + 1)$ with $x_1 = 1, \ldots, L_1$, the particle does not move, which means that the horizontal boundary is a reflecting surface. If the target site belongs to the left or to the right vertical boundary, that is to say it is of the form $(0, x_2)$ or $(L_1 + 1, x_2)$ with $x_2 = 1, \ldots, L_2$, the particle exits the system and the walk is stopped. Moreover, we shall consider a rectangular obstacle inside the strip, in the sense that, when one of the sites of this region will be chosen as target site for the move of the particle, the particle will not move. Thus, all the

sites in the obstacle are not accessible to the walker. The width and the height of the obstacle will be denote, respectively, by W and H.

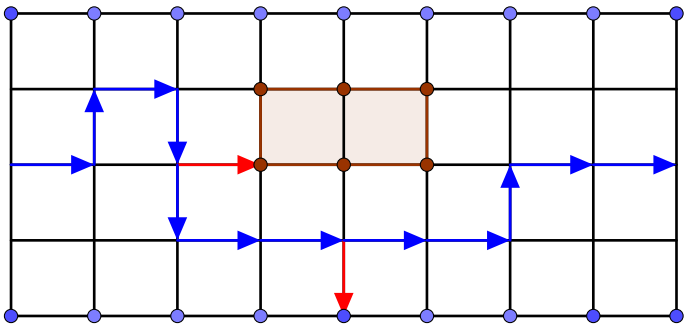

Figure 1.1: A possible trajectory in blue: when a particle tries to jump on a site occupied by the obstacle or by the horizontal boundary, it does not move (red arrows).

As for the case of the linear Boltzmann dynamics, the *residence time* is defined as the mean time that the particle started at a uniformly chosen random site with abscissa $x_1 = 1$ takes to exit the strip through the right boundary. Sometimes, we shall address to the residence time as to the *total* residence time to stress that it refers to the total time that the particle spends inside the strip. More precisely, one could consider the walk on the infinite strip $\mathbb{Z} \times \{1, \dots, L_2\}$ and define the residence time as the mean of the first hitting time for a particle started at a site $(1, x_2)$, with $x_2 = 1, \dots, L_2$ chosen at random with uniform probability, to the set of sites with $x_1 = L_1 + 1$ conditioned to the event that the particle reaches such a subset before visiting the set of sites with abscissa $x_1 = 0$.

We shall compute the residence time by simulating many particles and averaging the time that each of them needs to exit, paying attention to the fact that only those particles which effectively exit through the right boundary will contribute to the average, whereas those exiting through the left boundary will be discarded.

Similarly to the case discussed in Section 1.3 we find that the residence time is not monotonic with respect to the geometrical parameters of the obstacle, such as its position and its size. We show, also, that obstacles can increase or decrease the residence time with respect to the empty strip case depending on their side lengths and on their position. In some cases, one of these parameters controls a transition from the increasing to the decreasing effect. We stress that in some cases discussed later the residence time measured in presence of an obstacle is smaller than the one measured for the empty strip, that is to say, the obstacle is able to select those particles that cross the strip faster.

We now discuss our results for different choices of the obstacle and we postpone a possible interpretation to the end of this section. The geometrical parameters of the strip are $L_1 = 200$ and $L_2 = 50$. All the details about the numerical simulations are in the figure captions. The statistical error, since negligible, is not reported in the picture.

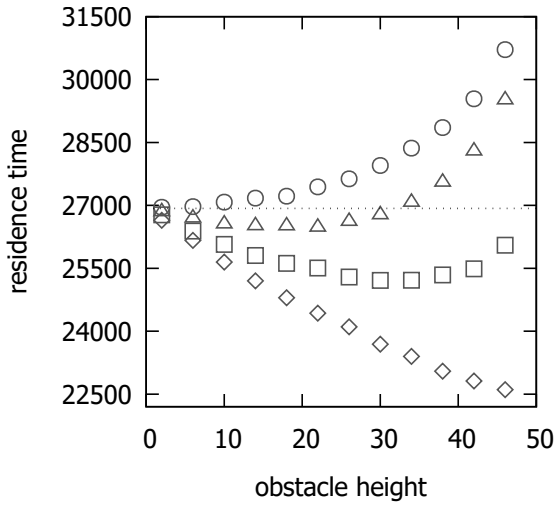

Figure 1.2: Residence time vs. obstacle height. The obstacle is placed at the center of the strip and its with width is $W = 2$ (disks). $W = 20$ (triangles), $W = 40$ (squares), and $W = 60$ (diamonds). Simulation parameters: $L_1 = 200$, $L_2 = 50$, total number of inserted particles $5 \cdot 10^7$. The total number of particles exiting through the right boundary decreases when the obstacle height is increased from $2.49 \cdot 10^5$ (empty strip) to $1.69 \cdot 10^5$ (disks), $0.99 \cdot 10^5$ (triangles), $0.68 \cdot 10^5$ (squares), and $0.52 \cdot 10^5$ (diamonds). The dashed line at about 26930 represents the value of the residence time measured for the empty strip.

In Figure 1.2 we plot the residence time as a function of the obstacle height. The obstacle is placed at the center of the strip and its width is $W = 2$ (disks), $W = 20$ (triangles), $W = 40$ (squares), and $W = 60$ (diamonds). In the case of a thin barrier, starting from the empty strip value, the residence time increases with the height of the obstacle. For a wider obstacle, an a priori not intuitive result is found: the dependence of the residence time on the obstacle height is not monotonic. In the case $W = 20$, starting from the empty strip value, the residence time decreases up to height 20 and then increases to values above the empty strip one. This effect is even stronger if the width of the obstacle is further increased.

In Figure 1.3 the residence time as a function of the obstacle width is plotted. The obstacle is placed at the center of the strip and its height is $H = 40$. When the

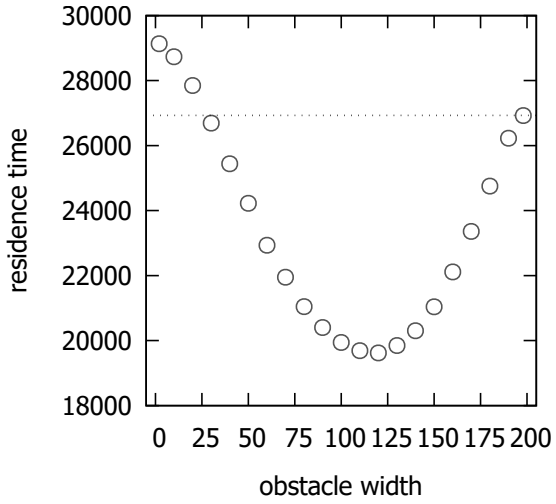

Figure 1.3: Residence time vs. obstacle width. The obstacle is placed at the center of the strip and its height is $H = 40$. The total number of particles exiting through the right boundary decreases when the obstacle width is increased from $2.49 \cdot 10^5$ (empty strip) to $0.5 \cdot 10^5$. The parameters of the simulation and the dashed line are as in Figure 1.2.

barrier is thin the residence time is larger than the one measured in the empty strip case, but, when the width is increased, the residence time decreases and at about 26 it becomes smaller than the empty case value. The minimum is reached at about 120 (recall the the length of the strip is $L_1 = 200$ in this simulation), then the residence time increases to the empty strip value which is reached when the obstacle is as long as the entire strip. This is indeed obvious, since in such a case the lattice is made of two independent channels having the same length as the original strip.

In Figure 1.4 a centered square obstacle is considered. The residence time as a function of its side length is reported. Although small oscillations, reasonably due to numerical approximations, are visible, the behavior appears to be monotonically decreasing.

Finally, in Figure 1.5 we show that, and this is really surprising, the residence time is not monotonic even as a function of the position of the center of the obstacle. Disks refer to a squared obstacle of side length 40, whereas triangles refer to a thin rectangular obstacle with width $W = 2$ and height $H = 40$. In both cases the residence time is not monotonic and attains its minimum value when the obstacle is placed in the center of the strip. In the squared obstacle case, when the abscissa of the center of the obstacle lies between 75 and 125 the residence time in presence of the obstacles is smaller than the corresponding value for the empty strip. On the other hand, for the

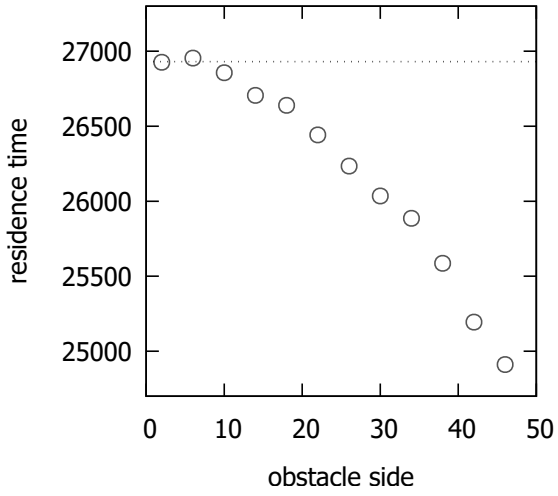

Figure 1.4: Residence time vs. squared obstacle side length. The squared obstacle is placed in the middle of the strip. The total number of particles exiting through the right boundary decreases when the obstacle side length is increased from $2.49 \cdot 10^5$ (empty strip) to $0.63 \cdot 10^5$ for side length equal to 46. The parameters of the simulation and the dashed line are as in Figure 1.2.

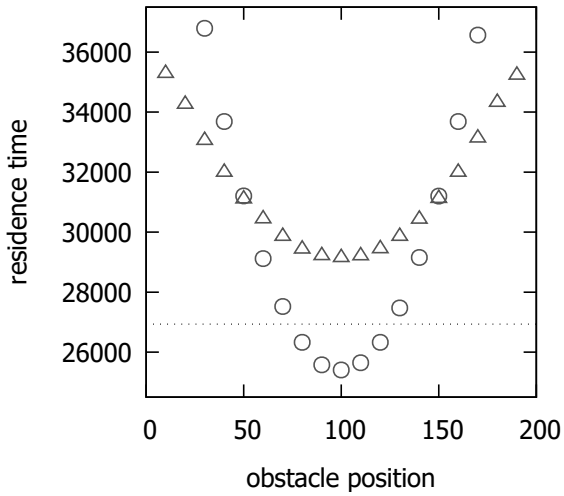

Figure 1.5: Residence time vs. position of the center of the obstacle. Disks refer to a squared obstacle with side length 40, whereas triangles refers to a rectangular obstacle with width $W = 2$ and height $H = 40$. The total number of particles exiting through the right boundary is approximately $1.24 \cdot 10^5$ (disks) and $2.01 \cdot 10^5$ (triangles) and depends poorly on the obstacle position. The parameters of the simulation and the dashed line are as in Figure 1.2.

thin rectangular obstacle, even if the non–monotonic behavior is found, the residence time is always larger than in the empty strip case. This fact is consistent with the results plotted in Figure 1.2.

The results that we found in the numerical experiments reported in Figures 1.2–1.5 can be summarized as follows: the residence time strongly depends on the obstacle geometry and position. In particular it seems that large centered obstacles favor the selection of particles crossing the strip faster than in the empty strip case.

In order to explain our observations, as we made in Section 1.3, we partition the strip into three parts: the rectangular region on the left of the obstacle, the rectangular region on the right of the obstacle and the remaining central part containing the obstacle. As we will see later, the residence time behavior is consequence of two effects in competition: the total time spent by the particles in the channels between the obstacle and the horizontal boundary is smaller than the total time spent in the central part of the strip in the empty case. On the contrary, the total time spent both in the left and in the right part of the strip is larger with respect to the empty case. Both these two effects can be explained remarking that, when the obstacle is present, it is more difficult for the walker to enter the central region of the strip, namely, one of the channels flanking the obstacle. The total residence time trend depends on which of the two effects dominates the dynamics of the walker.

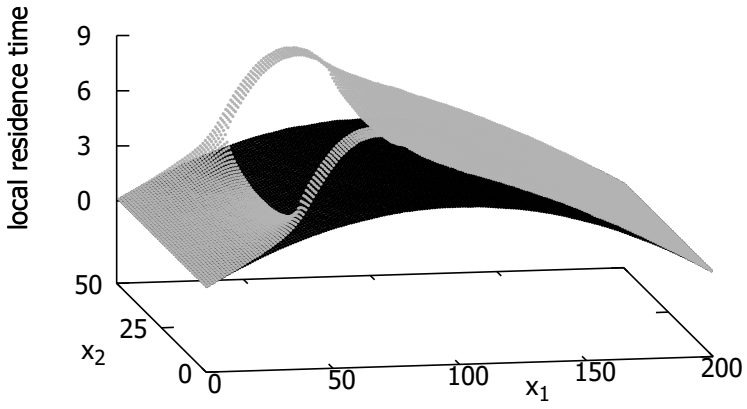

Figure 1.6: Mean time spent by the walker crossing the strip in each site of the strip (local residence time) for the empty strip case (black) and in presence of the obstacle (gray). Data are those of the experiment described by the disks in Figure 1.5. The obstacle is a squared obstacles with side length 40 placed at the site with abscissa 60.

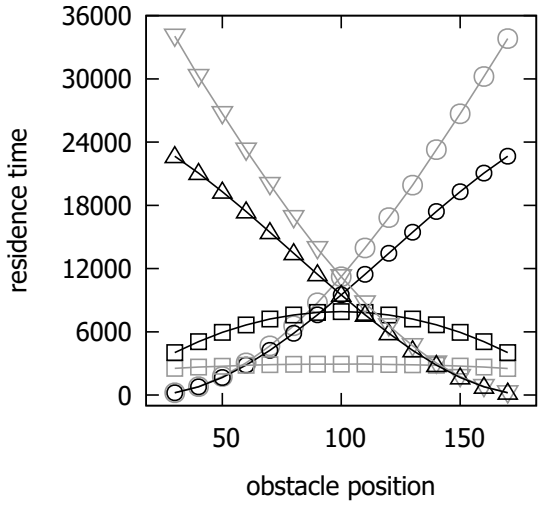

Figure 1.7: Total residence time in the left (circles), central (squares), and right (triangles) part of the strip in presence of the obstacle (gray) and in the empty strip case (black). The experiment associated with the disks in Figure 1.5 is considered.

To illustrate our interpretation of the phenomenon we describe in detail the walker behavior referring to the experiment associated with the disks in Figure 1.5. In Figure 1.6 we plot the mean time spent by the walker crossing the strip in each site of the strip. This quantity will be addressed as the *local residence time*. The gray surface in the picture refers to the obstacle case, whereas the black surface is related to the empty strip case. The data in the picture have been collected in the case in which the center of a squared obstacle with side length 40 is placed at the site with coordinates $(80, 25)$. The graph shows that in average in each site of the strip the particle spends a time larger than the time it spends at the same site in the empty strip case. This seems to be in contrast with the fact that the (total) residence time in the strip can be smaller when the obstacle is present. Indeed, this can happen since the sites of the strip falling in the obstacle region are never visited by the walker. It can then happen that the sum of the local residence times associated with sites in the central part of the strip in presence of the obstacle is smaller than the same sum computed in the empty strip case.

Results in Figure 1.6 can be interpreted as follows. The local residence times in the left and in the right regions are larger with respect to the empty case since for the particle it is more difficult to access the central region and, thus, it will spend more time in the lateral parts of the strip. On the other hand, once the particle enters into one of the two central channels, it will take in average the same time to get back to one of the two lateral parts of the strip that it would take in absence of the obstacle.

But, since, the number of the available sites in the central part is smaller when the obstacle is present, the local residence time will be larger.

The Figure 1.6 gives some new insight in the motion of the walker, but it is not sufficient to explain the residence time behavior discussed above. In order to get some in- sight into this, we compute the respective times spent by the particle in the left, central and right region of the strip. This is done in Figure 1.7, where data referring to the experiment associated with the disks in Figure 1.5 are reported. First, one should note that the total residence time in the left and in the right part of the strip are increased when the obstacle is present, this is due to the fact that for the particle it is more difficult to enter the central part when the obstacle is present. Moreover, precisely for the same reason the trajectory of the walker from its starting point to its exit from the strip will visit the channels in the central region of the strip a number of time smaller than the number of times that the particle visits the central region of the strip in the empty strip case. Thus, the residence time in the central part of the strip results to be smaller when the obstacle is present.

Hence, the behavior of the (total) residence time data reported as disks in Figure 1.5 can be explained as follows: if the center of the obstacle is close to the left boundary (say its abscissa is smaller than 75) the effect in the right region of the strip dominates the one in the central region and the (total) residence time is increased (the effect in the left region in this case is negligible). On the other hand, if the center of the obstacle is close to the center of the strip (say its abscissa is between 75 and 125) the effect in the central region dominates and the (total) residence time is decreased. Finally, if the center of the obstacle is close to the right boundary (say its abscissa is larger than 125) the effect in the left region of the strip dominates the one in the central region and the (total) residence time is increased (the effect in the right region in this case is negligible).

The behavior of the residence time in connection with all the experiments illustrated in Figures 1.2–1.5 can be explained similarly.

2.2 The 1D model

In this section we propose a one–dimensional reduction of the problem based on a symmetric simple random walk with two defect sites. We actually prove that the behaviors of the 1D system are similar to those discussed above and that the Monte Carlo data are fully supported by exact analytical computations.

We consider a simple random walk on $\{0, 1, \ldots, L\}$. The sites 0 and L are absorb-

ing, so that when the particle reaches one of these two sites the walk is stopped. All the sites $1, \dots, L-1$ are *regular* excepted for two sites called *defect* or *special* sites. The *first* or *left* defect site is the site $n+1$ and the *second* or *right* defect site is the site $n+h+2$, with $n = 1, 2, \dots, L-5$ and $h = 1, 2, \dots, L-n-4$. The parameters n and h are chosen in such a way that the left defect site cannot be 1, the right defect site cannot be $L-1$, and there is at least one regular site separating the two defect sites. The number of regular sites on the left of the left defect site is n and the number of regular sites in the region between the two defect sites is h. We let $w = L-(n+h+3)$ be the number of regular sites on the right of the right defect site.

At each time step the walker try to move with the following rule: if it is on a regular site, then it jumps to its left or to its right with probability $1/2$. If it is at the left defect site it jumps with probability λ to the right, with probability $1-\lambda-\epsilon$ to the left, and with probability ϵ it does not move. If it is at the right defect site it jumps with probability λ to the left, with probability $1-\lambda-\epsilon$ to the right, and with probability ϵ it does not move. Here, $\lambda \in (0,1)$ and $\epsilon \in [0,1)$.

The array $1, \dots, L-1$ will be called the *lane*. The sites 0 and L will be, respectively, called the *left* and *right exit* of the lane.

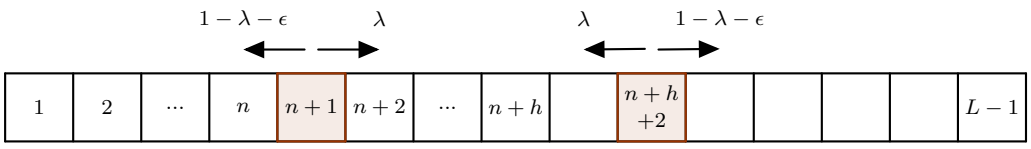

Figure 2.8: The lane. Particles on the singular sites $n+1$ and $n+h+2$ do not move with probability ϵ.

This 1D model is a toy model for the 2D system that we have discussed in Section 2.1. Indeed, the left defect site $n+1$ mimics the sites in the first column of the 2D strip on the left of the obstacle: the 2D walker in such a column has a probability to move to the right smaller than the probability to move to the left. Similarly, the right defect site $n+h+1$ mimics the sites in the first column to the right of the obstacle. It is important to stress that the sites $n+1+1, \dots, n+h$ are regular, since when the 2D walker enters one of the two channels flanking the obstacle its probability to move to the right is equal to that to move to the left.

In this framework the residence time is defined by starting the walk at site 1 and computing the typical time that the particle takes to reach the site L provided the walker reaches L before 0. In other words we compute the time that the particle takes to exit the lane through the right exit. More precisely, we let x_t be the position

of the walker at time t and denote by $\mathbb{P}_k$ and $\mathbb{E}_k$ the probability associated to the trajectories of the walk and the related average operator for the walk started at $x_0 = k$ with $k = 1, \dots, L-1$. We let

$$T_i = \inf\{t > 0,\, x_t = i\} \tag{2.1}$$

be the *first hitting time to* i, with the convention that $T_i = \infty$ if the set $\{t > 0,\, x_t = i\}$ is empty, i.e., the trajectory does not reach the site i. The main quantity of interest is the *residence time* or *total residence time*

$$R = \mathbb{E}_1[T_L | T_L < T_0] = \sum_{t=1}^{\infty} t \mathbb{P}_1[T_L = t | T_L < T_0] \ . \tag{2.2}$$

Note that the residence time is defined for the walk started at $x_0 = 1$ and the average is computed conditioning to the event $T_L < T_0$, namely conditioning to the fact that the particle exits the lane through the right exit.

As in the 2D case discussed in Section 2.1, we shall compute numerically the residence time by simulating many particles and averaging the time that each of them takes to exit through the right ending point, discarding all the particles exiting through the left ending point. But we stress that in this 1D model it is also possible to compute exactly the residence time. In this section we shall discuss our findings and in each plot the solid lines will represent the exact result which will be discussed in the following Section 2.3.

We now discuss our results for different choices of the parameter which are the analog of the cases considered in Section 2.1 for the 2D model. All the details about the numerical simulations are in the figure captions. The statistical error, since negligible, is not reported in the picture. The simulation are carried out with the following choice of the parameters:

$$\epsilon = \frac{1}{2} p \quad \text{and} \quad \lambda = \frac{1}{2}(1-p) \tag{2.3}$$

with $p \in [0, 1)$, so that $\epsilon \in [0, 1/2)$ and $\lambda \in (0, 1/2]$. Note that with such a choice the probability to move left (resp. right) for the particle sitting at the left (resp. right) defect site is $1 - \lambda - \epsilon = 1/2$. Note that for p equal zero we recover the symmetric simple random walk, which mimics the 2D empty strip.

The case reported in Figure 2.9 is the analog of the case discussed in Figure 1.2 in the 2D setting. Indeed, the residence time is plotted as a function of the parameter p increasing from 0 to 0.99 and this mimics the increase of the height of the obstacle considered in Figure 1.2. Moreover, the two defect sites are symmetric with respect

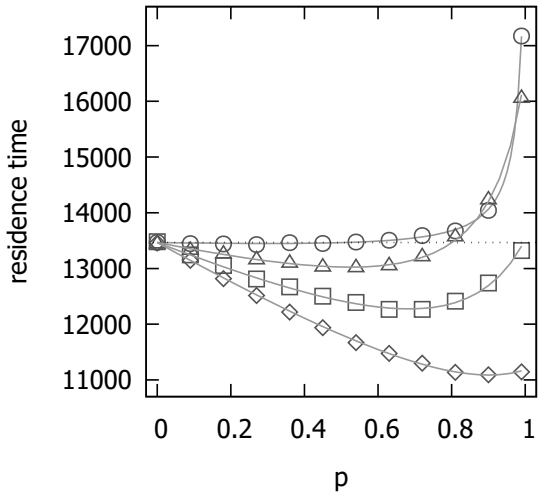

Figure 2.9: Residence time vs. p. Simulation parameters: total number of inserted particles $5 \cdot 10^7$, $L = 201$, $n = 98$ and $h = 2$ (disks), $n = 89$ and $h = 20$ (triangles), $n = 79$ and $h = 40$ (squares), and $n = 69$ and $h = 60$ (diamonds). The total number of particles exiting through the right exit decreases, when p grows, from $2.48 \cdot 10^5$ (no defect is present, namely, $p = 0$) to $1 \cdot 10^5$ (disks), $0.22 \cdot 10^5$ (triangles), $0.12 \cdot 10^5$ (squares), and $0.08 \cdot 10^5$ (diamonds), for $p = 0.99$. The dashed line at about 13465 represents the value of the residence time measured in absence of defect sites ($p = 0$). The solid line is the exact solution.

to the middle point of the lane and the number of regular sites between them is chosen equal to 2, 20, 40, and 60 mimicking the different obstacle widths considered in Figure 1.2. The data show a behavior similar to that reported in Figure 1.2 in the 2D case: in the case $h = 2$ (the defect sites are close to each other) the residence time increases with p. For a wider obstacle, the non–monotonic behavior is recovered. In the case $h = 20$, starting from the empty strip value, the residence time decreases up to $p \sim 0.55$ and then it increases to values above the $p = 0$ case. This effect is even stronger if p is further increased.

The case reported in Figure 2.10 is the analog of the case discussed in Figure 1.3 in the 2D setting. Indeed, the residence time is plotted as a function of the parameter h increasing from 2 to 198 with the two defect sites symmetric with respect to the middle point of the lane. This case mimics the increase of the width of the centered rectangular obstacle reported in Figure 1.3. When h is small the residence time is larger than the one measured for $p = 0$, but, when h is increased, the residence time decreases and at about 25 it becomes smaller than the $p = 0$ case. The minimum is reached at about 120 (recall the lane is long 201 sites in this simulation), then the

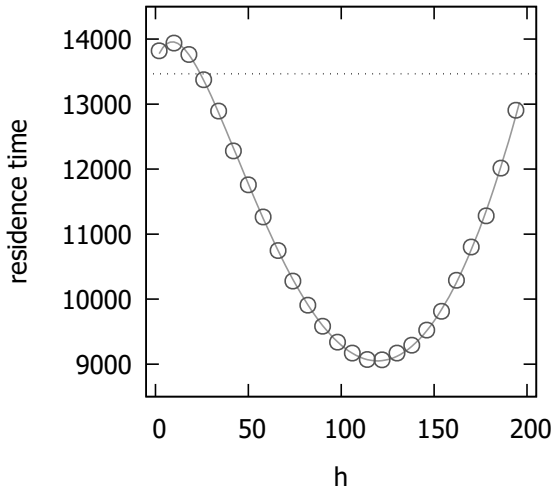

Figure 2.10: Residence time vs. h (even) for $p = 0.84$, $L = 201$, $n = (L - h - 3)/2$, and total number of inserted particles $5 \cdot 10^7$. The dashed and the solid lines are as in Figure 2.9. The total number of particles exiting through the right exit decreases when h is increased from $2.31 \cdot 10^5$ for $h = 2$ to $0.41 \cdot 10^5$ for $h = 194$.

residence time increases towards the $p = 0$ value.

In this 1D setting it is not really clear how to construct an analog for the experiment in Figure 1.4, where a squared centered obstacle was considered. On the other hand, the case reported in Figure 2.11 is the analog of the case discussed in Figure 1.5 in the 2D setting. Indeed, the residence time is plotted as a function of the parameter n in the two cases $h = 40$ (disks) and $h = 2$ (triangles). This case mimics the increase of the abscissa of the center of the obstacle reported in Figure 1.5. In both cases the residence time is not monotonic and attains its minimum value when the defect sites are symmetric with respect to the center of the lane. In the $h = 40$ case, when n lies approximately between 50 and 110 the residence time is smaller than the corresponding value for the case $p = 0$. On the other hand, for $h = 2$, even if the non–monotonic behavior is recovered, the residence time is always larger than the one measured in the $p = 0$ case. This fact is consistent with the results plotted in Figure 2.9.

In order to explain our findings, similarly to what we did in the 2D case, we partition the lane into three parts: the part of the lane on the left of the left defect (left region), the part of the lane between the two defect sites (central region), and the part of the lane on the right of the right defect (right region). As in the 2D case, the residence time behavior is consequence of two effects in competition: the total time spent by the particles in the central region is smaller than the total time spent in the same region in absence of defect sites ($p = 0$). On the contrary, the total time spent

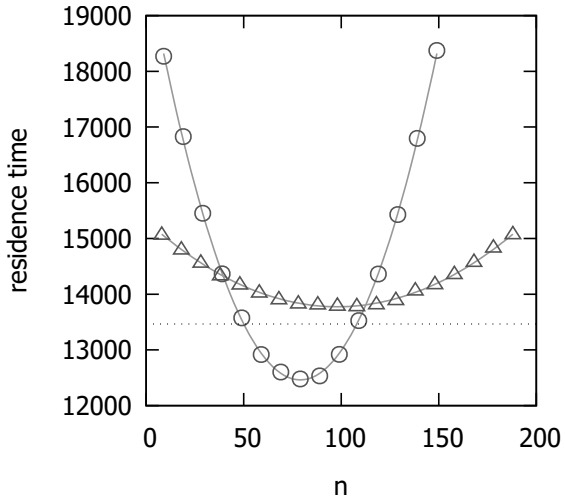

Figure 2.11: Residence time vs. n for $p = 0.84$, $L = 201$, $h = 40$ (disks), $h = 2$ (triangles), and total number of inserted particles $5 \cdot 10^7$. The dashed and the solid lines are as in Figure 2.9. The total number of particles exiting through the right exit is approximatively equal to $1.2 \cdot 10^5$ (disks) and $2.3 \cdot 10^5$ (triangles).

both in the left and in the right region is larger with respect to the time spent there in the $p = 0$ case. Both these two effects can be explained remarking that, in presence of defect sites, it is more difficult for the walker to enter the central region of the lane. The total residence time trend depends on which of the two effects dominates the dynamics of the walker.

These remarks are illustrated in Figure 2.12, data referring to the experiment associated with the disks in Figure 2.11 are reported. Again, one notes that the total residence time in the left and in the right regions of the lane are increased when the defect sites are present, this is due to the fact that for the particle it is more difficult to enter the central region in such a case. Moreover, precisely for the same reason the trajectory of the walker from its starting point 1 to its exit from the lane will visit the central region of the lane a number of time smaller than the number of times that the particle visits such a region in the $p = 0$ case. Thus, the residence time in the central region results to be smaller in presence of the defect site. Finally, similarly to what we did in the 2D case, the results in Figure 2.12 allows a complete interpretation of the residence time behavior depicted by the disks in Figure 2.11 (note that the maximum value of the variable n for the disks in Figure 2.11 is 150).

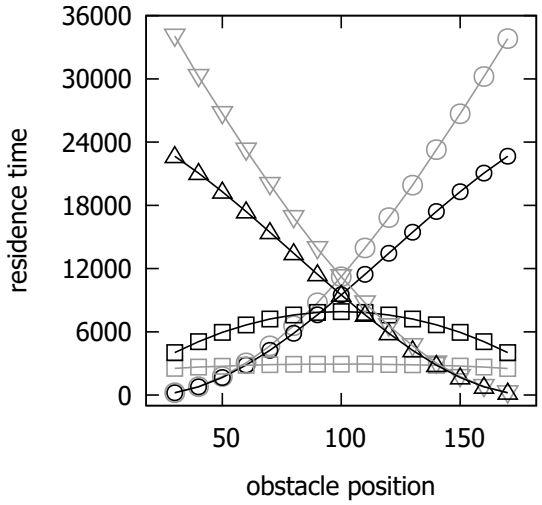

Figure 2.12: Total residence time in the left (circles), central (squares), and right (triangles) region of the lane in presence of the defect sites (gray) and in the $p = 0$ case (black). The experiment associated with the disks in Figure 2.11 is considered.

2.3 Analytic results

In this section we derive exact, though not explicit, expressions for the residence time defined in Section 2.2. To compute the residence time, we shall make use of the following result on a five state chain: the states are S, A, B, C, and D. The jump probabilities are as depicted in the figure 3.13 and the chain is started at time 0 in B. We prove that the probability Q_k, with $k \geq 1$, for the chain to reach D before S and return $k-1$ times to the site B before reaching D is

$$Q_k = p_B p_C [r_B + q_B p_A + p_B q_C]^{k-1} \quad , \tag{3.4}$$

where $r_B = 1 - (p_B + q_B)$. Indeed,

$$Q_k = p_B p_C \sum_{r=0}^{k-1} \binom{k-1}{r} (p_B q_C)^{k-1-r} \sum_{s=0}^{r} \binom{r}{s} (q_B p_A)^s (r_B)^{r-s}$$

where r counts the number of times that, starting from B, the chain either jumps to A or it stays in B and s counts the number of times that starting from B it jumps to A. The equation (3.4) is then proven by using the binomial theorem. We now consider again the 1D walk defined in Section 2.2. To compute the residence time we introduce the *local times*, i.e., the time spent by a trajectory at site i defined as

$$\tau_i = |\{t > 0, x_t = i\}| \tag{3.5}$$

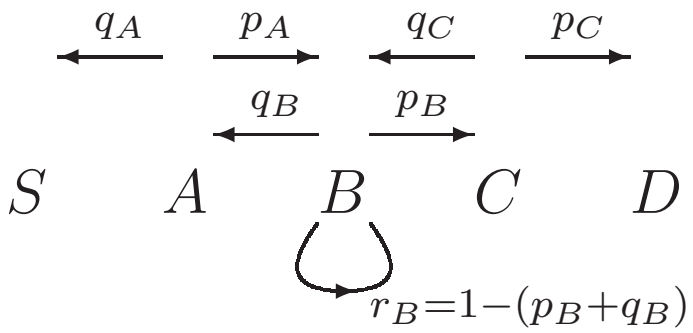

Figure 3.13: Schematic representation of the five state chain model.

for any $i = 1, \ldots, L-1$, where the cardinality $|\cdot|$ denotes the number of elements of a set. Provided T_L is finite, we have that

$$T_L = \sum_{i=1}^{L-1} \tau_i \quad . \tag{3.6}$$

Hence the residence time R defined in (2.2) can be expressed as

$$R = \sum_{i=1}^{L-1} \mathbb{E}_1[\tau_i | T_L < T_0] \tag{3.7}$$

and each term of the sum above can be proven to be

$$\mathbb{E}_1[\tau_i | T_L < T_0] = \frac{\mathbb{P}_1[T_i < T_0]}{\mathbb{P}_1[T_L < T_0]} \frac{p_B p_C}{[1 - (r_B + q_B p_A + p_B q_C)]^2} \quad , \tag{3.8}$$

where we defined the quantities

$$\begin{aligned} p_A &= \mathbb{P}_{i-1}(T_i < T_0), \quad & q_A &= \mathbb{P}_{i-1}(T_0 < T_i), \\ p_B &= \mathbb{P}_i(x_1 = i+1), \quad & q_B &= \mathbb{P}_i(x_1 = i-1), \\ p_C &= \mathbb{P}_{i+1}(T_L < T_i), \quad & q_C &= \mathbb{P}_{i+1}(T_i < T_L). \end{aligned} \tag{3.9}$$

Note that $p_A + q_A = 1$ and $p_C + q_C = 1$. Indeed, one has to average over all the trajectories of the walk the random variable returning the total number of visits of the site i. Hence, we have

$$\mathbb{E}_1[\tau_i | T_L < T_0] = \sum_{k=1}^{\infty} k \mathbb{P}_1[\{i \text{ visited } k \text{ times}\} | \{T_L < T_0\}]$$

and, using the definition of conditional probability and the Markov property,

$$\mathbb{E}_1[\tau_i | T_L < T_0] = \sum_{k=1}^{\infty} k \frac{\mathbb{P}_1[\{T_i < T_0\}]}{\mathbb{P}_1[\{T_L < T_0\}]} \mathbb{P}_i[\{T_L < T_0\} \cap \{k-1 \text{ returns to } i\}] \, .$$

The last probability appearing in the above expression is nothing but the quantity Q_k defined for the five state chain with the jump probabilities defined as in (3.9). Finally, (3.8) follows by noting that

$$\sum_{k=1}^{\infty} kQ_k = \frac{p_B p_C}{[1-(r_B + q_B p_A + p_B q_C)]^2} \quad .$$

Our strategy to compute the residence time is the following: for any $i = 1, \ldots, L-1$ we shall compute $\mathbb{E}_1[\tau_i | T_L < T_0]$ identifying the correct values of p_A, q_A, p_B, q_B, p_C, and q_C to be used, whose definition depends on the choice of the site i. Finally, the sum (3.7) will provide us with the residence time.

2.3.1 Residence time in the symmetric case

In the symmetric case, namely, $\epsilon = 0$ and $\lambda = 1/2$, by using the gambler's ruin result we have that

$$\mathbb{P}_1[T_0 < T_L] = \frac{L-1}{L} \tag{3.10}$$

and

$$\mathbb{P}_1[T_L < T_0] = \frac{1}{L} \quad . \tag{3.11}$$

This is a very classical problem in probability theory which can be found in any probability text book, see, for example, [28, paragraphs 2 and 3, Chapter XIV].

The residence time computation, which, in the gambler language, is the average duration of the game conditioned to the fact that the gambler wins, is not immediate. We use the formulas (3.7)–(3.9) proven above by defining suitably the five state chain jump probabilities. More precisely, $p_A = (i-1)/i$ is given by (3.10) with the initial point 1 replaced by $i-1$ and L replaced by i, $q_A = 1/i$ is similarly given by (3.11), $p_B = q_B = 1/2$ (and hence $r_B = 0$), $p_C = 1/(L-i)$ is given by (3.11) with the initial point 1 replaced by $i+1$ and L replaced by $L-i$, and $q_C = (L-i-1)/(L-i)$ is given similarly by (3.10). Moreover, since from (3.10) it also follows that $\mathbb{P}_1[T_L < T_0] = 1/L$ and $\mathbb{P}_1[T_i < T_0] = 1/i$, from (3.8) a straightforward computation yields

$$\mathbb{E}_1[\tau_i | T_L < T_0] = \frac{2}{L}(Li - i^2)$$

and, computing the sum in (3.7), we finally have

$$R = \frac{1}{3}(L-1)(L+1) \quad . \tag{3.12}$$

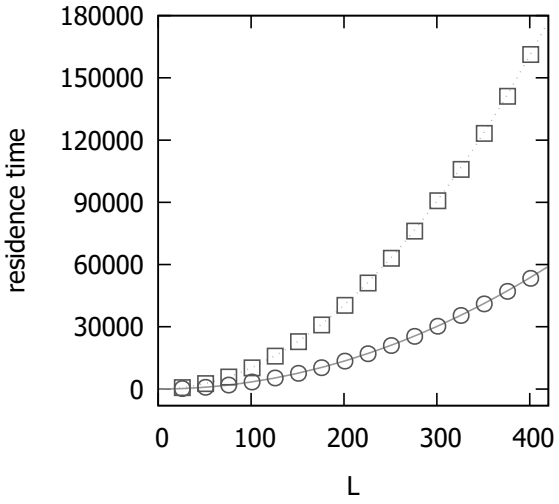

Figure 3.14: Residence time vs. L for the lane with no singular sites (symmetric case). The solid line is the exact solution (3.12), whereas circles are the average results of a Monte Carlo simulation with $5 \cdot 10^8$ particles started at the site 1. The squares represent the average duration of a Monte Carlo simulation of the symmetric random walk started from 0 and ended in L or $-L$, while the dashed line is the his expected duration L^2

In figure 3.14 the numerical estimate of the residence time in this symmetric case is compared to the exact result (3.12) and with the numerical estimate of the mean time that a symmetric walk started at 0 takes to reach either $-L$ or $+L$. It is interesting to remark that the mean time that a symmetric walk started at 0 takes to reach either $-L$ or $+L$ is L^2. This time can be computed as the average duration of the gambler's game. Thus, conditioning the particle to exit through the right end point decreases by a multiplicative factor the mean time that the particle needs to reach the distance L from the starting point, but it does not change the diffusive dependence on the length L of the lane.

2.3.2 Crossing probability in the general case

We now come back to the general 1D model introduced in Section 2.2. As a first step in the residence time computation, we have to calculate the *crossing probability* $\mathbb{P}_1[T_L < T_0]$ which appears at the denominator in (3.8). We first note that, by using repeatedly the Markov property, one gets

$$\mathbb{P}_1[T_0 < T_L] = 1 - p_1 p_2 p_3 p_4 p_5 \tag{3.13}$$

and, as a consequence

$$\mathbb{P}_1[T_L < T_0] = p_1 p_2 p_3 p_4 p_5 \tag{3.14}$$

where

$$\begin{aligned} &p_1 = \mathbb{P}_1[T_0 > T_{n+1}],\ p_2 = \mathbb{P}_{n+1}[T_0 > T_{n+2}], \\ &p_3 = \mathbb{P}_{n+2}[T_0 > T_{n+h+2}],\ p_4 = \mathbb{P}_{n+h+2}[T_0 > T_{n+h+3}], \\ &p_5 = \mathbb{P}_{n+h+3}[T_0 > T_L]. \end{aligned}$$

The five probabilities $p_1, \dots, p_5$ can be computed explicitly and the remaining part of this section is devoted to the computation of these quantities. For p_1 one has to use (3.11) with L replaced by $n+1$ to deduce that

$$p_1 = \frac{1}{n+1} \quad . \tag{3.15}$$

To compute p_2, we first note that, once the particle is in n, the probability to come back to $n+1$ before reaching 0 is equal to $n/(n+1)$, as it follows by using (3.10) with the initial point 1 replaced by n and L replaced by $n+1$. Hence,

$$p_2 = \sum_{r=0}^{\infty} \sum_{k=0}^{r} \binom{r}{k} \Big[(1-\varepsilon-\lambda)\frac{n}{n+1}\Big]^{r-k} \varepsilon^k \lambda$$

where r counts the number of times that, starting from $n+1$, the walker either jumps to n or it stays in $n+1$ and k counts the number of times that the walker stays in $n+1$. Using the binomial theorem, we get

$$p_2 = \frac{\lambda}{1 - [(1-\varepsilon-\lambda)n/(n+1) + \varepsilon]} \, . \tag{3.16}$$

In order to compute p_3, note that, using (3.10) and (3.11) with initial point $n+2$ and replacing L with $h+1$, one has $\mathbb{P}_{n+2}[T_{n+1} < T_{n+h+2}] = h/(h+1)$ and $\mathbb{P}_{n+2}[T_{n+h+2} < T_{n+1}] = 1/(h+1)$. Hence,

$$p_3 = \frac{1}{h+1} \sum_{k=0}^{\infty} \Big(\frac{h}{h+1}\Big)^k p_2^k = \frac{1}{1+h(1-p_2)} \, , \tag{3.17}$$

where k counts the number of times that, starting from $n+2$, the walker reaches $n+1$ before $n+h+2$.

To compute p_4, we first need to calculate $\xi = \mathbb{P}_{n+h+1}[T_0 > T_{n+h+2}]$. Starting from $n+h+1$ the probability to reach $n+h+2$ before $n+1$ is $\mathbb{P}_{n+h+1}[T_{n+h+2} < T_{n+1}] =$

$h/(h+1)$, where we used (3.10) with initial point $n+h+1$ and L replaced by $h+1$. Hence, $\mathbb{P}_{n+h+1}[T_{n+1} < T_{n+h+2}] = 1/(h+1)$. Thus,

$$\xi = \frac{h}{h+1} + \frac{1}{h+1} p_2 \frac{1}{h+1} \sum_{k=0}^{\infty} \left(p_2 \frac{h}{h+1} \right)^k$$

where k counts the number of times that the walker returns to $n+1$ after having visited it for the first time. We have also used that $\mathbb{P}_{n+2}[T_{n+1} < T_{n+h+2}] = h/(h+1)$. With some algebra we find the expression

$$\xi = \frac{p_2 + h(1-p_2)}{1 + h(1-p_2)} \quad . \tag{3.18}$$

Now, we have all the ingredients to compute p_4. Indeed,

$$p_4 = (1-\varepsilon-\lambda) \Big[\sum_{r=0}^{\infty} \sum_{k=0}^{r} \binom{r}{k} \varepsilon^k (\lambda\xi)^{r-k} \Big]$$

where $r-k$ counts the number of times that the walker starting from $n+h+2$ jumps to $n+h+1$ and where k counts the number of times that the walker stays at $n+h+2$. A simple calculation provides the result

$$p_4 = \frac{1-\varepsilon-\lambda}{1-(\lambda\xi+\varepsilon)} \quad . \tag{3.19}$$

Finally, to compute p_5 we remark that $\mathbb{P}_{n+h+3}[T_L < T_{n+h+2}] = 1/(w+1)$ and $\mathbb{P}_{n+h+3}[T_{n+h+2} < T_L] = w/(w+1)$, as it can be deduced by (3.11) and (3.10) by using as initial point the point $n+h+3$ and replacing L by $w+1$. Then,

$$p_5 = \frac{1}{w+1} \sum_{k=0}^{\infty} \left(\frac{w}{w+1} p_4 \right)^k = \frac{1}{1+w(1-p_4)} \quad . \tag{3.20}$$

Finally, plugging the equations (3.15)–(3.20) in (3.14), we find the expression

$$\mathbb{P}_1[T_L < T_0] = \frac{\lambda}{(1+h)(1-\varepsilon-2\lambda)+\lambda L} \tag{3.21}$$

for the probability that the particle started at the site 1 reaches L before visiting 0. It is interesting to remark that in the case $\varepsilon = 0$ and $\lambda = 1/2$ the expression (3.11) valid in the symmetric case is recovered.

2.3.3 Residence time in presence of defects

The last step, necessary to complete our algorithm to compute the residence time, is that of listing the expression that must be used for the probabilities (3.9) for the

different choices of i on the lattice. In this last section, in order to get simpler formulas, we focus on the case that has been studied numerically, that is to say, we choose the parametrization (2.3). First of all we note that the expression (3.21) of the probability that the particle started at the site 1 reaches L before visiting 0 simplifies to

$$\mathbb{P}_1[T_L < T_0] = \frac{1-p}{p(1+h)+(1-p)L} \quad . \tag{3.22}$$

The site i in the lattice can be chosen in nine possible different ways: in the bulk of the three regions on the left, between and on the right of the defect sites, as one of the four sites neighboring the defects and as one of the two defect site. We list only five cases, the remaining four can be deduced exchanging the role of the parameters n and w. Note that we shall only list either p_A or q_A and p_C or q_C; the missing parameter can be deduced by the equations $p_A + q_A = 1$ and $p_C + q_C = 1$.

Case $1 \le i \le n-1$. First note that $\mathbb{P}_1[T_i < T_0] = 1/i$ is given by (3.11) with initial site 1 and L replaced by i. Moreover, $p_A = (i-1)/i$ follows from (3.10) with initial site $i-1$ and L replaced by i. We trivially have that $p_B = q_B = 1/2$. Finally, $p_C = (1-p)/[p(1+h)+(1-p)(L-i)]$ follows from (3.22) with initial site $i+1$ and L replaced by $L-i$.

Case $i = n$. First note that $\mathbb{P}_1[T_i < T_0] = 1/n$ is given by (3.11) with initial site 1 and L replaced by n. Moreover, $p_A = (n-1)/n$ follows from (3.10) with initial site $n-1$ and L replaced by n. We trivially have that $p_B = q_B = 1/2$. Finally, we note that q_C has the same structure as p_4, thus, by exchanging the role of n and w, from (3.16), (3.18), and (3.20) we have that $q_C = 1/[2-p-(1-p)\zeta]$ where

$$\zeta = \frac{\pi + h(1-\pi)}{1+h(1-\pi)} \quad \text{and} \quad \pi = \frac{1-p}{2-p-\frac{w}{w+1}} \quad . \tag{3.23}$$

Case $i = n+1$. First note that $\mathbb{P}_1[T_i < T_0] = 1/(n+1)$ is given by (3.11) with initial site 1 and L replaced by $n+1$. Moreover, $p_A = n/(n+1)$ follows from (3.10) with initial site n and L replaced by n. We trivially have that $p_B = (1-p)/2$ and $q_B = 1/2$. Finally, we note that q_C has the same structure as ξ, thus, by exchanging the role of n and w, from (3.18) we have that $q_C = \zeta$, see (3.23).

Case $i = n+2$. First note that $\mathbb{P}_1[T_i < T_0] = p_1 p_2$, hence, using (3.15) and (3.16), an easy computation yields $\mathbb{P}_1[T_i < T_0] = (1-p)/[(n+1)(2-p-n/(n+1))] = (1-p)/(2+n-p(n+1))$ since, with the parametrization that we are adopting in this section

$$p_2 = \frac{1-p}{2-p-n/(n+1)} \quad .$$

Moreover, $p_A = p_2$ by definition and $p_B = q_B = 1/2$. Finally, we note that q_C has the same structure as ξ with h replaced by $h-1$. Thus, by exchanging the role of n and w, from (3.18) we have that $q_C = [\pi + (h-1)(1-\pi)]/[1 + (h-1)(1-\pi)]$, with π defined in (3.23).

Case $n+3 \leq i \leq n+h$. First note that $\mathbb{P}_1[T_i < T_0] = p_1 p_2 \bar{p}_3$, where $\bar{p}_3$ has the structure of p_3 with h replaced by $i-(n+2)$. Hence (3.17) gives us $\mathbb{P}_1[T_i < T_0] = (p_1 p_2)/(1 + (i-n-2)(1-p_2))$ with p_1 and p_2 as in the previous case. Moreover, p_A has the same structure as ξ with h replaced by $i-n-2$ so $p_A = (p_2 + (i-n-2)(1-p_2))/(1 + (i-n-2)(1-p_2))$ and $p_B = q_B = 1/2$. Finally, we note that q_C has the same structure as ξ with h replaced by $n+h+1-i$. Thus, by exchanging the role of n and w, from (3.18) we have that $q_C = [\pi + (n+h+1-i)(1-\pi)]/[1 + (n+h+1-i)(1-\pi)]$, with π defined in (3.23).

Chapter 3

Pedestrian dynamics in dark regions

We introduce a simple lattice model without exclusion in order to study the motion of pedestrians. The model, despite the basic rules of its dynamics, captures some interesting features of the difficulty in obtaining an optimal strategy of evacuation in a very difficult situation (no visibility, no external lead to the exits). We introduce a buddying threshold (of no-exclusion per site) mimicking the tendency of pedestrians to form groups (herding effect) and to cooperate. We examine how the dynamics of the crowd is influenced by the tendency to form big groups. We observe that the more the tendency to form large groups is present, i.e. the bigger the buddying threshold is, the more the evacuation will be inefficient. We find very interesting results in the investigation of how obstacles influence the dynamics. A strong asymmetry emerges in the effect of the same obstacle placed in different position.

3.1 The model

This lattice model has been introduced in [17, 18] by adapting some ideas introduced in [3] to study the ionic currents in cell membranes and further developed in [4].

The lattice we consider is a finite square $\{1, 2, \ldots, L\} \times \{1, 2, \ldots, L\} \subset \mathbb{Z}^2$ with odd side length L. Inside this lattice square we may consider the presence of an obstacle of size $l_o \times l_v$, a rectangular subset of the previous square $\{x_o, x_o+1, \ldots, x_o+l_o-1\} \times \{x_v, x_v+1, \ldots, x_v+l_v-1\}$ such that $3 \leq x_o$; $x_o + l_o \leq L-1$ and $3 \leq x_v$; $x_v + l_v \leq L-1$. We define as our domain Λ the set difference of the previous two sets. In the sequel we will call Λ the *corridor*.

Let $e_1 = (1, 0)$ and $e_2 = (0, 1)$ denote the coordinate vectors in $\mathbb{R}^2$. Every element

x of Λ will be called a *cell* or *site*. The external boundary of the corridor is made of four segments made of L cells each; the point at the center of one of these four sides, e.g. the right side, is called *exit*. The sites, not belonging to Λ, on the boundary of rectangular obstacle are called internal boundary.

We consider the motion of N individuals in the corridor Λ, so N will be a positive integer. We consider the state space $X = \{0, \dots, N\}^\Lambda$ and for any state $n \in X$ we denote by $n(x)$ the number of individuals at the site x. The model does not have an exclusion rule: we do not control how many agents can be at a cell x. Although some states of the system would be unlikely, in principle $n(x)$ can be any integer in $[0, N]$ for a generic site x.

We define a Markov chain n_t on the finite state space X with discrete time $t = 0, 1, \dots$. The parameters of the process are the integer $T \geq 0$ called *threshold* and $W \geq 0$ called *wall stickiness*. We finally define the function $S : \mathbb{N} \to \mathbb{N}$ as

$$S(k) = \begin{cases} 1 & \text{if } k > T \\ k + 1 & \text{if } k \leq T \end{cases}$$

for any $k \in \mathbb{N}$. Note that for $k = 0$ we have $S(0) = 1$.

When a particle try to move, it jumps on a nearest neighbor or it stays at rest according to probabilities depending on the position of the particle and the state of the system. The probabilities are defined as:

$$p(x, y) = \frac{w(x, y)}{D(x)}, \qquad y \in \{x, x + e_1, x - e_1, x + e_2, x - e_2\} \tag{1.1}$$

where the denominator

$$D(x) = w(x, x) + \sum_{i=1}^{2} w(x, x + e_i) + \sum_{i=1}^{2} w(x, x - e_i)$$

is just a factor to normalize the weights and obtain a probability, while the weights $w(x, y)$ take into account the position of the particle and the number of particles present in the sites y.

For any cell x situated in the interior of the corridor Λ, i.e. if all the nearest neighbors y of x are in Λ, $y = x \pm e_i$, $i = 1, 2$, and for the state $n \in X$, we define

$$w(x, x) = S(n(x))$$
$$w(x, y) = S(n(y)).$$

The function $S(\cdot)$ will return a value dependent on our choice of the buddying threshold T. It is worth stressing that T is a threshold in the probability that such a cell is

likely to be occupied. If $n(x) > T$, so there are too much particles in the site x, the function $S(n(x))$ will take value 1 and $p(x, y)$ the value $1/D(x)$. This does not mean that T acts as a threshold in $n(x)$, the number of individuals per cell.

If the cell x is one of the four corners $\{(1, 1), (1, L), (L, 1), (L, L)\}$ of the corridor Λ, only two sites y among nearest neighbors of x are internal to Λ, while two sites z are cells out of Λ on the boundary. For the state $n \in X$, we define the weights

$$\begin{aligned} w(x, x) &= S(n(x)) + 2W \\ w(x, y) &= S(n(y)) + W, \\ w(x, z) &= 0. \end{aligned}$$

In this case we are introducing the additional term W that is mimicking the stickiness of the wall. That is this parameter takes into account the possibility that people prefer to move nearby the wall in condition of lack of visibility.

Consider now the case in which the particle is on a cell that has a neighbor site on the external or on the internal boundary. For $x \in \Lambda$ neighboring the boundary (but neither in the corners, nor neighboring the exit), y nearest neighbors in Λ, z nearest neighbor out of Λ on the boundary and for the state $n \in X$, we define the weights

$$\begin{aligned} &w(x, x) = S(n(x)) + W \\ &w(x, y) = S(n(y)) && \text{if y is in the interior of } \Lambda \\ &w(x, y) = S(n(y)) + W, && \text{for y neighboring the boundary } \Lambda \\ &w(x, z) = 0. \end{aligned}$$

Finally, we have to define the weights if x is the site in Λ neighboring the exit. We propose two different choices mimicking two different situations. If the exit is clearly identifiable when particles are in the closest cell, we should consider particles to exit with probability 1. We will call this case *sure exit*.

If the exit is not clearly identifiable, we altough assume it is the most likely site to jump to and we treat it as if it were occupied by the threshold number of pedestrians. More precisely, in this case for $n \in X$, we define the weights

$$\begin{aligned} &w(x, x) = S(n(x)) \\ &w(x, y) = S(n(y)) && \text{if y is in the interior of } \Lambda \\ &w(x, y) = S(n(y)) + W, && \text{for y neighboring the boundary } \Lambda \\ &w(x, \text{exit}) = T + 1. \end{aligned}$$

We will call this case *threshold exit*.

Note that if we consider the threshold to be 0 (so pedestrians are not attracted by other people), we recover particles moving via independent symmetric random walks.

In the sequel until explicitly stressed out we are firstly considering the case of absence of the obstacle into the square lattice. All the simulations are for $L = 101$.

3.2 Parallel vs. serial update

We consider at the initial time $t = 0$ the N particles to be located randomly in the corridor Λ. We draw the initial position of each particle on the cell chosen randomly with uniform probability $1/(L^2 - l_o l_v)$, where $l_o l_v$ is the number of cells occupied by of the obstacle. Let us consider the first time step: all the probabilities $p(x, y)$ governing the jumps of each particle are defined by (1.1) looking at the state of the system at time $t = 0$. We propose two different definitions of the dynamics. As the first case, we consider all the particles to update their position simultaneously at each time step (parallel update). The second possibility is to consider just one particle to update its position at each time step (serial update). That is in this second case we draw at each time a particle uniformly among the N in Λ and we let it evolve its position.

Note that to have comparable results we have to rescale the time interval in the serial update case as follows: observing that in the case of parallel rule we let all N particles update their position, we consider as the new unit of time $t' = Nt$. In this way after a unit time in both cases, parallel and serial update, we consider N updates in particles positions. This choice reflects the idea that at each time we consider all the pedestrians to have the possibility to move one step.

In the sequel all the data plot for the serial update case will refer to the time unit t', so we will omit to stress it again.

We want to compare the behavior of the system in these two different cases, focusing on the *average outgoing flux*. This is defined as the ratio between the number of particles that exited the corridor in the time interval $[0, t_f]$ and the time t_f. In the simulation we use $t_f = 10^7$. To study the overall exit flux we consider the stationary case in which the same number of particles is present in the corridor at every time. This means that when a particle finds the exit and goes out from the lattice, we insert a new one at the center of the opposite side of the lattice.

Let us consider as the first case the square lattice with no obstacle and the wall interaction $W = 0$. In figure 2.1 we show the stationary average flux for different choices of the threshold $T = 0$, 2, 5, 30, 300 and some values of N between 50 and 10000, for particles evolving following the parallel update rule and for the two different

choices of the exit rule that we previously described. We can stress some evidences.

As one should expect, the choice of the *sure exit* favors the outgoing flow. Indeed, in this case the particles in front of the exit go always out of Λ at the first next update of their position, while in the other case they can remain in Λ with probability bigger than 0. This is clearly visible for the case of $T = 0,\ 2$, but it is not so evident for choices of larger threshold. In figure 2.2 is presented a comparison between the data for the two different exit rules, for the values of the threshold $T = 5,\ 30,\ 300$. Since in the figure the black and the grey symbols for large values are indistinguishable, this picture shows that the difference between the two cases tends to vanish when T grows.

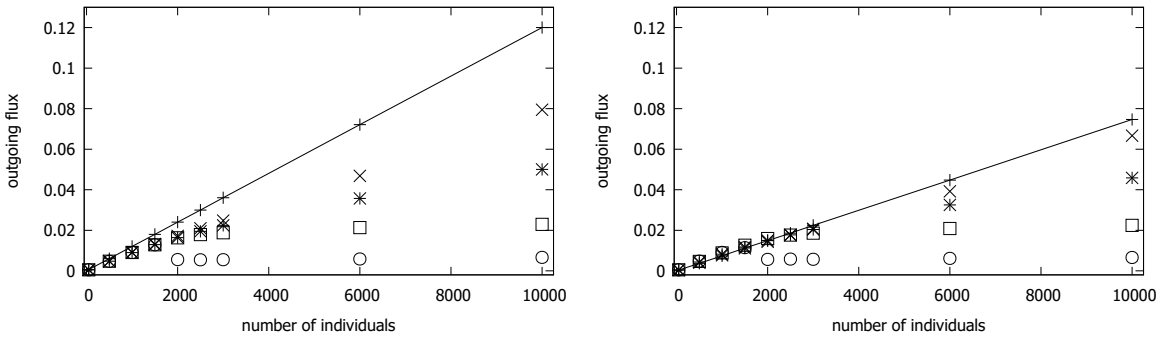

Figure 2.1: **Averaged outgoing flux vs. number of pedestrians.** The symbols $+$, $\times$, $*$, the squares and the circles represent respectively the cases $T = 0, 2, 5, 30, 300$, with $L = 101$, $W = 0$ and parallel update. The solid line has been obtained by fitting the Monte Carlo data corresponding to the case $T = 0$. On the left we show the simulation results for the choice of the *sure exit*, on the right the data refer to the *threshold exit*.

This fact can be explained as the consequence of our choice of the probability for a particle to go out in the case of the *threshold exit*. Indeed we can notice that in the case of small values of T, think for instance to 0 or 2, the weight we assign to the exit site, that is $T + 1$, is comparable to the weight of the nearest neighbor, so particles close to the exit often jump to one of the other sites. This effect is reduced if the value of T grows, since in that case the weight of the exit site is likely to be significantly larger than that one of the nearest sites, so the behavior of the system becomes really close to that one of the system in the case of sure exit.

This remark explains another phenomenon observed in figure 2.1 and stressed in the zoom in figure 2.3. If we consider the threshold exit rule, for small values of N, the

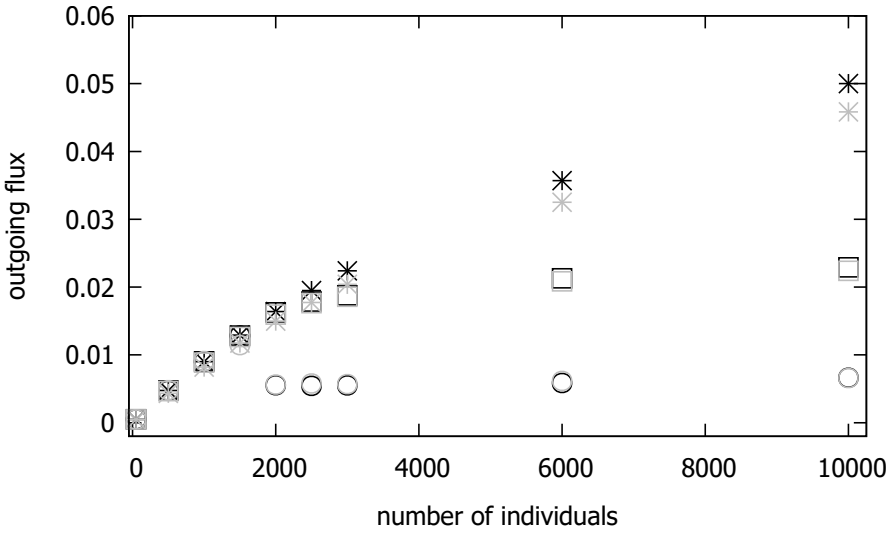

Figure 2.2: **Averaged outgoing flux vs. number of pedestrians.** We show a comparison of the simulation results for $T = 5$ ($*$), 30 (squares), 300 (circles), in the case of *sure exit* (in black), and in the case of *threshold exit* (in gray). Note that gray and black circles and squares are overlapping.

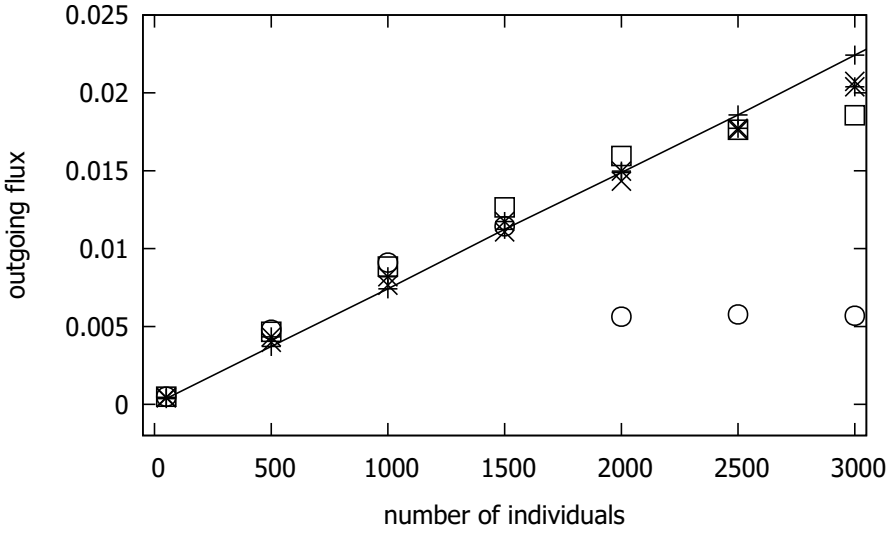

Figure 2.3: **Averaged outgoing flux vs. number of pedestrians.** The symbols $+$, $\times$, $*$, the squares and the circles represent respectively the cases $T = 0, 2, 5, 30, 300$, with $L = 101$, $W = 0$ and parallel update. The solid line has been obtained by fitting the Monte Carlo data corresponding to the case $T = 0$. The data refer to the a zoom for $N \leq 3000$ of the case of *threshold exit* (figure 2.1, right picture).

average outgoing exit flux has a small increment in the case of large threshold with

respect to the independent random walk case ($T = 0$). This is due to the fact that in a regime of small number of particles, it is really unlikely to have many particles on the nearest neighbors of the sites closest to the exit, so the weight of the exit site is clearly much larger than the other nearest neighbors. Thus, the probability to jump out is significantly bigger for large T than in the case of small values of the threshold.

This phenomenon can be observed only in the case of small density of particles, and it is obviously not present if we choose the sure exit rule. If the density of particles grows, the interaction among particles plays a much more important role in the dynamics, influencing crucially the behavior of the overall flux, as we will comment later on, so this increased flux effect disappears.

As in figure 2.1, in figure 2.4 we propose the data plot of the average outgoing flux as function of the number of particles N for the serial update and for the different choices of the exit rule. Analogous consideration as we made before for the parallel update can be made.

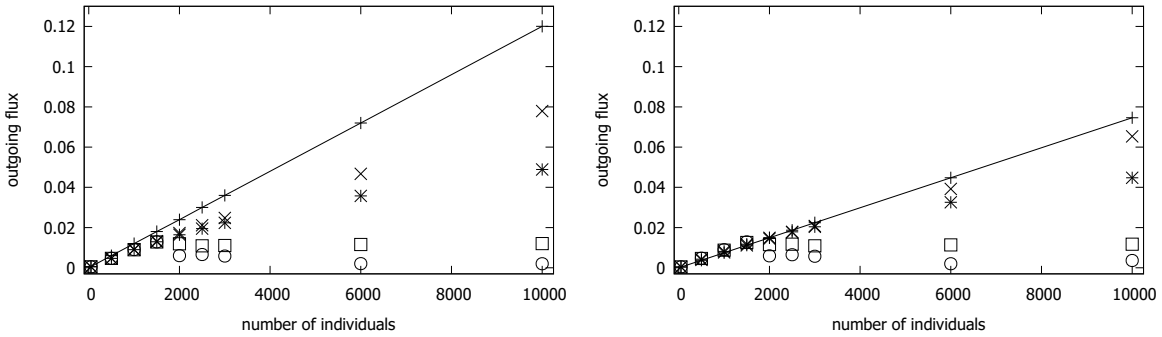

Figure 2.4: **Averaged outgoing flux vs. number of pedestrians.** The symbols $+$, $\times$, $*$, the squares and the circles represent respectively the cases $T = 0, 2, 5, 30, 300$, with $L = 101$, $W = 0$ and serial update. The solid line has been obtained by fitting the Monte Carlo data corresponding to the case $T = 0$. On the left we show the simulation results for the choice of the *sure exit*, on the right the data refer to the *threshold exit*.

Some general phenomena governing the dynamics of this model can be observed on how the value of the threshold influences the outgoing flux. We can see that when the number of particles is sufficiently small, i.e. the average density of particles is small, the outgoing flux does not differ substantially even changing $T > 0$. This happens because the effect of big values of T is to favor the formation of groups of particles moving together. These clusters of particles moves very slowly in the corridor, so their

presence decrease the outgoing flux, but they are not very stable especially if their size (the number of particles involved) is not very big.

Anyway, clusters of agents do not appear if the number of particles is too much small. In this case, it is difficult for a particle to encounter many others and form a stable cluster. The overall effect of a positive threshold is in this case just to favor interaction among a small groups of particles, obtaining a little slow down in the exit of particles with respect to the independent walk of particles ($T = 0$). This is easily observable for the sure exit case. In the case of threshold exit, this effect competes with the increase of probability to exit due to the weight of the exit site discussed before, giving an overall effect of increasing the flux.

What happen if the number of particles grows? When the number of agents is larger, the probability to form a big stable cluster of particles increases. Obviously, since the threshold represents the maximum size of an attractive group, the more the threshold is large the more it is easy to see the formation of big stable clusters of particles. Once the clusters are formed, it is therefore likely that agents will spend a substantial amount of "effortless" time in such large clusters that will ultimately prevent them from exiting as indicated in Fig. 2.5 that depicts cluster formation behavior for $N = 10000$ and $T = 300$.

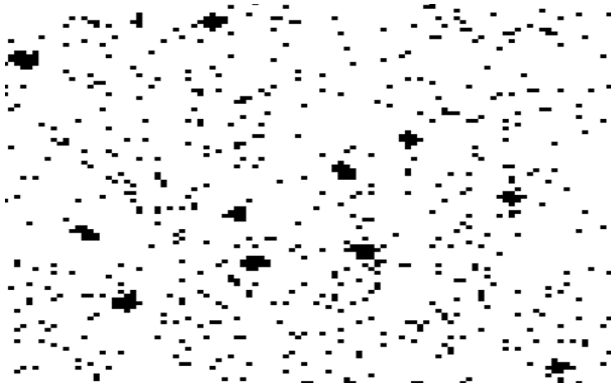

Figure 2.5: **Typical configuration.** Typical configuration of the system at large time in the case $T = 300$, $L = 101$, and $N = 10000$. White and black points denote, respectively, empty and occupied sites of the lattice.

This is shown in the data plots, figures 2.1 and 2.4. We see in the plot, for $N \leq 1500$, that the behavior of the outgoing flux for different T is qualitatively the same. This happens until the number of particles grows to 2000, where for large values of T (300 in the plot), we are in a regime of clusters formation. The resulting effect for $T = 300$ is a flux drop (the flux suddenly decreases). Once the system is in this cluster

formation regime, the increase of number of particles does not affect significantly the outgoing flux, so we see for instance that the outgoing flux for $T = 300$ and bigger values of N remains roughly constant.

If the system is not in a cluster formation regime the outgoing flux grows as a function of N. Note that for different values of threshold the system may reach the cluster formation regime for N bigger or never reach it (small values of T).

The choice of the update rule influences which values of the parameters of the system give a clustering regime. In the case of serial update, the system reaches it earlier, for smaller number of individuals N, and the flux stabilizes at a lower value. This is due to the fact that with the serial update rule the clusters of particles are more stable. Indeed, when the occupation number on a site exceeds the threshold, at the next time step if become unattractive for all particles neighboring it, and a parallel update favors to break the cluster. With the serial update rule, a cluster loses some particles but it is very difficult to break. Nevertheless, if T is sufficiently small, the system does not form clusters.

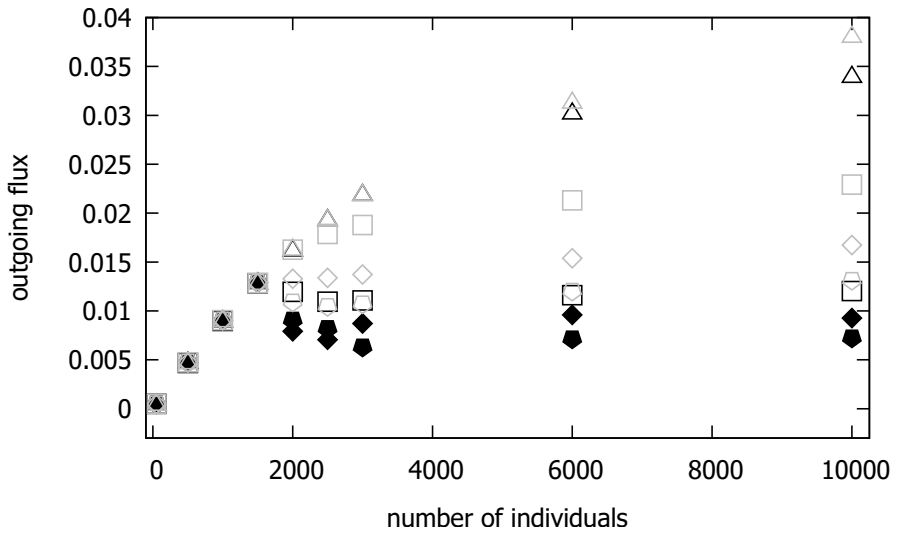

Figure 2.6: **Averaged outgoing flux vs. number of pedestrians.** The triangles, the squares, the diamonds and the pentagons represent respectively the cases $T = 10, 30, 60, 100$, with $L = 101$, $W = 0$ and serial update (in black) and parallel update (in grey). The case 0, 2, 5 are not reported since at this scale would be indistinguishable.

The comparison between the outgoing flux behavior with the different choices of the update rules is illustrated in figure 2.6. Note that in the figure we do not report the plot of the outgoing flux for $T \leq 5$ because the values measured for the flux are

very close, at this scale we cannot distinguish the plot for the two exit rules. For larger values of T we plot the outgoing flux as a function of N for $T = 10$, 30, 60, 100. As a test of the different behavior of the two cases, let us see for instance the squares in the picture, corresponding to the case $T = 30$. With the parallel update the flux is monotonic in N, while with the serial update the system is already in the clustering regime for $N = 2000$. For $T = 10$ the system shows the same behavior with the different rules until the number of particles grows up to 6000.

Totally analogous results hold in the case of threshold exit too.

In the sequel we will focus mainly on the parallel update and on the sure exit, so these choices will be assumed when it is not differently stressed.

3.3 The interaction with the wall

We study the dependence of the dynamics on the possible choice of the parameter $W \geq 0$, the wall stickiness. We introduce this parameter to take into account the possibility that the pedestrian may have the tendency to move close to the wall in condition of lack of visibility.

We can expect that the choice of a positive value for the parameter W can improve the outward flux. This intuition follows from the fact that the number of sites neighboring the boundary are of order L while the total number of sites is of order L^2. So the choice of the parameter $W > 0$ helps reducing the random walk on a number of sites of lower order and the individuals will find the exit earlier. On the other hand we can expect that the localization of the particles on the wall can favor the formation of clusters of particles, that we have seen to slow down the evacuation.

Our simulations show that the leading effect is the increase of the flux rate. In figure 3.7 we show the effect of the wall interaction on the outgoing flux. We plot the measured average outgoing flux for different values of $W \geq 0$. In the figure, to have a readable picture, we show the cases $T = 0$ in the left panel, and the cases $T = 5$ and $T = 300$ in the right panel, but the increasing effect is present for any value of the threshold. We use grey tones to distinguish the values assumed by $W = 0, 1, 3, 5, 10$, using lighter tone when W is increasing. For any fixed value of the threshold T, the flux is monotonic increasing in W. The increment is bigger when the clustering effect is not so strong, hence for small values of T.

It is interesting to notice that even if the measured value of the flux increases when W grows, for any fixed value of W the plot of the average flux as function of N has the same behavior of the one resulting in the case $W = 0$. To illustrate this

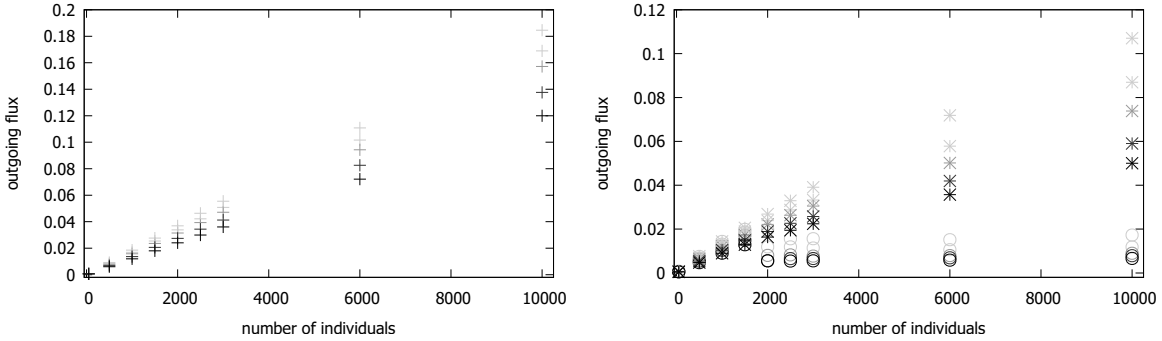

Figure 3.7: **Averaged outgoing flux vs. number of pedestrians.** Simulations with $L = 101$, parallel update, and, from the darkest to the lower grey, $W = 0, 1, 3, 5, 10$. On the left: plot of the average outgoing flux for $T = 0$ $(+)$. On the right: plot of the average outgoing flux for $T = 5$ $(*)$ and $T = 300$ (circles).

observation, we construct a plot analogous to the one we made for $W = 0$ in figure 2.1. The qualitative behavior of the outgoing flux as a function of N does not change for $W > 0$. We see in figure 3.8 illustrating the case $W = 3$ that both with the sure exit rule and with the threshold exit the plot are similar to those in figure 2.1.

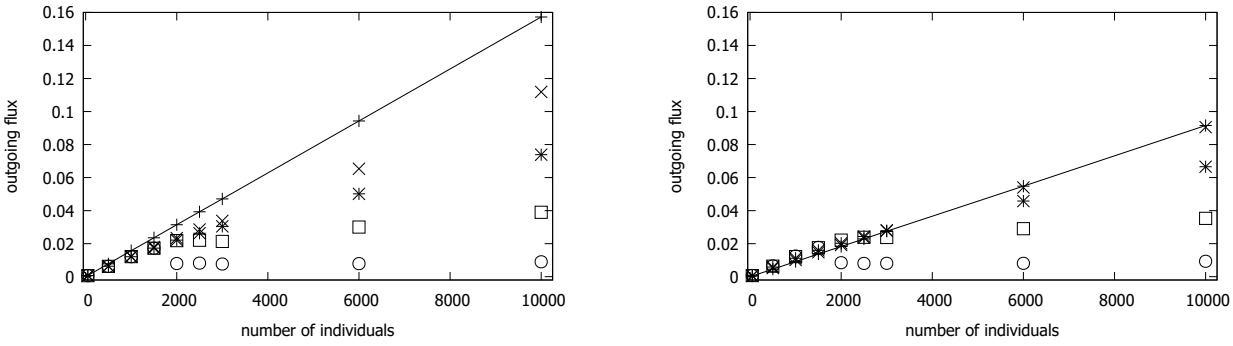

Figure 3.8: **Averaged outgoing flux vs. number of pedestrians.** The symbols $+$, $\times$, $*$, the squares and the circles represent respectively the cases $T = 0, 2, 5, 30, 300$, with $L = 101$, $W = 3$, and parallel update. The solid line has been obtained by fitting the Monte Carlo data corresponding to the case $T = 0$. On the left we show the simulation results for the choice of the *sure exit* on the right the data refer to the *threshold exit*.

We remark also that even in this case, as observed earlier for $W = 0$, the clustering regime starts for $T = 300$ when the number of individuals grows up to 2000. For small

number of particles ($N \leq 1500$) the measured outgoing fluxes for any fixed value of the parameter W are really close. So the measured flux does not depend on T for these values of N.

3.4 The role of the obstacle

We have seen even in the study of the residence time that it is not always obvious to understand the effect of a different geometry induced by an obstacle on the dynamics. Note also that for the value $T = 0$, particles move performing independent symmetric random walks. Nevertheless, the results we found in Chapter 2 are not directly applicable to this model, not even for $T = 0$. This is due to the different boundary conditions.

We expect that the obstacle can influence the resulting outgoing flux, because of excluded volume, in two different ways. On the one hand it can make easier for a particle to find the exit, for instance making more difficult to reach a region far from the exit, on the other the presence of an obstacle can favor the clustering and influence in which region the cluster is formed. How will the positioning of the obstacle affect the measured flux? Does exist a suitable positioning of the obstacle that can maximize the flux?

We can notice in our simulation that if the obstacle is sufficiently small it does not visibly affect the flux.

Let us start considering a small square obstacle placed at the center of the lattice. The obstacle is 21×21. In figure 4.9 we see the gray symbols representing the flux measured in presence of the obstacle to be really close to that one measured for the empty lattice. An interesting remark is that differently to the empty lattice case, when $W = 0$ the flux drop for $T = 300$ happens for a smaller N (1500 in the figure).

We consider now the case of a bigger obstacle. In figure 4.10 we show the behavior of the flux if it is present a squared obstacle with side 41 with center in the center of the corridor. For small values of the threshold there is not a great difference in the average exit flux. We can see it for $T = 0$, 2, 5. It is instead interesting to note the clustering induced by the obstacle for large values of T. The flux drop for $T = 300$ happens for $N = 1500$ both if $W = 0$ and if $W = 3$. We recall that in absence of obstacle we observe this flux drop for $T = 300$ for the first time if $N = 2000$. Even for $T = 30$, the flux in the case $W = 0$ is reduced by the cluster formation (see the squares in figure 4.10, in the left panel, the grey symbols are always below the black).

We recall here that in the previous models in Chapters 1, 2, a squared obstacle at

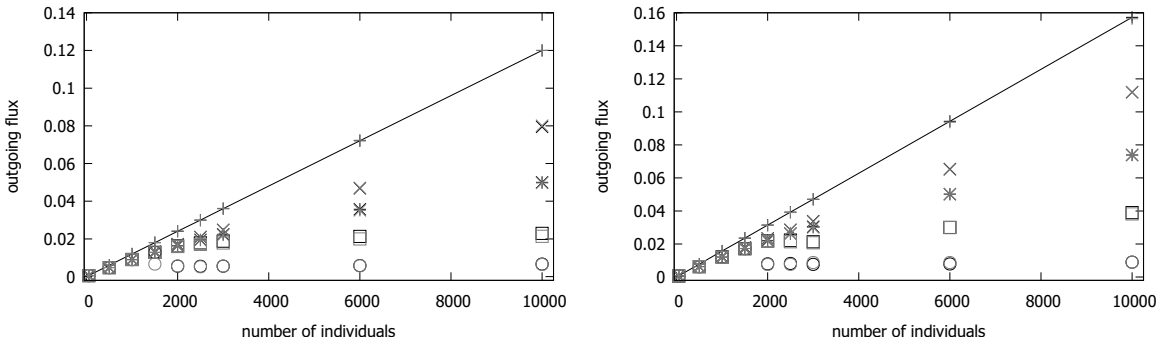

Figure 4.9: **Averaged outgoing flux vs. number of pedestrians.** The symbols $+$, $\times$, $*$, the squares and the circles represent respectively the cases $T = 0, 2, 5, 30, 300$, with parallel update, $L = 101$ and a squared obstacle with side 21 placed in the lattice with center in $(51, 51)$. The gray symbols represent the case of presence of the obstacle, while the black symbols refer to the empty lattice. The solid line has been obtained by fitting the Monte Carlo data corresponding to the case $T = 0$. On the left we show the simulation results for $W = 0$, on the right the data refer to $W = 3$.

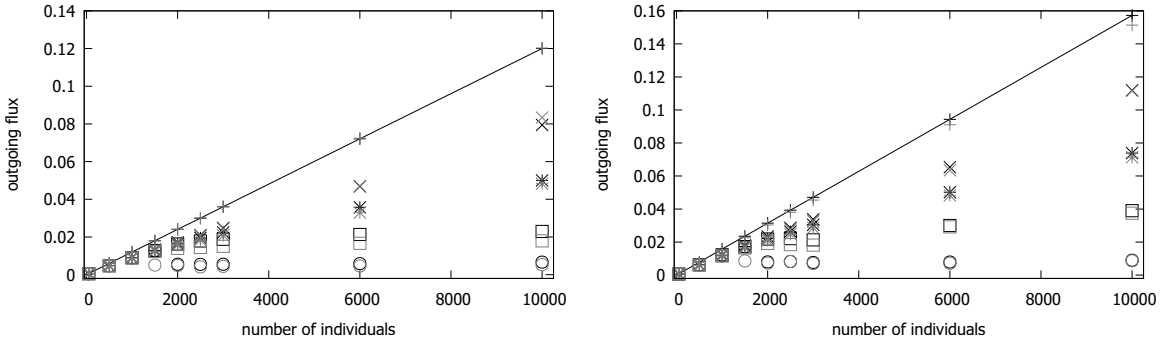

Figure 4.10: **Averaged outgoing flux vs. number of pedestrians.** As in figure 4.9, with a squared obstacle with side 41 and center in $(51, 51)$.

the center of the strip produced a smaller residence time, i.e., it selected the particles that cross the strip in a smaller time. Moreover, we found the residence time to be symmetric in the position of the obstacle with respect to the center of the obstacle.

The same does not happen now. We find here a strong asymmetry. Let us first consider the same 41×41 obstacle, but we consider it to be closer to the exit than to the opposite side of the lattice. In figure 4.11 we show the data for the square with center in $(71, 51)$. We find out that this obstacle close to the exit produces a loss in

the outgoing flux (in figure we find the grey symbols always below the blacks, both if $W = 0$ and if $W = 3$). It is interesting to notice that now the clustering effect does not appear for smaller N with respect to the case of the empty corridor (without obstacle).

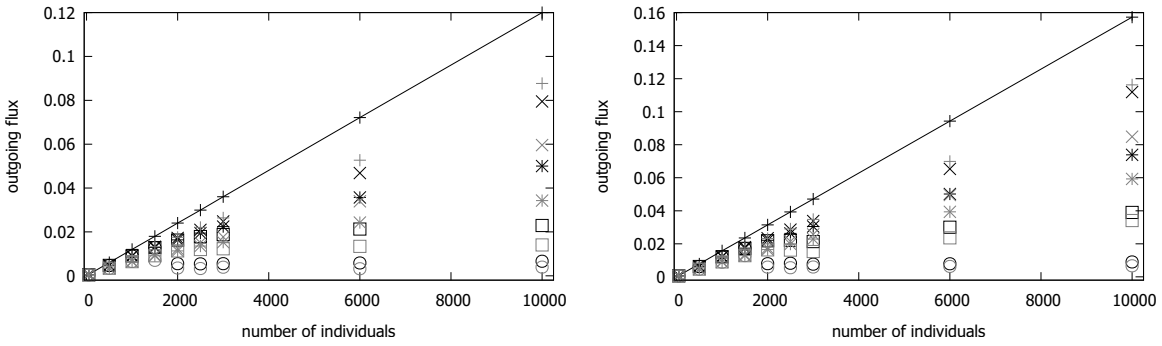

Figure 4.11: **Averaged outgoing flux vs. number of pedestrians.** As in figure 4.9, with a squared obstacle with side 41 and center in $(71, 51)$.

So we observed that an obstacle close to the exit cannot increase the average flux. What if the same 41×41 obstacle is in the left half of the lattice? Consider now the square with center in $(31, 51)$. We can see in Fig. 4.12 that in this geometry the outgoing flux increases if the threshold is not too much large ($T \leq 5$ in the plot). On the contrary, if the threshold is large, $T \geq 30$ in the figure, we can observe that the clustering regime is reached earlier than in the empty corridor case. Indeed, there is a loss in the outgoing flux for $T = 30$ and $W = 0$, and the clustering appears at $N = 1000$ for the parameters $T = 300$ and $W = 0$, while at $N = 1500$ for $T = 300$ and $W = 3$.

These two phenomena are more evident if the obstacle has larger side, while for a smaller obstacle the effect on the flux is negligible. We keep the center to be in $(31, 51)$. In the left panel of figure 4.13 we represent the effect of a larger squared obstacle of side 51 on the measured flux, with $W = 0$. It is evident that the clustering is present for $T = 300$ and $N = 1000$. On the contrary, in figure 4.13, right panel, the squared obstacle has side 21, so we see a negligible effect on the outgoing flux, except that the clustering appears for $T = 300$ at $N = 1500$, earlier if there is the obstacle with respect to the empty lattice.

Summarizing, we find a strong dependence on the position of the obstacle. If the obstacle is closer to the exit than to the opposite side, the flux decreases. On the contrary, if the obstacle is close to the entrance and far from the exit, the flux

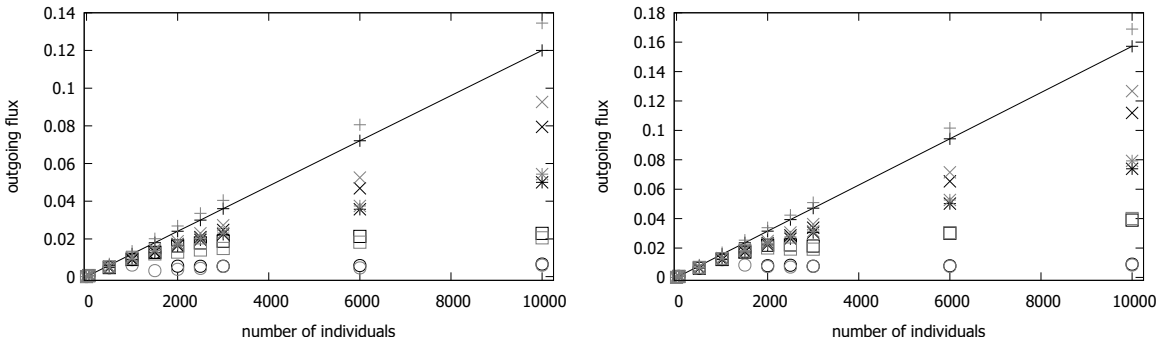

Figure 4.12: **Averaged outgoing flux vs. number of pedestrians.** As in figure 4.9, with a squared obstacle with side 41 and center in $(31, 51)$.

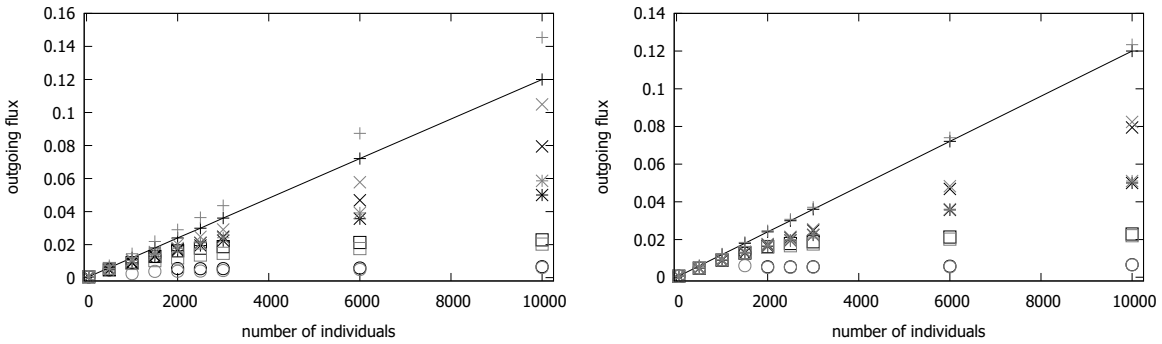

Figure 4.13: **Averaged outgoing flux vs. number of pedestrians.** As in figure 4.9, with $W = 0$. Left panel: a squared obstacle with side 51 the right and center in $(31, 51)$ is placed in the corridor. Right panel: the obstacle has side 21 and center in $(31, 51)$.

increases for T small. But if the threshold is large, an obstacle close to the entrance point favors the formation of clusters.

Our interpretation of the results is that the obstacle close to the exit, making more difficult to reach the region on the right of the obstacle where there is the exit, produces a decreasing in the outgoing flux with respect to the empty lattice case.

An obstacle close to the other side, making difficult for a particle to reach again the region on the left of the obstacle once it is on the right side, keeps the particles longer in the region with the exit, favoring the exit. However, since the obstacle reduces the free region close to the entrance point, it makes more likely the formation of a big stable cluster in that region. This may produce a decreasing in the flux, if

the threshold is sufficiently big and the number of individuals sufficiently large.

3.5 Evacuation time

We are interested in evaluating the evacuation time, i.e., the average time needed to let all the individuals leave the corridor.

We will consider the following experiment: we dispose N agents randomly in the corridor, we let start the dynamics accordingly with the description of the model in Sect. 3.1, but we do not consider any new individual entering in the corridor. We observe which is the time needed to the last agent to exit from the corridor. The average time measured repeating this experiment will be called *evacuation time*.

The results discussed above on the outgoing flux let us argue which behaviors would be observed for the evacuation time. Note that since the number of agents is decreasing during the evolution of the system, it will be more difficult to enter in a clustering regime, i.e., it is necessary a larger number of particles to reach it. Because of the results on the effect of an obstacle on the the outgoing flux of the previous section, we expect to find analogously that the evacuation time is smaller with respect to the case of empty corridor if the obstacle is far from the exit. On the contrary, the more an obstacle is close to the exit, the more we expect the evacuation time to be large.

We plot in figure 5.14 the evacuation time as a function of the number of individuals N, for $W = 0$, and values for T from 0 to 300, in the geometry of the empty lattice.

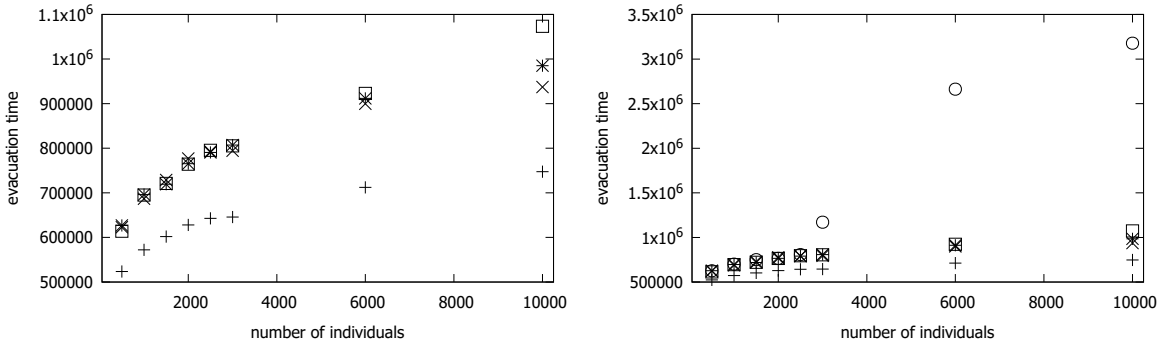

Figure 5.14: **Averaged evacuation time vs. number of pedestrians.** The symbols $+$, $\times$, $*$, the squares and the circles represent respectively the cases $T = 0, 2, 5, 30, 300$, with $L = 101$, $W = 0$, and no obstacles in the corridor. On the left we excluded the results for $T = 300$ to have a more readable figure, on the right we have the same picture added of the data for $T = 300$.

We can observe that the evacuation time is monotone in T for fixed N if N is large, while is essentially not depending on $T > 0$ if N is small. The independent random walk for $T = 0$ guarantees the minimum evacuation time. Note also that the system reaches the clustering regime only for large values of the threshold T and for large N, for $N \geq 3000$ when $T = 300$ in the plot. Note that in this clustering regime there is a clear growth in the evacuation time.

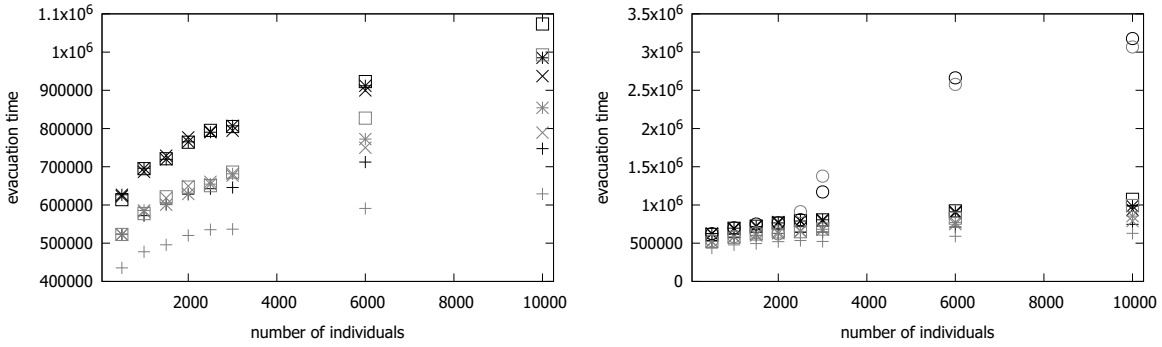

Figure 5.15: **Averaged evacuation time vs. number of pedestrians.** The symbols $+$, $\times$, $*$, the squares and the circles represent respectively the cases $T = 0, 2, 5, 30, 300$, with $L = 101$, $W = 0$, and a squared obstacle with side 41 and center in $(31, 51)$ in the corridor. The gray symbols represent the case of presence of the obstacle, while the black symbols refer to the empty lattice. On the left we excluded the results for $T = 300$ to have a more readable figure, on the right we have the same picture added of the data for $T = 300$.

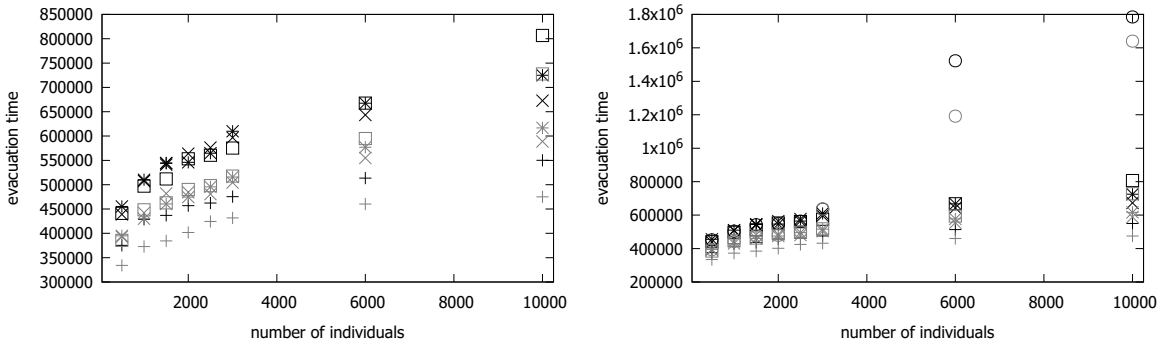

Figure 5.16: **Averaged evacuation time vs. number of pedestrians.** As in figure 5.15, here $W = 3$.

The presence of the obstacle in the corridor produces the expected effect on the evacuation time. As we made in the previous section we consider a large squared

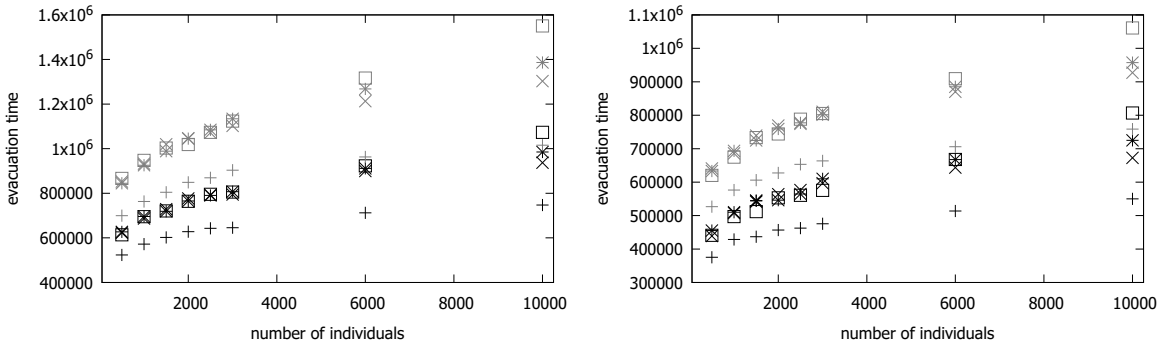

Figure 5.17: **Averaged evacuation time vs. number of pedestrians.** The symbols $+$, $\times$, $*$ and the squares represent respectively the cases $T = 0, 2, 5, 30$, with $L = 101$ and a squared obstacle with side 41 and center in $(71, 51)$ in the corridor. The gray symbols represent the case of presence of the obstacle, while the black symbols refer to the empty lattice. On the left we show the simulation results for $W = 0$, on the right the data refer to $W = 3$.

obstacle with side 41 and we consider it to be in the left half of the corridor or in the right half. We report in figures 5.15–5.16 the comparison of the average evacuation time calculated for the empty corridor (black symbols) and for the presence of the obstacle of side 41 with center again in $(31, 51)$ (grey symbols). We consider the cases of no influence by the wall on the dynamic ($W = 0$) in figure 5.15 and the case of positive W in figure 5.16. The presence of the obstacle in the left half of the corridor, far from the exit, produces a reduction of the evacuation time in most of the considered data. It is interesting to observe that for $W = 0$ and $T = 300$ (figure 5.15, right picture) the clustering effect starts for a smaller number of agents with respect to the empty corridor case, so for $T = 300$ and N between 2500 and 3000 the evacuation time is longer if the obstacle is present. Once the clustering regime is reached in both cases (large N), the obstacle yields again a shorter evacuation time.

In figure 5.17 we consider the presence of the same square obstacle in the right half of the corridor, closer to the exit. We compare the evacuation time in presence of this obstacle (gray symbols) and in absence of obstacles (black symbols). The center of the obstacle is now put in $(71, 51)$. As in the case of the evaluation of the outgoing flux we find this positioning to be unfavorable, i.e., it produces an increment in the evacuation time, both if $W = 0$ (left picture) and if $W = 3$ (right picture).

Chapter 4

Lorentz Model

The 2D Lorentz gas model is a system of non–interacting particles moving in a region where static small disks (scatterers) are distributed according to a Poisson probability measure. Particles perform uniform linear motion up to the contact with a disk where they are elastically reflected.

The Lorentz process has been firstly studied in [30] in the Boltzmann–Grad limit. In a low density limit (in the scatterers) in [6], the authors studied the stationary configuration and the mass flow of the system in the case of an infinite $2D$ slab, exploiting the reduction of the limit problem to a one–dimensional problem.

We expect that a similar result can be proved in our more complex geometry: the horizontal strip with one or more large fixed reflective obstacle, vertical sides in contact with two mass reservoirs, and horizontal sides behaving as specular reflective boundaries, even if the limit problem is not one–dimensional anymore. A possible strategy could be to make use of the linear Boltzmann equation as an intermediate step between the Lorentz model and the macroscopic Laplace problem with mixed boundary conditions.

4.1 The model

The Lorentz model is a system of light particles moving according to the laws of Newtonian mechanics in the two-dimensional space, where there is also a random distribution of scatterers. We consider as in Chapter 1 as domain a subset Ω of the finite strip $(0, L_1) \times (0, L_2) \subset \mathbb{R}^2$. This strip has two open boundaries, that we think as the left side $\partial\Omega_L = \{0\} \times (0, L_2)$ and the right side $\partial\Omega_R = \{L_1\} \times (0, L_2)$. The system is in contact on the left side and on the right side with two mass reservoirs at equilibrium with particles densities ρ_L and ρ_R, respectively. Particles traveling into

Ω are instead specularly reflected upon colliding with the upper side $(0, L_1) \times \{L_2\}$ and lower side $(0, L_1) \times \{0\}$ of the strip.

The scatterers we consider are fixed hard disks at rest with radius ε. The scatterers are distributed in Ω uniformly in space according to a Poisson law of mean $\lambda_\varepsilon > 0$, so that the probability of finding exactly n scatterers in a measurable set of $A \subset \Omega$ with measure $|A|$ is

$$e^{-\lambda_\varepsilon |A|} \frac{\lambda_\varepsilon^n |A|^n}{n!}. \tag{1.1}$$

We denote this probability by $\mathbb{P}_\varepsilon$ and we call $\mathbb{E}_\varepsilon$ the associated expectation.

A light particle moving in the domain Ω travels freely in Ω up to the instant of contact with a scatterers, then it is elastically reflected.

We consider the case in which large fixed obstacles are placed in the strip so that the domain Ω is a connected set. These obstacles are convex sets with smooth reflective boundaries. We consider a generic configuration of a finite number of obstacles with positive mutual distance and positive distance from the sides of the strip. In the sequel we will call $\partial\Omega_E$ the union of the obstacle boundaries and the upper and lower sides of the strip. Therefore, when a particle reaches $\partial\Omega_E$ it experiences a specular reflection.

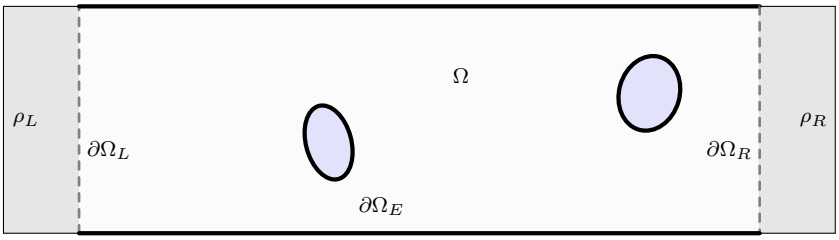

Figure 1.1: Domain Ω: strip with large fixed obstacles, where $\partial\Omega_L$ and $\partial\Omega_R$ are the vertical open boundaries and $\partial\Omega_E$ are reflective boundaries.

Since all collisions preserve the energy, the modulus of the velocity of a particle moving in Ω is constant. We consider it to be equal to one, so that the phase space is $\Omega \times S^1$, where $S^1 := \{v \in \mathbb{R}^2 : |v| = 1\}$.

For any arrangement of n scatterers drawn according to the Poisson law with mean λ_ε, we denote the centers of the scatterers by $\mathbf{c}_n = (c_1, c_2, \ldots, c_n)$. We define $\Psi^{-s}_{\mathbf{c}_n}(x, v)$ as the flow backward in time from a point $(x, v) \in \Omega \times S^1$ for a time $s > 0$ and for the configuration of scatterers individuated by $\mathbf{c}_n$. So $\Psi^{-t}_{\mathbf{c}_n}(x, v)$ describes the backward dynamics for a time t of a particle put in the point $(x, v) \in \Omega \times S^1$. We

recall that these trajectories are elastically deflected at contact with the scatterers and with the elastic boundary $\partial\Omega_E$. When following the time flowing from 0 to t, we define the function $\tau = \tau(x, v, t, \mathbf{c}_n)$ as the time the trajectory leaves a reservoir and it enters into the strip, reaching finally the position (x, v) at time t. So if the backward trajectory starting from (x, v) at time t reaches the boundary $\partial\Omega_L \cup \partial\Omega_R$ in the time interval $[0, t]$, this happens after a backward time $t - \tau$. If the trajectory $\Psi^{-s}_{\mathbf{c}_N}(x, v)$ never hits the boundary $\partial\Omega_L \cup \partial\Omega_R$ for times $s \in [0, t]$ we put $\tau = 0$.

The flow previously defined allows us to define the particle density of the system at time $t > 0$ as

$$f_\varepsilon(x, v, t) = \mathbb{E}_\varepsilon[f_B(\Psi^{-(t-\tau)}_{\mathbf{c}_n}(x, v))\chi(\tau > 0)] + \mathbb{E}_\varepsilon[f_0(\Psi^{-t}_{\mathbf{c}_n}(x, v))\chi(\tau = 0)], \tag{1.2}$$

where we are considering as initial datum for f_ε at time 0 a function $f_0(x, v) \in L^\infty(\Omega \times S^1)$ and as boundary datum f_B (not depending on t):

$$f_B(x, v) := \begin{cases} 1/2\pi\, \rho_L & x \in \partial\Omega_L,\ v \cdot n > 0 \\ 1/2\pi\, \rho_R & x \in \partial\Omega_R,\ v \cdot n > 0. \end{cases} \tag{1.3}$$

Here $1/2\pi$ is the density of the uniform distribution on S^1 and $n = n(x)$ is the inward pointing normal of Ω at $x \in \partial\Omega$.

We are representing the density f_ε as the sum of two contributions: the first one due to the trajectories leaving a reservoir at a positive time (so transporting the value f_{B} for the density), the second one due to particles that fulfill their motion into Ω for every time $s \in [0, t]$ (so transporting the value f_0).

Note that: *i*) the configurations of scatterers with the center of an obstacle in the disk of center x and radius ε cannot contribute to the expectation in (1.2) (they have to be forbidden). ii) We allow overlapping of scatterers. iii) The dynamics $\Psi^{-t}_{\mathbf{c}_n}$ is defined only almost everywhere with respect to $\mathbb{P}_\varepsilon$: for instance a trajectory hitting the set of zero measure intersection of two scatterers is not well defined beyond the collision.

We deal with the problem of finding a stationary state for the system. So we are wondering if there exists $f^S_\varepsilon(x, v)$ not dependent on t such that for any $t \geq 0$ solves the equation

$$f^S_\varepsilon(x, v) = \mathbb{E}_\varepsilon[f_B(\Psi^{-(t-\tau)}_{\mathbf{c}_n}(x, v))\chi(\tau > 0)] + \mathbb{E}_\varepsilon[f^S_\varepsilon(\Psi^{-t}_{\mathbf{c}_n}(x, v))\chi(\tau = 0)]. \tag{1.4}$$

4.2 Expected results

We are interested in studying the limit of f_ε^S as the scale parameter ε goes to 0. We scale the scatterers density as

$$\lambda_\varepsilon = \varepsilon^{-1}\eta_\varepsilon\lambda \tag{2.5}$$

where $\lambda > 0$ is a fixed parameter and η_ε is diverging, but

$$\eta_\varepsilon^7 \varepsilon^{\frac{1}{2}} \to 0 \text{ as } \varepsilon \to 0. \tag{2.6}$$

Note that we are considering a dilute configuration of obstacles. Indeed $\lambda_\varepsilon \to \infty$ but the typical area occupied by the scatterers in a region of measure one is of the order of $\lambda_\varepsilon\varepsilon^2 \to 0$. On the other hand the inverse of the mean free path is of the order of $\lambda_\varepsilon\varepsilon = \eta_\varepsilon\lambda \to \infty$, so we expect a diffusive behavior in the limit. Recall that in the classical Boltzmann-Grad limit $\eta_\varepsilon = 1$.

Our conjecture is that for ε sufficiently small there exists a unique stationary solution $f_\varepsilon^S(x,v) \in L^\infty(\Omega \times S^1)$ for the equation (1.4), that for $\varepsilon \to 0$, f_ε^S converges to ρ, where ρ is solution of the Laplace problem on Ω with mixed boundary conditions:

$$\begin{cases} \Delta\rho(x) = 0 & x \in \Omega \\ \rho(x) = \rho_L & x \in \partial\Omega_L \\ \rho(x) = \rho_R & x \in \partial\Omega_R \\ \partial_n\rho(x) = 0 & x \in \partial\Omega_E. \end{cases} \tag{2.7}$$

This should be true in the $L^\infty(\Omega \times S^1)$ setting.

A possible strategy is to compare the Lorentz model with the model described by the linear Boltzmann equation on the same domain Ω. Then we could exploit the results on the linear Bolzmann equation in the domain Ω that we proved in Chapter 1: Theorems 1.1 and 1.2. These results allow to reach the macroscopic picture for the limiting stationary density given by (2.7).

The proof of the asymptotically equivalence of the Lorentz process and the linear Boltzmann dynamics for $\varepsilon \to 0$ with (2.5)-(2.6) consists in estimating the events that prevent markovianity of the Lorentz gas in the same spirit of [6, 21, 22]. To do this a Gallavotti's argument as in [30] is needed (see also [8, 48]).

We introduce a decomposition analogous to the one introduced in (4.12) for the g_ε^S. We write the density $f_\varepsilon(x,v,t)$ solution of the Lorentz process defined in (1.2) separating the trajectories remaining in Ω for every time in $[0,t]$ and the trajectories that come from the boundary $\partial\Omega_L \cup \partial\Omega_R$ for a positive time $\tau \in [0,t]$:

$$f_\varepsilon(x,v,t) = f_\varepsilon^{out}(x,v,t) + f_\varepsilon^{in}(x,v,t),$$

where

$$f_\varepsilon^{out}(x,v,t) := \mathbb{E}_\varepsilon[f_B(\Psi_{\mathbf{c}_n}^{-(t-\tau)}(x,v))\chi(\tau>0)] \tag{2.8}$$

and

$$f_\varepsilon^{in} = \mathbb{E}_\varepsilon[f_0(\Psi_{\mathbf{c}_n}^{-t}(x,v))\chi(\tau=0)]. \tag{2.9}$$

We introduce the flow $F_\varepsilon(t)$ that takes account only of trajectories that stay internal to Ω for all times $s\in[0,t]$:

$$(F_\varepsilon(t)h)(x,v) = \mathbb{E}_\varepsilon[h(\Psi_{\mathbf{c}_n}^{-t}(x,v))\chi(\tau=0)] \quad h\in L^\infty(\Omega\times S^1) \tag{2.10}$$

and we observe that $f_\varepsilon^{in}(t) = F_\varepsilon(t)f_0$.

To prove the results on stationary solution of the Lorentz process we need to prove the following estimates, that we believe to hold:

Let us fix $T>0$. Considering the g_ε^{out} defined in (4.12), for any $t\in[0,T]$

$$\|f_\varepsilon^{out}(t) - g_\varepsilon^{out}(t)\|_{L^\infty(\Omega\times S^1)} \le C\varepsilon^{1/2}\eta_\varepsilon^3 t^2(1+t); \tag{2.11}$$

For any $t\in[0,T]$ and any $h\in L^\infty(\Omega\times S^1)$

$$\big\|\big(F_\varepsilon(t) - S_\varepsilon(t)\big)h\big\|_\infty \le C\|h\|_\infty\varepsilon^{1/2}\eta_\varepsilon^3 t^2(1+t). \tag{2.12}$$

We believe that those estimates can be proven via a direct estimate of the bad events preventing the Markovianity: recollision and interference events (see [6, 30]). The estimate proposed in [6] does not apply directly on our problem due to the presence of the reflective boundaries of the obstacle and of the strip. A more accurate study of the possible trajectories should be made, taking carefully into account the new configurations of the scatterers that due to the presence of those boundaries yields an interference or a recollision event.

Our aim is to complete this study in the near future.

Bibliography

[1] G. Albi, M. Bongini, E. Cristiani, D. Kalise. Invisible control of self-organizing agents leaving unknown environments. *SIAM Journal on Applied Mathematics*, 76(4):1683–1710, 2016.

[2] F. Alonso-Marroquin, S. I. Azeezullah, S. A. Galindo-Torres, L. M. Olsen-Kettle. Bottlenecks in granular flow: When does an obstacle increase the flow rate in an hourglass? *Phys. Rev. E*, 85:020301, 2012.

[3] D. Andreucci, D. Bellaveglia, E. N. M. Cirillo, S. Marconi. Monte Carlo study of gating and selection in potassium channels. *Physical Review E* 84:021920, 2011.

[4] D. Andreucci, D. Bellaveglia, E. N. M. Cirillo. A model for enhanced and selective transport through biological membranes with alternating pores. *Mathematical Biosciences* 257, 42–49, 2014.

[5] D. Andreucci, D. Bellaveglia, E. N. M. Cirillo, S. Marconi. Effect of intracellular diffusion on current–voltage curves in potassium channels, *Discrete Contin. Dynam. Syst. Ser. B* 19, 1837—1853, 2014.

[6] G. Basile, A. Nota, F. Pezzotti, M. Pulvirenti. Derivation of the Fick's law for the Lorentz model in a low density regime. *Commun. Math. Phys.*, 336, Issue 3, 1607–1636, 2015.

[7] N. Bellomo, C. Dogbe. On the modeling of traffic and crowds: A survey of models, speculations, and perspectives. *SIAM Review*, 53(3):409–463, 2011.

[8] C. Boldrighini, L. A. Bunimovich, Y. G. Sinai. On the Boltzmann equation for the Lorentz gas. *J. Stat. Phys.* 32, 477—501, 1983.

[9] D. Braess, A. Nagurney, T. Wakolbinger. On a paradox of traffic planning. *Transportation Science*, 39(4):446–450, 2005.

[10] C. Cercignani, R. Illner, M. Pulvirenti. *The Mathematical Theory of Dilute Gases.* Applied Mathematical Sciences 106, Springer-Verlag, New York, 1994.

[11] A. Ciallella. On the linear Boltzmann transport equation: a Monte Carlo algorithm for stationary solutions and residence times in presence of obstacles, *Conference Proceedings, Aimeta 2017, Salerno*, 952–960, 2017.

[12] A. Ciallella, E. N. M. Cirillo. Linear Boltzmann dynamics in a strip with large reflective obstacles: stationary state and residence time, *Kinetic & Related Models* **11**, 1475—1501, 2018.

[13] A. Ciallella, E. N. M. Cirillo, J. Sohier. Residence time of symmetric random walkers in a strip with large reflective obstacles, *Physical Review E* **97**, 052116, 2018.

[14] A. Ciallella, E. N. M. Cirillo, P. L. Curseu, A. Muntean. Free to move or trapped in your group: Mathematical modeling of information overload and coordination in crowded populations, *Mathematical Models and Methods in Applied Sciences* **28**, 1831—1856, 2018.

[15] E. N. M. Cirillo, O. Krehel, A. Muntean, R. van Santen. Lattice model of reduced jamming by a barrier, *Phys. Rev. E*, 94:042115, 2016.

[16] E. N. M. Cirillo, O. Krehel, A. Muntean, R. van Santen, A. Sengar. Residence time estimates for asymmetric simple exclusion dynamics on strips, *Physica A: Statistical Mechanics and its Applications*, 442 : 436–457, 2016.

[17] E. N. M. Cirillo, A. Muntean. Can cooperation slow down emergency evacuations? *Comptes Rendus Macanique* **340**, 626–628, 2012.

[18] E. N. M. Cirillo, A. Muntean. Dynamics of pedestrians in regions with no visibility — a lattice model without exclusion, *Physica A: Statistical Mechanics and its Applications*, 392(17): 3578–3588, 2013.

[19] E. Cristiani, D. Peri. Handling obstacles in pedestrian simulations: Models and optimization, *Applied Mathematical Modelling*, 45: 285–302, 2017.

[20] D. Desirable, P. Dupont, M. Hellou, S. Kamali-Bernard. Cellular automata in complex matter, *Complex Syst.* 20, 67-–91, 2011.

[21] L. Desvillettes, M. Pulvirenti. The linear Boltzmann equation for long-range forces: a derivation from particle systems. *Models Methods Appl. Sci.* 9, 1123—1145, 1999.

[22] L. Desvillettes, V. Ricci. A rigorous derivation of a linear kinetic equation of Fokker—Planck type in the limit of grazing collisions, *J. Stat. Phys.* 104, 1173—1189, 2001.

[23] A. J. Ellery, M. J. Simpson, S. W. McCue, R. E. Baker. Characterizing transport through a crowded environment with different obstacle sizes, *The Journal of Chemical Physics*, 140(5):054108, 2014.

[24] R. J. Ellis. Macromolecular crowding: obvious but underappreciated, *Trends Biochem. Sci.* 26: 597–604, 2001.

[25] R. Escobar, A. De La Rosa. Architectural Design for the Survival Optimization of Panicking Fleeing Victims. In W. Banzhaf, J. Ziegler, T. Christaller, P. Dittrich, and J.T. Kim, editors, *Advances in Artificial Life, Proceedings of the 7th European Conference, ECAL, 2003, Dortmund, Germany, September 14–17, 2003, Proceedings. Lecture Notes in Computer Science, vol. 2801.*, 97–106, Springer, Berlin, 2003.

[26] R. Esposito, M. Pulvirenti. From Particles to Fluids. *Hand-Book of Mathematical Fluid Dynamics*, vol.III, 1–82. North-Holland, Amsterdam, 2004.

[27] L. C. Evans. *Partial Differential Equations*, Graduate Studies in Mathematics, Vol. 19 Amer. Math. Soc., 1998.

[28] W. Feller. *An Introduction to Probability Theory and its Applications*, volume 1. John wiley & Sons, Inc, New York – London – Sidney, 1968.

[29] B. W. Fitzgerald, J. T. Padding, R. van Santen. Simple diffusion hopping model with convection. *Phys. Rev. E*, 95:013307, 2017.

[30] G. Gallavotti. Grad–Boltzmann limit and Lorentz's Gas. In:*Statistical Mechanics. A short treatise.* Appendix 1.A2. Springer, Berlin, 1999.

[31] D. Genovese, J. Sprakel. Crystallization and intermittent dynamics in constricted microfluidic flows of dense suspensions, *Soft Matter* 7, 3889–3896 , 2011.

[32] M. D. Haw. Jamming, two-fluid behavior, and self-filtration in concentrated particulate suspensions, *Phys. Rev. Lett.* 92, 185506, 2004.

[33] D. Helbing, I. Farkas, P. Molnàr, T. Vicsek. Simulation of pedestrian crowds in normal and evacuation situations, In M. Schreckenberg and S. D. Sharma, editors, *Pedestrian and Evacuation Dynamics*, 21–58, Springer, Berlin , 2002.

[34] D. Helbing. Traffic and related self-driven many-particle systems, *Rev. Mod. Phys.*, 73:1067–1141, 2001.

[35] D. Helbing, L. Buzna, A. Johansson, T. Werner. Self-organized pedestrian crowd dynamics: Experiments, simulations, and design solutions, *Transportation Science*, 39(1):1–24, 2005.

[36] D. Helbing, I. Farkas, T. Vicsek. Simulating dynamical features of escape panic, *Nature*, 407:487–490, 2000.

[37] D. Helbing, P. Molnár, I. J. Farkas, K. Bolay. Self-organizing pedestrian movement, *Environment and Planning B: Planning and Design*, 28(3):361–383, 2001.

[38] F. Höfling, T. Franosch. Anomalous transport in the crowded world of biological cells, *Reports on Progress in Physics*, 76(4):046602, 2013.

[39] R. L. Hughes. The flow of human crowds, *Annual Review of Fluid Mechanics*, 35:169–182, 2003.

[40] K. Kosmidis, P. Argyrakis, P. Macheras. A reappraisal of drug release laws using Monte Carlo simulations: the prevalence of the Weibull function, *Pharm. Res.* 20 (7) 988-–995, 2003.

[41] O. A. Ladyzhenskaya. *The Boundary Value Problems of Mathematical Physics*, Springer-Verlag, Berlin, 1985.

[42] H. A. Lorentz. Le mouvement des electrons dans les metaux, *Arch. Neerl. Sci. Exact Natur.* 336–371, 1905.

[43] M. Matsumoto, T. Nishimura. Mersenne Twister: A 623-dimensionally equidistributed uniform pseudorandom number generator, *ACM Trans. on Modeling and Computer Simulation* Vol. 8, No. 1, 3–30, 1998.

[44] M. Matsumoto, T. Nishimura. A Nonempirical Test on the Weight of Pseudorandom Number Generators, in: *Monte Carlo and Quasi-Monte Carlo methods* 2000, pp. 381–395, Ed. K.T. Fang, F.J.Hickernel, and H. Niederreiter, Springer-Verlag, 2002.

[45] M. A. Mourão, J. B. Hakim, S. Schnell. Connecting the dots: The effects of macromolecular crowding on cell physiology, *Biophysical Journal*, 107:2761–2766, 2017.

[46] P. Papagiannis, L. Beaulieu, F. Mourtada. Computational Methods for Dosimetric Characterization of Brachytherapy Sources, *Comprehensive Brachytherapy Physical and Clinical Aspects*, 85–104, Taylor & Francis, 2012.

[47] D. G. Rees, H. Totsuji, K. Kono. Commensurability-dependent transport of a Wigner crystal in a nanoconstriction, *Phys. Rev. Lett.* 108, 176801, 2012.

[48] H. Spohn. The Lorentz flight process converges to a random flight process, *Commun. Math. Phys. 60*, 277-–290, 1978.

[49] M. J. Saxton. Anomalous diffusion due to obstacles: a Monte Carlo study, *Biophysical Journal*, 66: 394–401, 1994.

[50] K. To, P. Y. Lai, H. K. Pak. Jamming of granular flow in a two-dimensional hopper, *Phys. Rev. Lett.*, 86: 71–74, 2001.

[51] I. Zuriguel, A. Garcimartín, D. Maza, L. A. Pugnaloni, J. M. Pastor. Jamming during the discharge of granular matter from a silo, *Phys. Rev. E*, 71:051303, 2005.

[52] I. Zuriguel, A. Janda, A. Garcimartín, C. Lozano, R. Arévalo, D. Maza. Silo clogging reduction by the presence of an obstacle, *Phys. Rev. Lett.*, 107:278001, 2011.

[53] I. Zuriguel. Invited review: Clogging of granular materials in bottlenecks, *Papers in Physics*, vol. 6, 060014, 2014.